

Quantum Features of the Cosmological Horizon

Eleanor Harris

A thesis presented for the degree of
Doctor of Philosophy



Department of Mathematics
King's College London
United Kingdom
June 2023

Abstract

This thesis explores the thermodynamics of the cosmological horizon, aiming to make progress towards a better understanding of the microscopic nature of its entropy. We utilise the constrained nature of low-dimensional theories of gravity to do so and investigate timelike boundaries in these theories, with an emphasis on the stretched horizon holographic picture. Throughout, we make use of the Euclidean continuation of de Sitter to the sphere.

Given the success of the AdS/CFT correspondence, one might attempt to embed a piece of de Sitter inside an anti-de Sitter geometry, and then describe the expanding region from the AdS boundary. In two dimensions, there exist dilaton potentials that give rise to such geometries and, by studying this problem in the presence of a timelike boundary, we demonstrate how to stabilise such solutions against thermal fluctuations. We then propose a dual matrix model living at the AdS boundary that should describe the interior spacetime, including the expanding region. Having proposed such a duality, a key method for testing it would be to compare correlation functions in the bulk and boundary. However, for de Sitter this poses a puzzle: in the saddle point approximation two-point functions can be calculated as a weighted sum over geodesic lengths. Such correlation functions are known to exist for any two points in de Sitter, but geodesics do not exist between arbitrary points. The puzzle is resolved by including complex length saddles that appear upon analytic continuation from the sphere.

Additionally, one can use the semi-classical relationship between three-dimensional gravity and Chern-Simons theory to explore thermodynamic contributions to the de Sitter horizon. The Euclidean gravitational path integral provides the exact, all-loop quantum corrected de Sitter entropy. To better understand the microscopic origin of this entropy, one hopes to find an analogous Lorentzian calculation that produces this result. This takes the form of an edge-mode theory living close to the cosmological horizon with a complexified gauge group, leading to an unbounded spectrum. To make progress, we study an analogous Abelian theory and see that there is an entanglement character to the entropy of the horizon. Finally, we summarise some new results on edge-mode theories arising from general boundary conditions.

Acknowledgements

I would like to begin by expressing my immeasurable gratitude to my supervisor, Dionysios Anninos. Your seemingly infinite passion for physics has truly inspired me throughout the last four years, and whenever I'm in any doubt, a conversation with you always reminds me to just focus on the physics and remember that it's incredible that we get paid to play around with maths all day. I would like to thank you for your kind and patient approach to mentorship; for always making yourself available for silly questions, and for telling me never to apologise for asking them. In a poorly-constructed de Sitter pun, there seems to be no boundary to the amount of support and encouragement you give your students. I am furthermore very appreciative for the fun and interesting projects that you have proposed over the course of this doctorate, which as well as being engaging have certainly expanded my horizons into new areas of physics. I could absolutely not have done this without your supervision.

Secondly, I would like to thank my amazing collaborators who worked on the various projects that contributed to this thesis; Shira Chapman, Kévin Nguyen, Sameer Sheorey, and David Vegh. You were all wonderful and very fun to work with. I would like to express particular gratitude to Damián Galante for always making himself available to answer questions and give advice. More broadly, I would also like to express my appreciation for the theory group at King's College London; it has been a pleasure to conduct research in such a friendly and open environment. I would further like to thank STFC for financially supporting this doctorate.

Of course, it would be remiss of me not to acknowledge my fellow PhD students at King's, whose unfaltering willingness to go to the pub at the end of a long day was vital to the completion of this PhD. The group is too big to list all your names individually, but you all know who you are. A special shout-out to Ben Pethybridge though for offering to proofread parts of this thesis for me.

I would also like to thank my family: to my mum for endlessly supporting me and always knowing the right words to say at the end of a tough week; to my dad for believing in me and keeping me inspired with a constant stream of wonderful pop-science articles; and to my aunt Rosie, whose encouragement and kindness was integral to getting me to the end of this PhD.

Moreover, I also would like to express my gratitude to my partner Mike, for doing a very good impression of someone who is interested in hearing about niche topics in theoretical physics for four years straight. In all seriousness, your calm and collected attitude to every hurdle and your untiring encouragement and belief in me has been invaluable in helping me complete this PhD. To say I could not have done this without you is a huge understatement.

And last, but definitely not least, I would like to thank Abby. You may not have known much about the expansion of the universe, but my world is certainly much bigger for having had you in it.

Contents

Introduction	7
I Two spacetime dimensions	17
1 Interpolating between dS_2 and AdS_2	22
1.1 Two-dimensional dilaton-gravity theories	22
1.1.1 Equations of motion and solutions	23
1.1.2 Boundary conditions	24
1.1.3 Thermodynamics	25
1.2 Near-Nariai thermodynamics	27
1.2.1 Near-Nariai with a boundary	28
1.3 (A) dS_2 interpolating geometries	31
1.3.1 Geometry	32
1.3.2 Thermodynamic properties	33
1.3.3 Interpolating the stretched dS_2 horizon	36
1.4 Double interpolating geometries	38
1.4.1 Geometry	38
1.4.2 Thermodynamic properties	40
1.5 Dual theory proposal	42
2 Correlation functions in de Sitter space	44
2.1 The scalar two-point function in de Sitter	44
2.2 The geodesic approximation	48
2.2.1 Review of geodesics in dS_2	48
2.2.2 From geodesics to two-point correlators	50
2.3 Sphere two-point functions	51
2.3.1 Euclidean saddle points	52
2.3.2 Quadratic perturbations	54

2.3.3	Generalising to higher dimensions	55
2.4	Lorentzian two-point functions	56
2.4.1	Timelike separated points	57
2.4.2	Spacelike separated points	58
2.4.3	Spacelike separated points between stretched horizons	59
II	Three spacetime dimensions	63
3	Topological contributions to the de Sitter entropy	66
3.1	Chern-Simons theory on S^3 and dS_3	69
3.1.1	Chern-Simons theory on S^3	70
3.1.2	Chern-Simons on $S^2 \times \mathbb{R}$ and $D \times \mathbb{R}$	72
3.2	Abelian example	75
3.2.1	Three-sphere partition function	75
3.2.2	Classical edge-mode theory	78
3.2.3	Quantum edge-mode theory	79
3.2.4	Edge-mode symmetries.	82
3.2.5	Comments on the non-Abelian case	84
3.3	Complexified Abelian Chern-Simons: Lorentzian model	86
3.3.1	Lorentzian model	86
3.3.2	Lorentzian edge-mode theory & quantisation	87
3.3.3	Lorentzian edge-mode spectrum	89
3.3.4	Lorentzian model in Euclidean signature?	90
3.4	Complexified Abelian Chern-Simons: Euclidean model	92
3.4.1	Euclidean model on S^3	92
3.4.2	Euclidean edge-mode theory on the torus	93
3.5	Remarks on gravitation in three dimensions	94
3.5.1	Euclidean signature	95
3.5.2	Lorentzian signature	96
3.6	AdS_4/CFT_3 and S^3	98
4	An alternative edge-mode theory	103
4.1	General boundary conditions	103
4.2	Bogoliubov transformation	106
4.2.1	Original edge-mode theory	106
4.2.2	Diagonalising the new term	108

Conclusion	109
Future directions	110
Appendices	112
A Thermodynamics of finite boundary geometries	113
A.1 AdS ₂ JT gravity	113
A.2 Schwarzschild dilaton gravity	114
B Double interpolating geometry with finite boundary	116
C WKB approximation	119
D Quantum mechanical path integral	123
E Geodesic equation in higher dimensions	126
F Details on the stretched horizon	128
G Chern-Simons determinant on S^3	130
H Euclidean path-integral of Abelian edge-mode theory	134
I Lorentzian edge-mode Hamiltonian	136
J $SL(2, \mathbb{C})$ WZW central charge	138

Introduction

For more than twenty years we have had observational evidence that the expansion of the universe is accelerating, driven by a mysterious source which we refer to as dark energy [1–3]. This accelerated expansion causes galaxies to recede away from us in all directions, with the furthest away galaxies retreating the fastest. If a galaxy is far enough away such that the light it emits cannot overcome the expansion in order to reach us, it will be hidden behind our cosmological horizon – the ultimate barrier to our observations of the cosmos. Eventually, the expansion will push more and more galaxies beyond our cosmological horizon, and future civilisations may believe that the entire universe consists of just the stars of the Milky Way and Andromeda, since these will be all that they see when they peer up at the night sky. Such a future civilisation may not even be able to detect the presence of dark energy at all since they will have no distant supernovae to use to detect it, as we do today. On long enough timescales even the radiation of the cosmic microwave background - the imprint of light from the very early universe - will dwindle behind the cosmological horizon, cutting the inhabitants of Milkdromeda off from the history of the universe. Fortunately, we happen to live in an era where we can observe this accelerated expansion, and we are therefore conscious of the fact that a complete understanding of the universe must incorporate this phenomenon.

In fact, it seems that this is not the only occasion in the history of the universe that it has exhibited accelerated expansion. The first was the epoch directly after the Big Bang, where the universe rapidly increased in size to 10^{78} times its original volume in only around 10^{-33} seconds [4, 5]. We call this era inflation [6–9], and it is clearly a much more rapid flavour of expansion to that which we experience today, yet we are able to model both periods using the same mathematical description. A universe exhibiting accelerated expansion is described by solving Einstein’s equations with a positive cosmological constant, denoted by $\Lambda > 0$, the result of which is the de Sitter solution [10]. After inflation ended, the expansion of the universe slowed until dark energy started to drive the uptick that we see today. Experiments indicate that the observed value of the cosmological constant in our universe is $\Lambda_{\text{Obs}} \sim 10^{-52} m^{-2}$; an incredibly small, but notably positive quantity.

The cosmological horizon is a fascinating feature that begs to be better understood. The more familiar situation in which horizons occur in physics is in the study of black holes, which are comparatively understood in greater detail. There are certainly some key differences between the black hole and cosmological horizons, perhaps amongst the more glaring of which is their behaviour with respect to an observer. The position of the black hole horizon is independent of where we are when we measure it, while if one tries to move towards their cosmological horizon, it will always move away in such a way as to keep them in the centre. However, there are also some key similarities between the two. Bekenstein and Hawking proposed that we should associate an entropy to a black hole that is proportional to the surface area of its horizon [11, 12]. This entropy can be thought of as quantifying the lack of information that we have about the system; it is counting the possible configurations of all the particles that are inaccessible to us behind the black hole horizon. It is therefore somewhat surprising that this entropy is proportional to the area of the black hole horizon, rather than its volume, given one would expect that all the possible configurations of matter inside the black hole would fill its entire interior. In a complete theory of quantum gravity, we should be able to perform this counting of configurations (known as microstates) precisely, and we even know how to do so in some highly symmetric setups. Gibbons and Hawking proposed that, similarly to the black hole, we should also associate an entropy to the cosmological horizon, and that this entropy should also follow an area law [13, 14]. However, it is fair to say that the question of whether a horizon should have an associated entropy is much less well understood for the cosmological case. It is therefore important to search for a theory of quantum gravity that describes expanding spacetimes, since if we could achieve this then we would be able to count the microstates of the cosmological horizon precisely and thus verify the proposal. In this thesis, we will be examining the hypothesis that such a theory exists.

As already mentioned, accelerated expansion can be modelled by the de Sitter solution, which has $\Lambda > 0$, and it is therefore quantum features of this spacetime with which this body of work is concerned. We already have a good understanding of how quantum gravity works in a very closely related spacetime, which is appropriately known as anti-de Sitter since it is the solution to Einstein's equations with a negative cosmological constant, $\Lambda < 0$. The key to understanding quantum features of anti-de Sitter space lay in uncovering the correspondence between anti-de Sitter space and conformal field theory, which is abbreviated to AdS/CFT [15]. This correspondence states that a theory of quantum gravity in anti-de Sitter space can be completely described by a non-gravitating theory that resides at the boundary of AdS. This reduction in dimension of spacetime is known as holography, reflecting the fact

that the volume’s worth of information in the interior is expressed as a hologram on the surface area at the boundary. This harks back to our description of the black hole as having an entropy proportional to its surface area, rather than the volume of its interior. Indeed, holography has been very successfully applied to the case of black holes by, for example, studying black holes in anti-de Sitter spacetime [16–18]. We are very fortunate to be able to describe quantum gravity in any theory of gravity, but somewhat unfortunate in the sense that where we have been able to do so, it is not for the spacetime that describes the universe that we inhabit. It is still very much an open question whether it is possible to describe de Sitter holographically in a similar way to that which has been achieved for anti-de Sitter. In this thesis, our aim is to take some steps towards understanding quantum features of expanding spacetimes, and hence build towards a better understanding of the microscopic origin of the de Sitter horizon entropy.

One reason for the success of anti-de Sitter is that it possesses the virtue of a boundary at spatial infinity where gravity effectively ‘switches off’, allowing us to identify the holographic dual theory more easily. We call such a boundary timelike since it is extended in time. In de Sitter space, by contrast, the boundaries are in the far future and far past. This originally led to the dS/CFT proposal [19–21], which states that a conformal field theory living in the far future of de Sitter should describe the physics of the interior. This was certainly a useful step forward and may have applications for describing early universe inflation, since for that de Sitter era the accelerated expansion came to an end. We therefore presently exist as ‘metaobservers’ of inflation since the far future of the early universe exists in our past today. However, this setup is not as useful for describing the period of dark energy driven expansion that we experience today since we are confined to our current cosmological horizon, and it is impossible to make measurements in the infinite future. Therefore, it is widely thought that we should search for a quantum theory of de Sitter that is intrinsic to the piece of the universe that we have access to inside our de Sitter horizon. There are two main proposals for this, which are known as worldline holography [22, 23] and stretched horizon holography [24–27]. Both of these involve putting an artificial timelike boundary between us and our horizon. Worldline holography attempts to establish a holographic dual in the vicinity of an observer, who could be a person with a telescope on Earth, say. Stretched horizon holography, on the other hand, suggests that the natural placement of the holographic dual is very close to the cosmological horizon. Here, we will be investigating several versions of the latter setup. This picture has gained renewed interest in recent years [28–30], but it is fair to say that a deep understanding of holography in de Sitter is still lacking.

When we encounter a difficult problem, our job as physicists is to simplify it as much as possible, and then once the simpler system is understood, we can attempt to gradually add details back in. When we calculate the orbits of planets, for example, we do not attempt to keep track of every atom in the solar system. The method of simplification that we will employ in this body of work is to remove some spacetime dimensions from the problem, and work in theories of low-dimensional gravity. These are theories consisting of two or even just one spatial dimension, along with one timelike dimension. This strategy has a long and fruitful history in many areas of physics [16, 31–37]. The hope is that this lower dimensional system is constrained enough that we can perform experiments more concretely, and yet that we still retain some of the features that we are interested in studying in the higher dimensional theories. Indeed, this methodology has been particularly worthwhile in the analogous setup for black holes since theories of low-dimensional gravity often still exhibit horizons [37]. As we will see, the cosmological horizon is also retained in theories of lower-dimensional gravity, allowing us to more easily probe features that we are interested in understanding, such as the thermodynamic behaviour. Thus, eventually we may be able to uplift our findings to the real world of three space and one timelike direction. Occasionally, we will be able to extend our results to higher dimensions explicitly, but in other situations it may not yet be straightforward to do so. In such cases, it is not unreasonable to expect that the results we obtain will still be able to guide our understanding in four dimensions.

The results of this thesis are split into two main parts. In Part I, we discuss features of de Sitter in two dimensions. Recently, there has been an increased interest in applying the standard tools of AdS/CFT to probe the static patch of de Sitter. A non-comprehensive list includes [26, 38–53]. One approach is to study geometries that flow between an anti-de Sitter boundary and a de Sitter interior. One could then attempt to probe the expanding region from the boundary. In dimensions $d > 2$, solutions with dS_d embedded within AdS_d either defy the null energy condition, or contain black hole horizons which cloak the de Sitter piece of the geometry from being examined using the boundary theory [54, 55]. However, in two dimensions there are no such impediments, and these solutions have been dubbed interpolating geometries [56, 57]. The thermodynamics of such theories in the presence of a timelike boundary are examined in Chapter 1, where we demonstrate how to stabilise the solution under thermodynamic fluctuations. This progress in establishing a thermodynamically stable realisation of dS_2 inside AdS_2 enables us to propose concrete microscopic models that could live at the AdS_2 boundary. These are matrix models whose degrees of freedom we expect will capture some of the physics of the expanding piece of the bulk geometry. In Chapter 2, we look at quantum fields in the presence of a fixed de Sitter background. It is

interesting to study whether scalar fields behave differently in the vicinity of a cosmological horizon compared to black holes. We utilise the worldline formalism and show that in order to correctly reproduce the large mass expansion of the correlator, it is necessary to include saddles of complex length in the geodesic approximation. These complex geodesics result in oscillatory behaviour in the two-point function, a behaviour which is not seen in the example of the AdS black hole in two dimensions.

In Part II, we study the de Sitter horizon in three dimensions, making use of the semi-classical relationship between Chern-Simons theory and three-dimensional gravity to explore thermodynamic contributions to the de Sitter horizon very precisely. In this setup, the Euclidean Chern-Simons path integral evaluated on the round three-sphere saddle gives the exact all-loop quantum corrected entropy of the de Sitter horizon. In Chapter 3, the goal is to investigate a corresponding Lorentzian computation for this entropy. To make progress, we can begin with a simpler Abelian model that has a complexified gauge group structure similar to that required for three-dimensional gravity with a positive cosmological constant. It follows that there exists an edge-mode theory living on a timelike boundary close to the de Sitter horizon. The previously discovered topological entanglement entropy [58, 59] in Chern-Simons theory then has a natural interpretation as a contribution to the entropy of the de Sitter horizon. We subsequently consider more general boundary conditions for the same setup in Chapter 4 and show that in fact there is no choice one can make to tame the unboundedness of the spectrum.

The remainder of this introduction is dedicated to reviewing some general features of de Sitter that will be useful for the rest of the thesis. The results of Part I first appeared in [60] and [61]. The content of Part II first appeared in [62] and Chapter 4 contains unpublished work with D. Anninos and K. Nguyen. At the beginning of each part, we will outline some more specific and technical details of gravity in two or three dimensions. The appendices contain further details of some of the calculations in the main text.

Geometry of de Sitter

It will be useful to review the geometry of de Sitter in general dimensions before specialising to two and three spacetime dimensions, as required later on. The de Sitter geometry is the maximally symmetric solution to Einstein's equations with positive cosmological constant, the value of which depends on the spacetime dimension d as

$$\Lambda = \frac{(d-2)(d-1)}{2\ell^2}. \quad (1)$$

Here ℓ characterises the curvature scale and is referred to interchangeably as the de Sitter length or the de Sitter radius. When $d = 2$ we set $\Lambda = 1/\ell^2$. This solution has constant positive curvature given by

$$R = \frac{d(d-1)}{\ell^2}. \quad (2)$$

One can view d -dimensional de Sitter space dS_d as the hypersurface embedded in $\mathbb{R}^{1,d}$ that is given by the equation

$$-X_0^2 + \sum_{i=1}^d X_i^2 = \ell^2, \quad (3)$$

This hyperboloid is shown in Figure 1. The hypersurface preserves an $SO(d, 1)$ subgroup of the Poincaré symmetries of $\mathbb{R}^{1,d}$, and this subgroup constitutes the isometry group of dS_d . The de Sitter metric induced on this hypersurface is given by specific parameterisations of the X_μ coordinates in the flat Minkowski metric,

$$ds^2 = -dX_0^2 + \sum_{i=1}^d dX_i^2. \quad (4)$$

For example, the global coordinate patch is given by setting

$$X_0 = \ell \sinh T, \quad X_i = \ell \omega_i \cosh T, \quad (5)$$

where $T \in \mathbb{R}$ is the global time coordinate and ω_i parametrises S^{d-1} . Plugging these coordinates into the $(d+1)$ -dimensional Minkowski metric (4) then leads to the global metric of d -dimensional de Sitter space,

$$\frac{ds^2}{\ell^2} = -dT^2 + \cosh^2 T d\Omega_{d-1}^2, \quad (6)$$

where $d\Omega_{d-1}^2$ is the round metric on unit $(d-1)$ -sphere. One can see that constant T slices are spheres that grow in size in the infinite past and future.

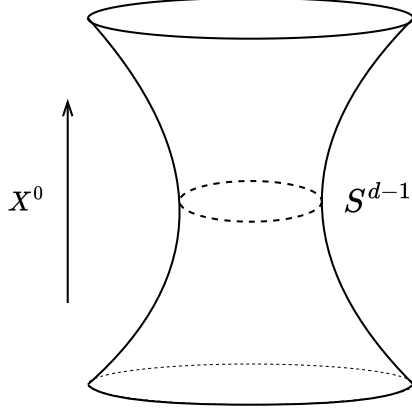


Figure 1: The d -dimensional hypersurface embedded in $\mathbb{R}^{1,d}$ that describes dS_d .

An inertial observer in this spacetime does not have access to the full geometry and is instead confined inside a cosmological event horizon. The causal region that such an observer has access to is described by the metric,

$$\frac{ds^2}{\ell^2} = -(1 - r^2)dt^2 + \frac{dr^2}{1 - r^2} + r^2 d\Omega_{d-2}^2, \quad (7)$$

where $t \in \mathbb{R}$ and $0 \leq r \leq 1$ for $d > 2$. However, when $d = 2$, the range of the radial coordinate is instead $-1 \leq r \leq 1$. The inertial observer sits at $r = 0$ in this spacetime and experiences a cosmological horizon at $r = 1$, and it is this horizon which we would like to characterise the features of. Note that this metric does not explicitly depend on the coordinate t , and hence (7) is referred to as the static patch metric. It is given by the choosing the embedding space coordinates in (4) to be

$$X_0 = \ell\sqrt{1 - r^2} \sinh t, \quad X_a = \ell r \omega_a, \quad a = 1, \dots, d - 1, \quad X_d = \ell\sqrt{1 - r^2} \cosh t. \quad (8)$$

The static patch region seen by an observer at $r = 0$ is indicated by the shaded region on the Penrose diagram in Figure 2. As already mentioned, we will be interested in timelike boundaries in the static patch, which correspond to lines of constant r in (7). In particular, the stretched horizon will be a surface of constant r that lies close to $r = 1$.

Of key importance to this body of work is the analytic continuation of de Sitter to Euclidean signature. Wick rotating $X_0 \rightarrow -iX_0$ in the embedding space description of de Sitter, equation (3) becomes the equation of an S^d embedded in \mathbb{R}^{d+1} , and the isometries become $SO(d + 1)$. Similarly, analytically continuing $T \rightarrow -i\theta$ in (6) gives

$$\frac{ds^2}{\ell^2} = d\theta^2 + \cos^2 \theta d\Omega_{d-1}^2, \quad (9)$$

which is the round metric on S^d . Surprisingly, analytically continuing equation (7) by taking $t \rightarrow -i\tau$ also leads to the round metric on S^d in a different coordinate system,

$$\frac{ds^2}{\ell^2} = (1 - r^2)d\tau^2 + \frac{dr^2}{1 - r^2} + r^2 d\Omega_{d-2}^2, \quad (10)$$

where in order to avoid a conical singularity, we must also periodically identify $\tau \sim \tau + 2\pi$. The fact that this is still the metric on S^d can be seen most clearly by performing this Wick rotation (along with $X_0 \rightarrow -iX_0$) in the choice of parameterisation in (8), then verifying that these obey the equation of the d -sphere. Therefore, despite describing seemingly very different regions of the Penrose diagram in Figure 2, the static patch and global metrics analytically continue to the same compact object in Euclidean signature, and upon evaluating the volume element, one can verify that they also have the same volume. The ‘observer dependence’ of the de Sitter horizon manifests itself in Euclidean signature by the fact that any S^{d-1} path on the S^d can be viewed as the Euclidean de Sitter horizon.

In analogy with the fact that the Euclidean continuation of a black hole spacetime leads to a thermal description with characteristic temperature given by the periodicity of the time coordinate, here we can read off the temperature of de Sitter to be $T_{\text{dS}} = 1/2\pi$. This is the temperature as measured by an inertial observer at $r = 0$.

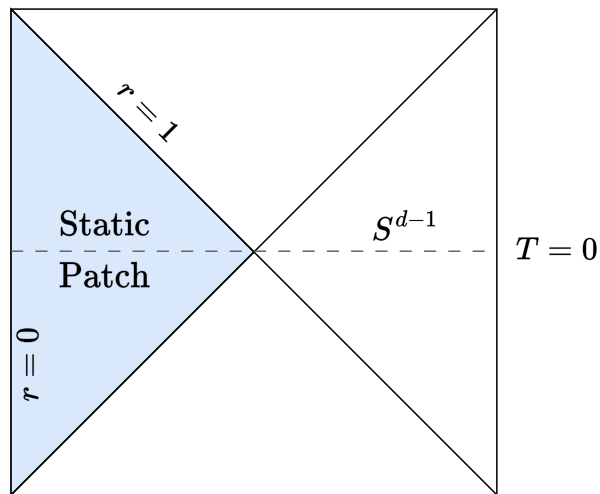


Figure 2: The Penrose diagram for de Sitter. Highlighted in blue is the static patch region which is casually accessible to an inertial observer at $r = 0$. This observer experiences a cosmological horizon at $r = 1$. Global time slices are $(d - 1)$ -spheres of radius $\ell \cosh T$, and the $T = 0$ time slice has been indicated explicitly.

Thermodynamics of de Sitter

Given that de Sitter seems to have an associated temperature T_{dS} , we can ask about the thermal properties of this spacetime. This works in close analogy to black hole thermodynamics. Consider the usual form of the thermal partition function in the canonical ensemble,

$$\log \mathcal{Z} = S - \frac{E}{T}, \quad (11)$$

where S is the entropy, E is the total energy and T is the temperature of the system which is kept fixed. Energy in general relativity is defined using the ADM formalism, which states that energy is given in terms of the asymptotic form of the metric. For the case of de Sitter, spatial slices are compact and therefore the ADM energy vanishes. This led to Gibbons and Hawking's proposal that the entropy of the de Sitter horizon should be given by the logarithm of the Euclidean gravitational path integral [13, 14],

$$\mathcal{Z}_{\text{grav}} = \sum_{\mathcal{M}} \int \mathcal{D}g e^{-S_E[g_{\mu\nu}]}, \quad (12)$$

where \mathcal{M} are compact manifolds and S_E is the Euclidean Einstein-Hilbert action,

$$S_E[g_{\mu\nu}] = -\frac{1}{16\pi G} \int d^d x \sqrt{g} (R - 2\Lambda). \quad (13)$$

Here R is the Ricci scalar (2), the metric g is that of Euclidean de Sitter (the round d -sphere), and G is Newton's constant. One can also include matter fields ϕ in the path integral, so that the above becomes

$$\mathcal{Z}_{\text{grav} + \text{matter}} = \sum_{\mathcal{M}} \int \mathcal{D}g \mathcal{D}\phi e^{-S_E[g_{\mu\nu}, \phi]}. \quad (14)$$

This proposal has also been more recently explored in [63–65]. We do not know how to compute this gravitational path integral exactly. However, equation (12) can be expanded in a semi-classical approximation around the round sphere saddle point solution, such that

$$\log \mathcal{Z}_{\text{grav}} \approx -S_E = S_{\text{dS}}, \quad (15)$$

where S_{dS} is the tree-level contribution to the de Sitter entropy, which is parametrically large in the semiclassical limit. We can use the semi-classical expansion to perform a simple check on the Gibbons-Hawking proposal. For example, for $d = 4$, the Euclidean action (13) can be

evaluated on-shell, leading to

$$S_{\text{dS}} = \frac{\pi \ell^2}{G} = \frac{\text{Area}}{4G}, \quad (16)$$

matching the classical result that the entropy should be proportional to the area of the horizon. It is thought that the entropy of the cosmological horizon in our universe is of order $S_{\text{dS}} \approx 10^{122}$. Therefore, given that the microscopic origin of this entropy is still an open question, we are in search of a huge number of microstates.

As previously mentioned, in this thesis we will be interested in the thermodynamics of time-like boundaries in de Sitter. In this case, the relevant temperature will be the Tolman temperature, which in the static patch coordinates (10) has inverse

$$\beta_T = \beta \sqrt{1 - r_b^2}, \quad (17)$$

where $\beta = 1/T_{\text{dS}} = 2\pi$ is the periodicity of the τ coordinate and $-1 \leq r_b \leq 1$ is the position of the timelike boundary. We will explore the thermodynamics with respect to this temperature in the remainder of this body of work.

Part I

Two spacetime dimensions

Introduction

Given the enormous success we have had in describing quantum features of anti-de Sitter spacetimes, one might ask whether it is possible to embed a piece of de Sitter within an anti-de Sitter geometry, and then use the tools of the AdS/CFT correspondence to capture the physics of this internal, expanding region. In dimensions greater than two, it has been shown that such a set-up either defies the null energy condition or that this geometry can only be realised if the de Sitter region is surrounded by a black hole horizon [54, 55], making it difficult to probe its microscopic structure. However, in two dimensions such geometries have been constructed and are known as either interpolating geometries or as Centaur geometries [56, 57, 66]. These geometries obey the null energy condition when viewed as pieces of higher-dimensional solutions [67] and offer the possibility of a holographic interpretation for the static patch of de Sitter. They can arise as dilaton-gravity models for certain choices of the dilaton potential. The solutions permit an asymptotically near-AdS₂ boundary of the type studied in [68]. For such a boundary, when the interpolating geometry ends at a dS₂ ‘black hole’ horizon one must grapple with a horizon of negative specific heat. Alternatively, one can choose a dilaton profile that decreases towards the near-AdS₂ boundary [56] leading to a dS₂ ‘cosmological’ horizon with positive specific heat, but now at the cost of a non-standard boundary behaviour for the dilaton. Neither of these features is an insurmountable obstacle in the search of a microscopic completion, but each adds an additional layer of difficulty. We will be focusing on the case where the AdS and dS regions are of the same dimension, but it is worth noting that another possibility is to consider geometries that interpolate between AdS_{*d*} and dS_{*D*} with $d \neq D$. Such a set-up was shown in [69] to obey the null energy condition for the case $d = 2$ and $D = 4$. The idea of rearranging the microphysical Hilbert space of quantum gravity in AdS to obtain de Sitter microstates also plays an interesting role in the approach of [46, 47, 70], and [28, 71].

In Chapter 1, we explore mechanisms for stabilising a portion of the dS₂ static patch within a near-AdS₂ world with ordinary boundary behaviour for the dilaton. We study Dirichlet boundary conditions at a finite proper distance from the horizon, following the method of

York [72, 73] applied to the de Sitter case [49, 74–77].¹ The temperature is fixed to be the Tolman temperature [83], which is the proper length of the Euclidean boundary S^1 . We begin by considering the thermodynamics of the dimensional reduction of the near-Nariai solution along the lines of [48, 56, 57]. Throughout, we will be in Euclidean signature, in which the near-Nariai geometry analytically continues to the round S^2 with a running dilaton. Because the geometry caps off in this way, it is a natural setting to ask about the effects of a Dirichlet boundary cutting the two-sphere. When we select the solution for which the dilaton has standard boundary behaviour, the piece of the geometry containing the ‘black hole’ dS_2 horizon is thermodynamically stable. The piece containing the ‘cosmological’ dS_2 horizon, which has a decreasing dilaton profile, is thermodynamically unstable.

We then consider the Dirichlet problem for the interpolating geometry, with standard boundary behaviour for the dilaton. We see that although for an asymptotic boundary the specific heat is negative, as the Dirichlet boundary is brought in a transition occurs rendering the specific heat positive, akin to a Hawking-Page phase transition [84]. To preserve a locally thermally stable interpolating solution that is asymptotically near- AdS_2 , with a large portion of Euclidean de Sitter in the interior, we construct interpolating geometries which include an additional piece of the Euclidean AdS_2 in the deep interior. Although the solution removes both Euclidean horizons of dS_2 , we note that we can tune the dilaton potential in such a way that the dS_2 portion has a region that is parametrically close to one with a cosmological horizon, evoking a stretched horizon picture. In Euclidean signature, this excision corresponds to removing a small disc surrounding the Euclidean horizon. As such, we end up with a geometry that is both thermally stable and encodes a stretched ‘cosmological’ dS_2 horizon, while being asymptotically near- AdS_2 . The stability of this geometry allows us to posit the form of a dual theory living at the asymptotically AdS_2 boundary by considering the interpolating geometry to be a deformation of JT gravity [85–87].

In Chapter 2, we shift focus slightly to study scalar two-point correlation functions in a fixed de Sitter background. Such correlation functions can give us an insight into how quantum fields behave in the presence of the cosmological horizon. Furthermore, a good understanding of two-point functions in de Sitter will allow us in the future to test the dual proposal put forward at the end of Chapter 1, by computing correlators in the bulk and comparing them to correlators computed in the boundary theory [88].

In the worldline formalism [89, 90], one can compute the correlator of a free massive scalar

¹Ordinary JT gravity with Dirichlet boundary conditions was considered, for example, in [78–82].

field between two points as a path integral over all paths connecting the points. In the large mass limit, one can take a saddle point approximation that reduces this path integral to a sum over geodesic lengths [91–93]. This is surprising since it is known that not all points in a Lorentzian spacetime can be connected by geodesics [94, 95].² For instance, in de Sitter space certain spacelike separated points are not connected by a geodesic. However, the two-point correlator for a free massive scalar field in the de Sitter invariant, Bunch-Davies state is known analytically for all points and all spacetime dimensions [97, 98]. We solve this apparent tension by considering the analytic continuation of de Sitter to the sphere where there always exist two geodesics that form a great circle between any two points. We compute the lengths of these geodesics as well as the one-loop correction to the Euclidean correlator coming from quadratic fluctuations of the geodesic length. We show that for certain points, it is necessary to keep the contributions from both Euclidean geodesics, even though on the sphere only one has the shortest length. Upon analytically continuing back to Lorentzian signature, we reproduce the precise form of the large mass two-point function, up to an overall coefficient. The geodesics that previously seemed to be missing between certain spacelike separated points turn out to have complex length when analytically continued to Lorentzian signature from the sphere. We see that it is crucial to include these complex saddles in the geodesic approximation in order to correctly reproduce the large-mass form of the correlator. We primarily work in two dimensions for simplicity, but ultimately extend our results to any spacetime dimension. Early work on static patch correlation functions includes [22, 99, 100]. Extremal surfaces in de Sitter (including geodesics in $d = 3$) have been studied in [101], while other extended objects such as Wilson lines have been studied in [102]. The geodesic approximation for late time correlators in dS_3 has recently been studied in [103], and [104] presents a related discussion on the role of complex geodesics in de Sitter space from the perspective of the heat kernel formalism. The geodesic approximation has also been widely used in the context of holography, starting with the work in [105, 106], where boundary conformal correlators of heavy operators were reproduced both at zero and finite temperature from a bulk geodesic calculation. Geodesics have also been used to explore dynamical settings in holography, such as in [107–109], and quantum chaos [110, 111].

Chapter 1 is organised as follows. In Section 1.1, we introduce a general class of Euclidean dilaton-gravity theories and provide general formulae for their thermodynamic properties in the presence of both a Dirichlet boundary at finite proper distance, as well as for an asymptotically AdS_2 boundary. In Section 1.2, we utilise these formulae in the near-Nariai limit of

²By the upper semi-continuity of arc-length, spacelike geodesics in Lorentzian manifolds always have (locally) maximal lengths [96]. However, it is possible to find scenarios where curve lengths connecting two points are unbounded from above, and in those cases, geodesics do not exist at all.

the black hole in dS_2 which in Euclidean signature is an S^2 . We show, as in [48], that the black hole is thermodynamically stable, while the cosmological horizon is thermodynamically unstable in this theory. In Section 1.3, we study the Dirichlet problem for the interpolating geometry and show that this saddle may be both stable, and thermodynamically favoured, depending on where we place the Dirichlet wall. We also posit that a region within this geometry may be interpreted as a completion of the stretched dS_2 cosmological horizon to a near- AdS_2 boundary. In Section 1.4, we introduce a dilaton-gravity theory permitting a solution which interpolates to a dS_2 region while being AdS_2 in the deep interior as well as near the boundary. We show that this saddle has positive specific heat, while also having the virtue of being asymptotically AdS_2 . First order phase transitions, reminiscent of the Hawking-Page transition [84], between the interpolating saddle and the AdS_2 black hole are discussed. Finally, in Section 1.5, we discuss the possibility of realising a boundary matrix model or SYK-type model that may capture some features of the expanding piece of the geometry. Appendices A and B summarise the thermodynamic properties of some further examples of dilaton potentials with finite boundaries.

Chapter 2 is organised as follows. In Section 2.1, we review the computation of the Wightman correlator in de Sitter and compute its large mass expansion. In Section 2.2, we review the calculation of Lorentzian geodesics in de Sitter, recovering the result that not all spacelike separated points in de Sitter are connected by a real geodesic. In Section 2.3, we move to the sphere and compute the Euclidean correlator in the geodesic approximation, including the one-loop corrections around each saddle point. We then extend our results to general dimensions. In Section 2.4, we analytically continue this result to Lorentzian signature to obtain the correct Lorentzian correlator. We apply our findings to several examples of timelike and spacelike geodesics, including those between opposite stretched horizons. In Appendix C, we recover the asymptotic form of the two-point correlator from a WKB approximation. In Appendix D, we solve the quantum mechanical path integral needed to compute one-loop corrections to the Euclidean correlator. In Appendix E, we discuss sphere geodesics in $d \geq 2$. Finally, in Appendix F we give details on the computation of correlations between stretched horizons.

Chapter 1

Interpolating between dS_2 and AdS_2

In this chapter, we explore a class of dilaton-gravity models that exhibit a dS_2 interior region and demonstrate ways to stabilise such solutions against thermal fluctuations. In two dimensions, Newton's constant G is dimensionless, and so in this chapter we choose to set $G = 1/8\pi$ for the brevity of expressions.

1.1 Two-dimensional dilaton-gravity theories

In this section, we introduce the general class of models we will be interested in. These are two-dimensional dilaton-gravity models whose field content is given by a two-dimensional metric, $g_{\mu\nu}$, and the dilaton field, ϕ . The Euclidean action governing the theory is given by

$$S_E = S_0 - \frac{1}{2} \int_{\mathcal{M}} d^2x \sqrt{g} \left(\phi R + \frac{1}{\ell^2} V(\phi) \right) - \int_{\partial\mathcal{M}} d\tau \sqrt{h} K \phi_b, \quad (1.1)$$

where the dilaton potential $V(\phi)$ will be a general function of ϕ unless otherwise specified. The theory is considered on a disc topology \mathcal{M} with boundary $\partial\mathcal{M} = S^1$. The trace of the extrinsic curvature normal to $\partial\mathcal{M}$ is given by K , and $\phi_b \equiv \phi|_{\partial\mathcal{M}}$ is the boundary value of the dilaton. The first term in (1.1) is the contribution from the constant part of the dilaton

$$S_0 = -\frac{\phi_0}{2} \int_{\mathcal{M}} d^2x \sqrt{g} R - \phi_0 \int_{\partial\mathcal{M}} d\tau \sqrt{h} K = -2\pi\phi_0\chi. \quad (1.2)$$

Due to the Gauss-Bonnet theorem, this term computes the Euler character χ of \mathcal{M} and so is topological. For a disc topology one has $\chi = 1$. In what follows, we will be interested in the canonical partition function for arbitrary $V(\phi)$ in the presence of a Euclidean boundary at finite proper distance from the Euclidean horizon.

1.1.1 Equations of motion and solutions

The equations of motion stemming from (1.1) are

$$\nabla_\mu \nabla_\nu \phi - g_{\mu\nu} \nabla^2 \phi + \frac{1}{2\ell^2} g_{\mu\nu} V(\phi) = 0, \quad (1.3)$$

$$R + \frac{1}{\ell^2} \partial_\phi V(\phi) = 0. \quad (1.4)$$

These equations can be rearranged, at least within a local neighbourhood of \mathcal{M} , as follows

$$-\nabla^2 \phi + \frac{1}{\ell^2} V(\phi) = 0, \quad (1.5)$$

$$R + \frac{1}{\ell^2} \partial_\phi V(\phi) = 0, \quad (1.6)$$

$$\nabla_\mu \xi_\nu + \nabla_\nu \xi_\mu = 0, \quad \xi^\mu \equiv \varepsilon^{\mu\nu} \partial_\nu \phi. \quad (1.7)$$

Therefore, even though it seems that (1.3) and (1.4) are overconstrained, recasting them in the form (1.5), (1.6), and (1.7) shows that there are only two second order equations acting on the degrees of freedom ϕ and R . The equation (1.7) moreover indicates that ξ^μ is a Killing vector field of $g_{\mu\nu}$. Using the existence of ξ^μ and the two diffeomorphisms we can place a general solution of (1.1) in the form

$$\frac{ds^2}{\ell^2} = N(r) d\tau^2 + \frac{dr^2}{N(r)}, \quad \phi(r) = r, \quad \tau \sim \tau + \beta. \quad (1.8)$$

Given this form of the metric, equation (1.5) then becomes

$$N'(r) = V(\phi), \quad (1.9)$$

which gives the following relation between the dilaton potential and the coefficient of the metric

$$N(r, r_h) = \int_{r_h}^r dr' V(r') > 0. \quad (1.10)$$

Since we are considering Euclidean solutions, this must be positive for all r . Noting that $N(r_h, r_h) = 0$, the metric (1.8) describes a Euclidean black hole solution with the horizon at r_h , and where $\phi(r_h) \equiv \phi_h$ is the value of the dilaton at the horizon. We emphasise that r_h is not an independent variable as it is fixed by the form of $N(r, r_h)$. Expanding (1.8) near to the horizon $r = r_h$ and imposing periodicity of $\tau \sim \tau + \beta$ to ensure smoothness of the

Euclidean solution leads to the relation

$$\beta = \frac{4\pi}{|V(r_h)|}. \quad (1.11)$$

This formula holds regardless of the asymptotic form of the potential. The usual JT gravity [112, 113] corresponds to the case where $V(\phi) = 2\phi$. For this potential (1.4) ensures that the curvature is constant and negative, giving an AdS₂ solution for the metric.

1.1.2 Boundary conditions

As boundary conditions, we consider the Euclidean Dirichlet problem for which the induced metric h at $\partial\mathcal{M}$ and the corresponding proper length β_T , as well as the boundary value of the dilaton ϕ_b on $\partial\mathcal{M}$ are fixed. The gauge parameter ξ_μ is required to vanish at $\partial\mathcal{M}$, to ensure the boundary condition on h is preserved and the location of the boundary is not disrupted (see for instance [114]).

The induced metric h can be arranged to be constant along $\partial\mathcal{M}$ by a judicious reparameterisation of the boundary time τ . In what follows, we moreover take ϕ_b to be constant along $\partial\mathcal{M}$. The physical motivation behind this choice of boundary condition stems from the Gibbons-Hawking prescription for Euclidean black hole thermodynamics [13, 14], whereby one views the Euclidean solutions on the disc as contributing to the thermal partition function of the underlying theory.¹ We will not necessitate that the boundary is asymptotically (near) AdS₂ for large part of our discussion, in line with the considerations of [48].

Given the solution (1.8) with (1.10), it is clear that a general choice of ϕ_b and h will not permit a real solution to our boundary value problem. For instance, let us consider the dilaton potential with $V(\phi) = -2\phi$, which yields $N(r, r_h) = r_h^2 - r^2$. Smoothness of the solution at the origin of the disc moreover fixes $r_h = 2\pi/\beta$ such that the proper size of the boundary circle is $\beta_T = \sqrt{4\pi^2 - \beta^2 r_b^2}$. Regardless of our choice for ϕ_b and assuming our solution is real, we have that $\beta_T \in (0, 2\pi)$ which is only a subset of the positive half-line. More markedly, for $\phi_b = 0$, only $\beta_T = 2\pi$ is permitted. In particular, going from a non-vanishing to a vanishing value of ϕ_b leads to a discontinuous jump in the allowed set of β_T . These restrictions on independent boundary data are a two-dimensional analogue of the obstructions arising when setting up the Dirichlet problem in four-dimensional general relativity [114–117] on manifolds with a boundary. In the case at hand, aside from such restrictions, the Dirichlet problem

¹Alternative boundary conditions could fix the trace of the extrinsic curvature K at $\partial\mathcal{M}$ or the normal derivative of ϕ at $\partial\mathcal{M}$, or more general combinations thereof.

is well-posed due to the absence of locally propagating gravitational degrees of freedom. Nonetheless, we must ensure that the Dirichlet data (β_T, ϕ_b) we consider are indeed sensible.

1.1.3 Thermodynamics

We would like to study the thermodynamics of the class of theories (1.1) in the presence of a finite boundary. One motivation for studying the finite boundary case is that certain geometries, such as the static patch of de Sitter space, do not afford an asymptotic boundary. In such circumstances, it is natural to consider a Dirichlet problem with a finite boundary. Our goal here is to present formulae for thermodynamic quantities at a finite boundary, generalising the results of [56, 118, 119].

We now evaluate the on-shell Euclidean action, which is related to the partition function by $-S_E = \log Z$. Given the Dirichlet problem under consideration, we have that Z is a function of ϕ_b and β_T . The induced metric h and ϕ_b at $\partial\mathcal{M}$ are given by

$$ds_{\text{bdy}}^2 = \ell^2 N(r_b, r_h) d\tau^2 \equiv h d\tau^2, \quad \beta_T = \beta \sqrt{N(r_b, r_h)}, \quad \phi_b = r_b. \quad (1.12)$$

The trace of the extrinsic curvature is

$$K = \frac{1}{h} K_{\tau\tau} = \frac{1}{2\sqrt{h}} \partial_{r_b} N(r_b, r_h). \quad (1.13)$$

We will further assume, for now, that the dilaton takes its minimal value at the Euclidean black hole horizon r_h . This is not necessarily the case; when the horizon is cosmological it will be located at the largest possible value of the dilaton, as will be discussed in the next section. The on-shell action is

$$S_E = \frac{\phi_0 \beta}{2} \int_{r_h}^{r_b} dr N''(r) - \frac{\phi_0 \beta}{2} N'(r_b) - \frac{\beta}{2} \int_{r_h}^{r_b} dr (-r N''(r) + N'(r)) - \frac{\beta}{2} N'(r_b) \phi_b. \quad (1.14)$$

Integrating the first term in the bulk action by parts and using (1.11), along with the fact that for a black hole horizon $V(r_h) > 0$ (otherwise (1.10) would not hold for r slightly greater than r_h), this evaluates to

$$\log Z = 2\pi (\phi_0 + \phi_b) + \beta_T \sqrt{N(r_b, r_h)}. \quad (1.15)$$

We see that the expression (1.15) takes the suggestive form $\log Z = S - E/T$ for a canonical thermal partition function. Indeed, we are interested in the thermodynamics experienced by an observer at a finite cutoff r_b . As such, the relevant temperature is the Tolman temperature

[72] which is precisely β_T in (1.12). To evaluate thermodynamic quantities, we must vary $\log Z$ with respect to β_T while keeping ϕ_b (and hence r_b) fixed. The following expressions prove to be useful

$$\partial_{\beta_T} N(r_b, r_h) = \frac{2V(r_h)^2 N(r_b, r_h)}{\beta_T (V(r_h)^2 + 2V'(r_h)N(r_b, r_h))}, \quad \partial_{r_h} N(r_b, r_h) = -V(r_h). \quad (1.16)$$

The thermal energy E , and entropy S are found to be

$$E = -\sqrt{N(r_b, r_h)}, \quad (1.17)$$

$$S = 2\pi(\phi_0 + \phi_h), \quad (1.18)$$

while the specific heat is given by²

$$C = \frac{\beta_T \sqrt{N(r_b, r_h)} V(r_h)^2}{V(r_h)^2 + 2V'(r_h)N(r_b, r_h)}, \quad (1.19)$$

in agreement with [118]. In the case where there are multiple possible saddles for a given β_T , the above formulae will hold at each saddle and the free energy must be computed to determine which solution is dominant. We observe that the entropy (1.18) is a function of quantities located at the Euclidean horizon, reflecting its more universal nature. This property was already observed in the early work of York [72] when placing a four-dimensional black hole in a box with Dirichlet conditions. The energy and specific heat depend more sensitively on the choice of boundary conditions. Consequently, though the entropy is insensitive to the location of the boundary, the thermal stability of a horizon may depend on this.

A special case of the above is when the dilaton potential at large values of ϕ takes the form $V(\phi) = 2\phi + \mathcal{O}(\phi^{-\epsilon})$. Here, our geometries acquire an asymptotic near-AdS₂ boundary such that the metric takes the asymptotic form $N(r_b, r_h) \approx r_b^2 - b$, and it follows from (1.12) that our thermodynamic quantities are computed (after a rescaling of r_b) with respect to the inverse temperature $\beta = 4\pi/V(\phi_h)$. Hence, for asymptotically near-AdS₂ configurations, our thermodynamic quantities are more closely associated to the behaviour of the spacetime at the horizon. Specifically, taking $\phi_b \gg 1$ while keeping β_T fixed, the quantities (1.17), (1.18), and (1.19) become

$$E_\infty = -\phi_b + \frac{b}{2\phi_b}, \quad S_\infty = 2\pi(\phi_0 + \phi_h), \quad C_\infty = -\frac{2\pi V(\phi_h)}{R(\phi_h)}, \quad (1.20)$$

²In the case where the dilaton decreases towards the AdS₂ boundary, rather than growing, these formulae will be modified to have an overall minus sign.

in agreement with the results of [56, 118, 119]. Stated otherwise, the more rigid nature of the near-AdS₂ boundary has allowed for the thermodynamic derivatives to occur with respect to the ordinary Gibbons-Hawking temperature β in (1.11), which is defined as the surface gravity at the horizon with a suitably normalised timelike Killing vector ∂_τ . One may also add boundary counterterms to the action by taking $K \rightarrow K - 1$ in equation (1.1) which has the effect of removing the divergent $-\phi_b$ contribution from the expression for E_∞ .

1.2 Near-Nariai thermodynamics

In this section, we compute thermodynamic properties of the dimensionally reduced near-Nariai black hole in the presence of a finite boundary. This geometry describes the near horizon limit of the Schwarzschild-de Sitter spacetime with near coincident horizons. The dilaton potential for this model is given by $V(\phi) = -2\phi$, which is plotted in Figure 1.1. The thermodynamics of this dilaton-gravity model were also discussed in [48, 56].

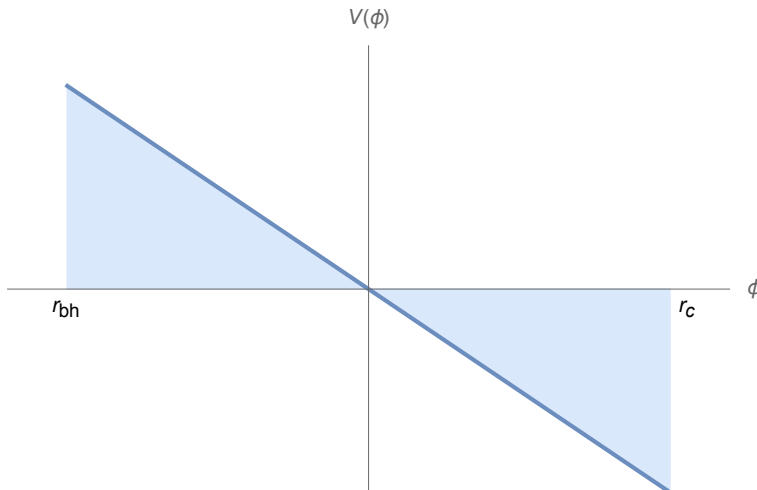


Figure 1.1: The dilaton potential $V(\phi) = -2\phi$ for the black hole in de Sitter. The solution caps off at the two horizons which have been indicated here as r_{bh} and r_c .

As in the previous section, we will consider the metric in Euclidean signature. Employing (1.10), we can confirm that the dilaton potential $V(\phi) = -2\phi$ produces the dS₂ geometry, whose solution reads

$$\frac{ds^2}{\ell^2} = (r_h^2 - r^2)d\tau^2 + \frac{dr^2}{(r_h^2 - r^2)}, \quad \tau \sim \tau + \beta, \quad \phi(r) = r, \quad (1.21)$$

where $r_h \leq r \leq -r_h$, with $r_h < 0$ and $\tau \sim \tau + \beta$. There are two Euclidean horizons at $r = \pm r_h$ – one is the black hole horizon which we will refer to as $r_{bh} = r_h < 0$, and the

other is the cosmological horizon which we call $r_c = -r_h > 0$. In Euclidean signature the space caps off at the two horizons and so this metric coincides with the round metric on the two-sphere, as illustrated in Figure 1.2. Taking $r_h = -1$ in (1.21), we retrieve equation (10) with $d = 2$. Since r_h is intrinsically linked to the temperature through (1.11) and we wish to consider thermal fluctuations of our system, it will be useful to keep r_h explicit here. Since the dilaton is also running, it is a near-dS₂ static patch.

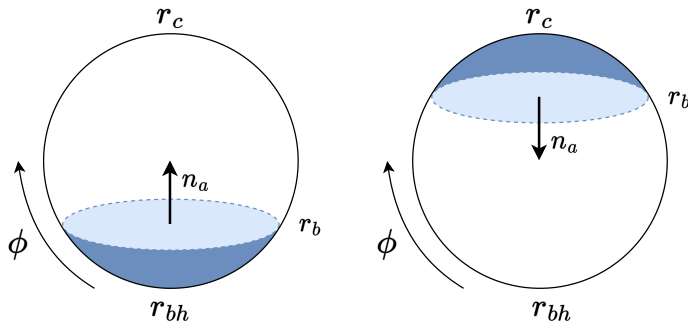


Figure 1.2: The Euclidean Nariai geometry is an S^2 . The choice of sign of the outward pointing normal vector is dependent on which horizon we choose to integrate from. The direction of increasing ϕ is indicated, which we will always take to increase from the back hole horizon towards the cosmological horizon.

As in the previous section, β is chosen to ensure smoothness of the Euclidean saddle. Now that there are two such potential singularities, we must have

$$\beta = \frac{4\pi}{|V(r_{bh})|} = \frac{4\pi}{|V(r_c)|} = \frac{2\pi}{|r_h|}. \quad (1.22)$$

From Figure 1.1 we see that the condition (1.22) is satisfied since $r_{bh} = -r_c = r_h$. We therefore have a \mathbb{Z}_2 symmetry $r \rightarrow -r$ in this metric which exchanges the two horizons. It is the sign of the dilaton that decides for us which is the cosmological horizon, and which is the black hole, and here we choose the dilaton to always grow away from the black hole horizon.

1.2.1 Near-Nariai with a boundary

In order to compute the thermal partition function, we place a boundary at some value $r = r_b \in (r_h, -r_h)$, where $\phi_b = r_b$ and β_T are fixed. The boundary can either surround the black hole or cosmological horizon. In fact, there is no choice of saddle here. Rather, all saddles must be included provided they satisfy the same Dirichlet boundary conditions. However, of all the saddles, one will generally dominate.

Thus, we must evaluate the thermodynamic quantities for both horizons in the presence

of a boundary at r_b . For the black hole horizon at $r = r_h$, the analysis of the previous section can be directly applied, resulting in

$$\log Z_{\text{bh}} = 2\pi(\phi_0 + r_h) + \beta_T \sqrt{r_h^2 - \phi_b^2}, \quad r_h = -\frac{2\pi|\phi_b|}{\sqrt{4\pi^2 - \beta_T^2}}. \quad (1.23)$$

An important difference for the cosmological horizon is that the outward pointing unit normal vector has the opposite sign to that of the black hole case, as shown in Figure 1.2. For this reason, the sign of the boundary term must be flipped in order to have a well-posed variational problem. Furthermore, for a cosmological horizon, (1.10) becomes

$$\int_r^{r_c} dr' V(r') < 0. \quad (1.24)$$

So, $V(r_c) < 0$ in order for this to hold for r slightly smaller than r_c . The end result is a change in the sign of the second term in equation (1.15), such that

$$\log Z_{\text{cos}} = 2\pi(\phi_0 - r_h) - \beta_T \sqrt{r_h^2 - \phi_b^2}. \quad (1.25)$$

We can now compute and compare various thermodynamic properties. The canonical free energies of the two saddles are

$$F_{\text{bh}} = -\frac{2\pi\phi_0}{\beta_T} + \frac{|\phi_b|\sqrt{4\pi^2 - \beta_T^2}}{\beta_T}, \quad (1.26)$$

$$F_{\text{cos}} = -\frac{2\pi\phi_0}{\beta_T} - \frac{|\phi_b|\sqrt{4\pi^2 - \beta_T^2}}{\beta_T}. \quad (1.27)$$

It follows that

$$\Delta F \equiv F_{\text{bh}} - F_{\text{cos}} = \frac{2|\phi_b|}{\beta_T} \sqrt{4\pi^2 - \beta_T^2} \geq 0, \quad (1.28)$$

where the inequality is saturated for $\phi_b = 0$.

The saddle with lowest free energy is the one with the cosmological horizon. However, we must also assess whether the saddle is stable under small thermal fluctuations. We thus compute the specific heat

$$C_{\text{bh}} = -C_{\text{cos}} = \frac{4\pi^2|\phi_b|\beta_T^2}{(4\pi^2 - \beta_T^2)^{3/2}} > 0. \quad (1.29)$$

We find that with Dirichlet boundary conditions, the black hole horizon of the near-Nariai geometry has positive specific heat while the cosmological horizon has negative specific heat [48]. This also resonates with the results of [77, 120]. In consequence, even though the cosmological saddle has lower free energy, it is thermally unstable in the setup under consideration. At least locally, the black hole saddle is the stable one, although it may be metastable at the non-perturbative level.

The energy can be computed in a similar fashion via (1.17). We find

$$E_{\text{bh}} = -E_{\text{cos}} = -\frac{|\phi_b|\beta_T}{\sqrt{4\pi^2 - \beta_T^2}}. \quad (1.30)$$

The energies of the black hole and cosmological horizons are equal and opposite. We can similarly calculate the entropy by either integrating from the black hole horizon, as in the left-hand side of Figure 1.2 or the cosmological one as in the right-hand side of the same figure. Using equation (1.18), we have

$$S_{\text{bh}} = 2\pi(\phi_0 + \phi_h), \quad (1.31)$$

$$S_{\text{cos}} = 2\pi(\phi_0 - \phi_h), \quad (1.32)$$

where $\phi_h = r_h < 0$ is the value of the dilaton at the horizon.

It is interesting to note that the total energy in the near-dS₂ static patch, which is given by ‘gluing’ the black hole saddle to the cosmological saddle along their common boundary yields a vanishing result

$$E_{\text{tot}} \equiv E_{\text{bh}} + E_{\text{cos}} = 0. \quad (1.33)$$

Adding the entropies together yields the total entropy of the near-dS₂ static patch to be

$$S_{\text{tot}} \equiv S_{\text{bh}} + S_{\text{cos}} = 4\pi\phi_0. \quad (1.34)$$

We can compare (1.33) and (1.34) to the result from calculating the classical contribution to the partition function over the whole two-sphere, where now there is no longer a boundary term for the action. One finds

$$S_E = \frac{\phi_0\beta}{2}(V(-r_h) - V(r_h)) - \frac{\beta r_h}{2}(V(-r_h) + V(r_h)). \quad (1.35)$$

Since for the Nariai geometry $V(r_h) = -2r_h$ the second term vanishes. The free energy F is related to the partition function by $\log Z = -\beta_T F = S - \beta_T E$. Since there is no spatial boundary anymore, the total energy of the full sphere vanishes. We therefore have that the total entropy is

$$S_{\text{full}} = -S_E = 4\pi\phi_0, \quad (1.36)$$

which exactly matches equation (1.34). It would be good to understand whether this agreement between the full two-sphere and the ‘glued’ saddles persists beyond the classical level by computing quantum corrections as in [121–123].

It is interesting to contrast (1.29) with the specific heat of the four-dimensional Nariai black hole, which has been reported in the literature [124,125] to be negative leading to an evaporating black hole (like that of the Schwarzschild black hole in flat space). The four-dimensional thermodynamic quantities rely on a more local treatment of the horizon thermodynamics. The temperature T , for instance, is given by the surface gravity at the Killing horizon with a suitably normalised Killing vector. If one computes the area, and hence the Bekenstein-Hawking entropy, of the black hole horizon as a function of T , one notes that it decreases with increasing T indicating a negative specific heat. For similar reasons the de Sitter horizon has been reported to have positive specific heat [98]. The difference in sign with the computations above is accounted for by the different definition of temperature, which is now given by the Tolman temperature β_T . This the near-Nariai black hole version [48] of York’s observation [72] that when placed in a box with Dirichlet conditions, the flat space Schwarzschild black hole can have positive specific heat.

In the following section we proceed to consider a different treatment of the boundary of the near-Nariai black hole geometry and show that one can recover a negative specific heat.

1.3 (A)dS₂ interpolating geometries

In this section, we explore an extension [56, 57] of the dS₂ dilaton potential, $V(\phi) = -2\phi$, that results in an asymptotically near-AdS₂ geometry ending at the near-Nariai black hole horizon. Our goal is to study the thermodynamic properties of such models in the presence of a Dirichlet boundary (a related discussion can be found in [78]). We end with a comment about the stretched dS₂ horizon in this framework.

1.3.1 Geometry

For the sake of concreteness, we focus on the dilaton potential

$$V(\phi) = 2|\phi| + \tilde{\phi}, \quad (1.37)$$

where $\tilde{\phi}$ is a real-valued parameter.³ The potential is shown in Figure 1.3. For a given temperature, this geometry will have up to two saddles. We shall refer to these as the interpolating geometry and the AdS₂ geometry. Although the potential $V(\phi)$ we study has a jump in its first derivative, the geometries it produces have continuous and differentiable metrics. We now provide the form of the metric for both $\tilde{\phi}$ positive as well as negative.

Case 1: $\tilde{\phi} \geq 0$

From equation (1.10) we can see that the metric for the interpolating geometry will be of the form (1.8) with

$$N^{D+}(r, r_D) = \begin{cases} (r - r_D)(\tilde{\phi} - r - r_D), & r_D \leq r \leq 0, \\ r^2 + r_D^2 + \tilde{\phi}(r - r_D), & 0 < r, \end{cases} \quad (1.38)$$

where r_D defines the Euclidean dS₂ black hole horizon. The Euclidean time periodicity is given by

$$\beta_D = \frac{4\pi}{|\tilde{\phi} - 2r_D|}. \quad (1.39)$$

We therefore have a portion of the two-sphere (Euclidean dS₂) for $r \leq 0$ (in particular, when $\tilde{\phi} = 0$ this is exactly the metric in (1.21)), and when $r > 0$ we have a Euclidean AdS₂ metric. Depending on the sign of $\tilde{\phi}$ the two-sphere is glued to a portion of a quotient of the hyperbolic disc ($\tilde{\phi} > 0$) or a portion of the hyperbolic strip ($\tilde{\phi} \leq 0$).

The metric of the AdS₂ saddle is

$$N^{A+}(r, r_A) = r^2 - r_A^2 + \tilde{\phi}(r - r_A), \quad 0 \leq r_A \leq r, \quad (1.40)$$

³It is worth emphasising that any $V(\phi)$, including smooth potentials, that have regions linear in ϕ with oppositely signed slopes and an asymptotic growth of the form $V(\phi) = 2\phi + \mathcal{O}(\phi^{-\epsilon})$ suffices for our purposes. A simple example is $V_\epsilon(\phi) = 2\phi \tanh \frac{\phi}{\epsilon}$ with $\epsilon > 0$ small. Moreover, although we have chosen the slope in (1.37) to have the same absolute value for $\phi > 0$ and $\phi < 0$ one can also consider cases where the slopes differ.

where r_A defines the location of the Euclidean AdS₂ black hole horizon. The Euclidean time periodicity is given by

$$\beta_A = \frac{4\pi}{|\tilde{\phi} + 2r_A|}. \quad (1.41)$$

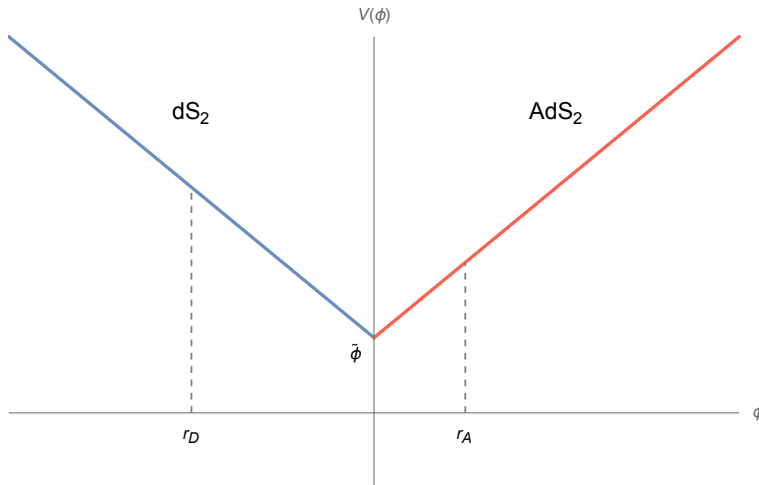


Figure 1.3: The dilaton potential for the interpolating geometry (1.37) with $\tilde{\phi} > 0$. The blue slope indicates where the potential describes a dS₂ geometry and the red slope shows where the geometry is Euclidean AdS₂. At a given temperature, there can be two saddles, indicated here at r_D and r_A .

Case 2: $\tilde{\phi} < 0$

When $\tilde{\phi} < 0$, we must further ensure that the metric is everywhere positive. The AdS₂ saddle will remain of the same form, but the range of r_A is modified as

$$N^{A-}(r, r_A) = r^2 - r_A^2 + \tilde{\phi}(r - r_A), \quad |\tilde{\phi}|/2 \leq r_A \leq r. \quad (1.42)$$

The interpolating solution similarly restricts the range of r_D , such that

$$N^{D-}(r, r_D) = \begin{cases} (r - r_D)(\tilde{\phi} - r - r_D), & r_D \leq r \leq 0, & r_D < \left(\frac{1+\sqrt{2}}{2}\right)\tilde{\phi}, \\ r^2 + r_D^2 + \tilde{\phi}(r - r_D), & 0 < r. \end{cases} \quad (1.43)$$

In the above we are assuming that the coordinate r can become large compared to $\tilde{\phi}$ and r_D . The periodicities β_D and β_A will be as for $\tilde{\phi} > 0$, namely (1.39) and (1.41) respectively.

1.3.2 Thermodynamic properties

As in the previous sections, we consider Dirichlet boundary conditions whereby the proper size of the boundary circle β_T and the boundary value of the dilaton ϕ_b are fixed. We take

$\phi_b > 0$ here since non-positive ϕ_b reproduces the near-Nariai black hole setup described in Section 1.2. In general, there are two solutions obeying the boundary conditions which we call r_D and r_A , as shown in Figure 1.3.

The temperatures of the interpolating geometry and the AdS₂ geometry are

$$\beta_T^D = \frac{4\pi}{|\tilde{\phi} - 2\phi_D|} \sqrt{r_b^2 + \phi_D^2 + \tilde{\phi}(r_b - \phi_D)}, \quad (1.44)$$

$$\beta_T^A = \frac{4\pi}{|\tilde{\phi} + 2\phi_A|} \sqrt{r_b^2 - \phi_A^2 + \tilde{\phi}(r_b - \phi_A)}, \quad (1.45)$$

where we have introduced the notation $\phi_D = r_D$ to be the value of the dilaton at the dS₂ black hole horizon and $\phi_A = r_A$ to be the value of the dilaton at the AdS₂ black hole horizon. We must set the temperatures equal to each other $\beta_T^D = \beta_T^A = \beta_T$ to compare their thermodynamic properties at a given temperature.

Case 1: $\tilde{\phi} \geq 0$

Let us begin by taking ϕ_b to be large compared to $\tilde{\phi}$ and $\phi_{A,D}$. The thermodynamics for the Euclidean AdS₂ solution (1.40) with $\tilde{\phi} = 0$ are reviewed in Appendix A. For non-vanishing $\tilde{\phi}$ we find a similar result for $\phi_A > 0$, namely

$$-\beta_T F_{\text{AdS}_2} = 2\pi \left(\phi_0 - \frac{\tilde{\phi}}{2} \right) + \frac{1}{2} \left(2\phi_b + \tilde{\phi} \right) \sqrt{\beta_T^2 + 4\pi^2}. \quad (1.46)$$

The specific heat follows readily

$$C_{\text{AdS}_2} = \left(\phi_b + \frac{\tilde{\phi}}{2} \right) \frac{4\pi^2 \beta_T^2}{(\beta_T^2 + 4\pi^2)^{3/2}}, \quad (1.47)$$

which is positive for all $\phi_b > 0$.

The other solution has $\phi_D < 0$ such that the region of the geometry near and including the horizon has positive curvature. For this interpolating solution, we have

$$-\beta_T F_{\text{interp}} = 2\pi \left(\phi_0 + \frac{\tilde{\phi}}{2} \right) + (\beta_T^2 - 4\pi^2) \sqrt{\frac{(\phi_b + \chi_+)(\phi_b - \chi_-)}{\beta_T^2 - 4\pi^2}}, \quad (1.48)$$

where for convenience we have defined $\chi_{\pm} \equiv \left(\frac{\sqrt{2} \pm 1}{2} \right) \tilde{\phi}$. In order to ensure the above expression is real we must lie in one of two regimes. The first, which connects to parametrically

large ϕ_b , is $\phi_b \geq \chi_-$ and $\frac{4\pi}{\tilde{\phi}} \sqrt{\phi_b(\phi_b + \tilde{\phi})} \geq \beta_T \geq 2\pi$, where the upper bound for β_T ensures the negativity of ϕ_D . Given F_{interp} , we can compute the specific heat of the interpolating saddle for this range:

$$C_{\text{interp}} = -\sqrt{(\phi_b + \chi_+)(\phi_b - \chi_-)} \times \frac{4\pi^2 \beta_T^2}{(\beta_T^2 - 4\pi^2)^{3/2}}. \quad (1.49)$$

For this case the specific heat C_{interp} is negative, and the only thermodynamically stable saddle is the Euclidean AdS₂ black hole. We thus retrieve, within this range of boundary conditions a near-Nariai black hole horizon with negative specific heat. The second regime is $0 < \phi_b < \chi_-$ and $\frac{4\pi}{\tilde{\phi}} \sqrt{\phi_b(\phi_b + \tilde{\phi})} < \beta_T < 2\pi$. For this case the specific heat C_{interp} is

$$C_{\text{interp}} = \sqrt{(\phi_b + \chi_+)(-\phi_b + \chi_-)} \times \frac{4\pi^2 \beta_T^2}{(4\pi^2 - \beta_T^2)^{3/2}}, \quad (1.50)$$

which is positive. Note that taking $\phi_b = 0$ in (1.50) recovers the result (1.29) for the black hole in the Nariai geometry up to an overall constant, as expected. Upon solving $\beta_T^D = \beta_T^A = \beta_T$, we see that

$$\phi_A = \frac{1}{2} \left(\frac{(2\phi_b + \tilde{\phi})(\tilde{\phi} - 2\phi_D)}{\sqrt{(2\phi_b + \tilde{\phi})^2 + 8\phi_D^2 - 8\tilde{\phi}\phi_D}} - \tilde{\phi} \right), \quad \phi_b > \chi_-. \quad (1.51)$$

A solution for ϕ_A for a given ϕ_D can only be found for large enough ϕ_b . Therefore, in the range $0 < \phi_b < \chi_-$ the interpolating geometry is the only saddle and is thermodynamically stable. We now explore the case $\tilde{\phi} < 0$.

Case 2: $\tilde{\phi} < 0$

We now consider the thermodynamic properties for $\tilde{\phi} < 0$. The Euclidean AdS₂ saddle will be thermodynamically stable, with the same free energy and specific heat as for $\tilde{\phi} > 0$, namely (1.46) and (1.47) respectively.

The interpolating saddle will now permit some additional properties. The free energy will still take the form (1.48), with the additional restriction coming from the requirement that the metric (1.43) remain positive for all r , namely that $\phi_D \leq \chi_+$. This additional restriction on the value of the dilaton at the horizon modifies the reality conditions for (1.48). We again find two possible regimes, the first being $\sqrt{2\pi} \left| \frac{2\phi_b + \tilde{\phi}}{\tilde{\phi}} \right| \geq \beta_T \geq 2\pi$ and $\phi_b \geq -\chi_+$. In this range the interpolating saddle has the same specific heat as in (1.49) and hence is unstable.

The other possibility is the regime $\sqrt{2\pi} \left| \frac{2\phi_b + \tilde{\phi}}{\tilde{\phi}} \right| < \beta_T < 2\pi$ and $0 < \phi_b < -\chi_+$. In this

case, the heat capacity is given by (1.50) and so is thermodynamically stable. Solving $\beta_T^D = \beta_T^A = \beta_T$, we find

$$\phi_A = \frac{1}{2} \left(\frac{(2\phi_b + \tilde{\phi})(\tilde{\phi} - 2\phi_D)}{\sqrt{(2\phi_b + \tilde{\phi})^2 + 8\phi_D^2 - 8\tilde{\phi}\phi_D}} - \tilde{\phi} \right). \quad (1.52)$$

Therefore, in this case for a given ϕ_D , there is always a ϕ_A provided that $|\tilde{\phi}|/2 < \phi_b < -\chi_+$. The difference in free energies between the stable interpolating saddle and the AdS₂ saddle is given by

$$F_{\text{interp}} - F_{\text{AdS}_2} = \frac{\sqrt{(\phi_b + \chi_+)(-\phi_b + \chi_-)(4\pi^2 - \beta_T^2)}}{\beta_T} + \frac{(2\phi_b + \tilde{\phi})\sqrt{\beta_T^2 + 4\pi^2 - 4\pi\tilde{\phi}}}{2\beta_T}. \quad (1.53)$$

For $\tilde{\phi} < 0$ this expression is positive. To give a numerical example, we can take $\tilde{\phi} = -1$, $\phi_b = 1$, and $\beta_T = 5$ which satisfy the conditions on β_T and ϕ_b . These values correspond to taking $\phi_D = -\frac{1}{2} - \frac{\pi}{\sqrt{4\pi^2 - 25}} \approx -1.33$ in (1.52) such that $\phi_A = \frac{1}{2} + \frac{\pi}{\sqrt{4\pi^2 + 25}} \approx 0.89$ lies in the allowed range for ϕ_A . They lead to a positive difference (1.53). So, the AdS₂ saddle will be thermodynamically favoured over the interpolating saddle. If instead $0 < \phi_b < |\tilde{\phi}|/2$, then there will be no AdS₂ saddle since $V(\phi_A) < 0$ in this range and we will have the same situation as in (1.50), with the interpolating saddle being the only stable solution.

1.3.3 Interpolating the stretched dS₂ horizon

We end this section by considering the interpolating solution for $\tilde{\phi} < 0$ in some more detail. For the purpose of our discussion, it will prove useful to slightly generalise the dilaton potential (1.37) to the following

$$V_\delta(\phi) = 2\phi \left(-\Theta(-\phi) + \frac{1}{\delta} \Theta(\phi) \right) + \tilde{\phi}, \quad (1.54)$$

with $\tilde{\phi} < 0$, and δ a small positive number. In order to have an interpolating solution with an asymptotic AdS₂ region, the horizon r_h must lie below the critical value $r_\delta \equiv \tilde{\phi}(1 + \sqrt{1 + \delta})/2$. At precisely $r_h = r_\delta$ the geometry caps off for a second time at $r = -\tilde{\phi}\delta/2$, creating a closed Euclidean universe.

If we now tune r_h to be parametrically close to and below r_δ and take $\phi_b \gg 1$, we find an asymptotically near-AdS₂ geometry which includes a significant portion of the two-sphere. The interpolating saddle stemming from $V_\delta(\phi)$ admits a portion of the two-sphere for which

the excised region is a disc of area $\sim \delta$. The excised region that would have contained the cosmological dS_2 horizon is replaced by a region of negative curvature that reaches all the way out to the AdS_2 boundary. The geometry and corresponding Penrose diagram is shown in Figure 1.4.

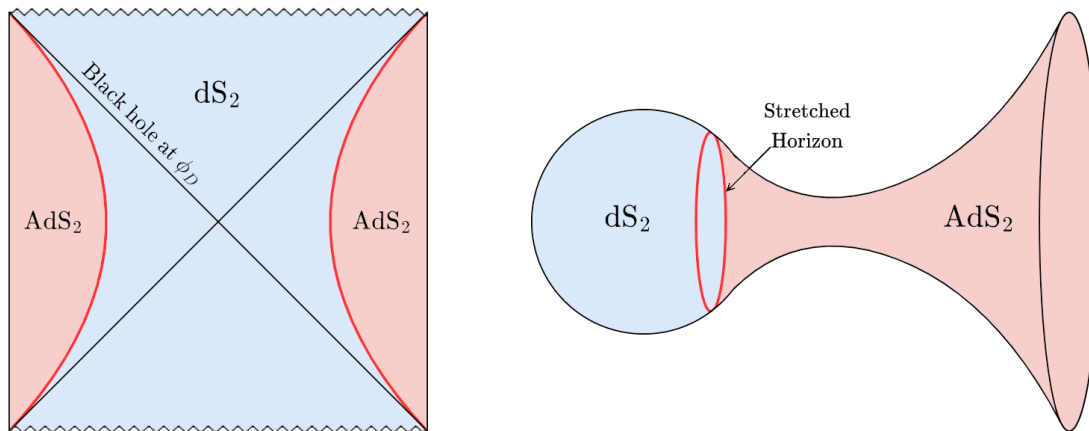


Figure 1.4: Left: The Penrose diagram of the interpolating geometry that contains the black hole in a de Sitter static patch in the deep interior and interpolates to an AdS_2 boundary. Right: The same geometry in Euclidean signature, where the Euclidean black hole horizon now caps off at the pole of the two-sphere.

An excision of this type is often considered when placing a stretched surface [24] a small region away from the dS_2 horizon and has been explored as a potential holographic screen of de Sitter in various works including [25–27, 30]. Though physically appealing, one of the challenges in making the stretched horizon picture precise is that the surface lies in the midst of a gravitating spacetime and it is difficult to obtain concrete observable quantities analogous to those at the boundary of AdS or the flat space S -matrix.⁴ Instead of placing a holographic theory at the stretched horizon, we might then view the interpolating geometry as an ultraviolet completion of the stretched dS_2 horizon with a near- AdS_2 boundary.

As it stands, the interpolating geometries we have discussed so far have negative specific heat whenever they are endowed with an asymptotically AdS_2 boundary. This can be ameliorated by bringing the near- AdS_2 boundary into the interior, by introducing a Dirichlet wall [78] along the lines we have discussed in the previous sections. This comes at the cost of sharp AdS/CFT type observables. In the next section we discuss a simple generalisation

⁴One approach is to set up a type of timelike Dirichlet boundary near the cosmological horizon, as explored in [49, 74–77]. However, at least in four and higher spacetime dimensions, caution must be exercised since this leads to various instabilities and issues with well-posedness of the Dirichlet problem [116, 117].

that admits a stretched dS_2 horizon that is capped off by a horizon with positive specific heat in the deep interior while preserving the asymptotic near- AdS_2 boundary.

1.4 Double interpolating geometries

In this section, we will propose a geometry that has some of the benefits of the interpolating geometry discussed in the previous section while also having the virtue of a positive specific heat, ensuring that the solution is locally thermodynamically stable. For the sake of concreteness, we will consider a theory with the following dilaton potential

$$V(\phi) = \begin{cases} 2\phi + \tilde{\phi} - 4x, & \phi \leq x, \\ 2|\phi| + \tilde{\phi}, & x < \phi, \end{cases} \quad (1.55)$$

where $x < 0$. As in the previous section, the potential can be viewed as an idealisation of a smooth potential where we have only retained the piecewise linear pieces.

We now discuss the asymptotically AdS_2 Euclidean saddles and their thermodynamic properties, while relegating the discussion with finite boundary to Appendix B. Here, we keep the slopes of each linear piece of $V(\phi)$ to have the same magnitude for the sake of simplicity. More generally, they can be taken to be different.

1.4.1 Geometry

The geometry is given by merging the interpolating geometry (1.38) to a second AdS_2 region in the deep interior at the distance $r = x$, as is shown in Figure 1.5. In the range $\tilde{\phi} < V(\phi) < \tilde{\phi} - 2x$, we therefore have three possible saddles which we label $\phi_1 < \phi_2 < 0 < \phi_3$. Outside of this range, the solution will only contain a stable AdS_2 black hole saddle if $\tilde{\phi} - 2x < V(\phi)$, or only the stable double interpolating geometry if $V(\phi) < \tilde{\phi}$.

Case 1: $\tilde{\phi} \geq 0$

The first saddle is for $r_1 < x$ and the metric for this system will have coefficients given by

$$N(r, r_1) = \begin{cases} (r - r_1)(r + r_1 + \tilde{\phi} - 4x), & \frac{4x - \tilde{\phi}}{2} \leq r_1 \leq r \leq x, \\ -r^2 + \tilde{\phi}r - 2x^2 + r_1(4x - r_1 - \tilde{\phi}), & x < r \leq 0, \\ r^2 + \tilde{\phi}r - 2x^2 + r_1(4x - r_1 - \tilde{\phi}), & 0 < r, \end{cases} \quad (1.56)$$

where the first condition on r_1 ensures that $V(r_1) \geq 0$. This describes a geometry which is AdS_2 in the deep interior, flowing to a piece of the Euclidean dS_2 static patch, and then flowing to another AdS_2 region near the boundary. The size of the static patch region is controlled by the two free parameters x and $\tilde{\phi}$.⁵

The second saddle has a Euclidean horizon located in the range $x \leq r_2 < 0$. This is the interpolating geometry described in Section 1.3 where the metric is precisely (1.38) with $r_D = r_2$. The final saddle has a Euclidean horizon located at $0 \leq r_3 \leq r$. For this range, the metric is (1.40) with $r_A = r_3$, which again is the AdS_2 saddle described in the previous section.

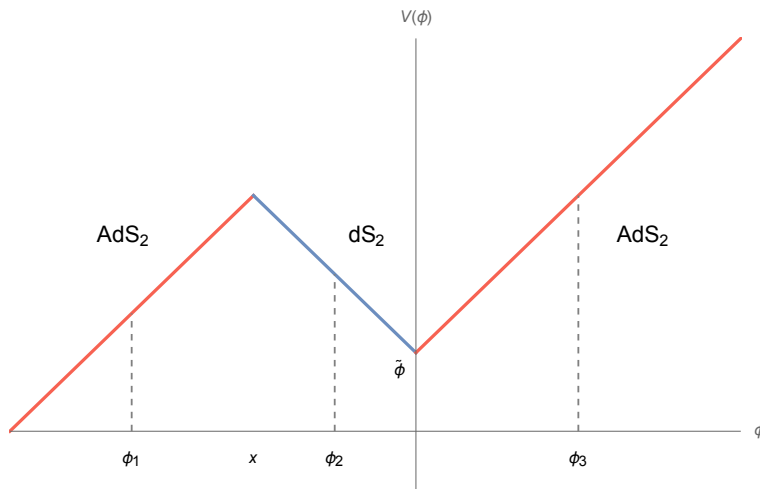


Figure 1.5: Plot showing the dilaton potential (1.55) with $\tilde{\phi} > 0$. This potential gives an AdS_2 geometry for $\phi \leq x$ and $\phi \geq 0$ but a dS_2 static patch in the region $x \leq \phi \leq 0$. At a given temperature, there may be up to three candidate black hole solutions.

Case 2: $\tilde{\phi} < 0$

In this case, the geometries are as above, but each saddle has an added restriction. Firstly, in order to have values of $r_h = r_1, r_2$ with $V(r_h) > 0$, we require $V(x) > 0$ such that $\tilde{\phi} > 2x$. This ensures that the lower bound on r_1 in (1.56) remains less than x when $\tilde{\phi} < 0$. To ensure the positivity of the metric (1.56) we must further have $4r_1(4x - \tilde{\phi} - r_1) > 8x^2 + \tilde{\phi}^2$. The restriction for the second saddle at r_2 is the same as in (1.43), namely $x \leq r_2 \leq \chi_+$ and for the third saddle at r_3 we have the same added restriction as in (1.42) that $|\tilde{\phi}|/2 \leq r_3$.

As for the interpolating solution with $\tilde{\phi} < 0$ discussed in the previous section, we can view

⁵By further adjusting the slopes of the linear pieces in $V(\phi)$, the AdS_2 in the deep interior can be made parametrically small.

the completion of the excised two-sphere as a way to push the stretched dS_2 horizon all the way to the near- AdS_2 boundary. This is shown in Figure 1.6. As we now explore, in the current setup the thermal stability properties are improved as compared to the previous case.

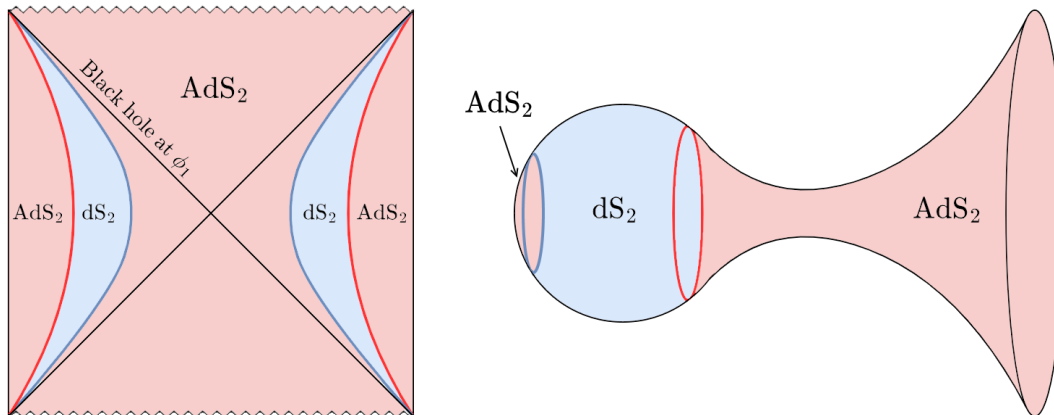


Figure 1.6: Left: Penrose diagram of the double interpolating geometry. Right: corresponding Euclidean geometry.

1.4.2 Thermodynamic properties

Let us introduce the notation $\phi_1 = r_1$, $\phi_2 = r_2$ and $\phi_3 = r_3$ as the values of the dilaton at each horizon. In what follows we will take $\phi_b \gg 1$ so that the boundary is asymptotically AdS_2 . The finite boundary case is treated in Appendix B. In this limit we can employ the asymptotic formulas (1.20). Along with these, in the large ϕ_b limit the difference in free energy of any two saddles ϕ_1 and ϕ_2 is given by [119]

$$\Delta F = F_2 - F_1 = \frac{1}{2\phi_b} [N(\phi_2, \phi_1) + V(\phi_1)(\phi_1 - \phi_2)]. \quad (1.57)$$

As $\phi_b \rightarrow \infty$, we have that $\beta_T \approx \beta\phi_b$, and so from the definition (1.11) we must also have $V(\phi_1) = V(\phi_2)$.

Case 1: $\tilde{\phi} \geq 0$

For $\phi_b \gg 1$ the first saddle at ϕ_1 will have heat capacity

$$C_1 = \pi(2\phi_1 + \tilde{\phi} - 4x), \quad (1.58)$$

which is positive due to the lower bound on r_1 in (1.56). As promised, this geometry has the benefit of being thermodynamically stable while also possessing an asymptotically AdS_2

boundary. The ground state with vanishing temperature is given by the configuration starting at the point $\phi_1 = 2x - \tilde{\phi}/2$ where the dilaton potential crosses the ϕ -axis.

The thermodynamic properties of the saddles at ϕ_2 and ϕ_3 were described in Section 1.3.2. For large ϕ_b , the saddle at ϕ_2 will have negative heat capacity (1.49) and hence will be thermodynamically unstable. The saddle at ϕ_3 will have heat capacity given by (1.47) and so will be thermodynamically stable. To see which saddle is thermodynamically favoured, we can use (1.57) with $V(\phi_1) = V(\phi_3)$, which leads to

$$\Delta F = F_3 - F_1 = \frac{x}{\phi_b} (2\phi_1 - 3x) . \quad (1.59)$$

This will be positive if $2\phi_1 < 3x$ and negative otherwise.

Thus, for temperatures satisfying $\beta > 4\pi/(\tilde{\phi} - x)$, the double interpolating solution containing a large portion described by Euclidean dS_2 dominates the thermodynamics in this model. Once β reaches the critical value $\beta = 4\pi/(\tilde{\phi} - x)$ we have a first order phase transition to the Euclidean AdS_2 black hole. In this case, the interpolating solution is metastable.

Case 2: $\tilde{\phi} < 0$

The model has two vanishing temperature configurations, one at $\phi_1 = 2x - \tilde{\phi}/2$, with x restricted to yield a positive metric, and the other at $\phi_3 = -\tilde{\phi}/2$. At finite temperature, the specific heat of the ϕ_1 saddle is (1.58) which remains positive. For $\phi_b \gg 1$, the saddle at ϕ_2 is again unstable and hence we again only have thermally stable saddles at ϕ_1 and ϕ_3 with their difference in free energies again given by (1.59).

Given that ΔF does not depend on $\tilde{\phi}$, the sign of $\tilde{\phi}$ will not affect which saddle dominates. Indeed, the model exhibits a first order phase transition at the critical temperature $\beta = 4\pi/(\tilde{\phi} - x)$ between a low temperature phase dominated by the double interpolating saddle, and a high temperature phase dominated by the Euclidean AdS_2 black hole.

To summarise, we have established the existence of dilaton-gravity models permitting locally (and even globally) thermally stable asymptotically near- AdS_2 geometries that encode a significant portion of the Euclidean dS_2 static patch in their interior. Slightly generalising the potential (1.55) to have different slopes in each linear regime, one can have asymptotically near- AdS_2 geometries that contain a stretched de Sitter horizon parametrically close to the actual cosmological dS_2 horizon. The geometries end at an AdS_2 black hole type horizon

with positive specific heat. Another way to stabilise the interpolating geometries in the deep interior might be to include an end-of-the-world brane, which would be interesting to explore.

1.5 Dual theory proposal

We have explored a variety of dilaton-gravity models whose solution space includes interpolating solutions containing a portion of the static patch of two-dimensional de Sitter space. In judiciously chosen circumstances, the stability properties of these geometries can be locally and even globally stable. In particular, the double interpolating solutions discussed in Section 1.4 have asymptotically near-AdS₂ solutions which contain a portion of the dS₂ static patch. Moreover, these solutions have positive specific heat and can be thermodynamically dominant over the AdS₂ black hole.

Given the presence of a near-AdS₂ boundary, one is tempted to investigate whether these models permit a microphysical realisation in terms of an AdS₂/CFT₁ type picture, or some other ultraviolet completion of dilaton-gravity. One such approach might be to consider the more general relation between dilaton-gravity models with general dilaton potential and matrix models [37, 85–87]. The challenge here is that the type of dilaton-potentials discussed in those works take a somewhat specific form

$$V_f(\phi) = 2\phi + \int_0^{2\pi} d\alpha f(\alpha) e^{-\alpha\phi}, \quad (1.60)$$

with $f(\alpha)$ small. Although it is suggested that the class of perturbative deformations in (1.60) might span to the larger class of holomorphic functions, $V_f(\phi)$ is subject to non-perturbative corrections. Whenever x is small and $\tilde{\phi}$ is positive, the potential (1.55), or a smoothed-out version, can be viewed as a perturbation $\delta V(\phi)$ of $V(\phi) = 2\phi$. So, provided that the deformed potentials (1.60) span a sufficiently large space of deformations, one might identify a corresponding matrix model. Employing the results of [85, 86], the corresponding eigenvalue distribution to linear order in the deformation (upon shifting ϕ such that $V_f(0) = 0$) reads

$$\rho(\lambda) = e^{S_0} \left(\frac{\sinh 2\pi\sqrt{\lambda}}{4\pi^2} + \frac{e^{2\pi\sqrt{\lambda}}\delta V(\sqrt{\lambda}) + e^{-2\pi\sqrt{\lambda}}\delta V(-\sqrt{\lambda})}{8\pi\sqrt{\lambda}} + \dots \right). \quad (1.61)$$

For the models we consider $\rho(\lambda)$ increases indefinitely, or at least up to some large cutoff, reflecting the near-AdS₂ boundary. For a closed Euclidean universe, as suggested by (1.61), perhaps one should take $\rho(\lambda)$ to fall back to a vanishing value [69, 126, 127], reflecting the presence of two horizons in dS₂ [27, 56]. It would be interesting to explore such matrix models

further.

More generally, one could ask whether the SYK model [128–130] permits deformations leading to theories such as (1.55). Since the vacuum is no longer pure AdS₂ in the interior, we expect that the SYK model is deformed by some relevant deformation. Relevant deformations are indeed permitted in SYK, and were explored in [67, 131] where flows between near-CFTs were identified. In particular, this was shown for the sum of two SYK Hamiltonians, $\hat{H}_{\text{tot}} = \hat{H}_q + s \hat{H}_{q/2}$, where

$$\hat{H}_q = i^{q/2} \sum_{i_1 \leq \dots \leq i_q \leq N} J_{i_1, \dots, i_q} \psi_{i_1} \dots \psi_{i_q}, \quad (1.62)$$

with J_{i_1, \dots, i_q} independently drawn from a suitable Gaussian ensemble, and ψ_i with $i = 1, \dots, N$ being Majorana fermions. Provided s is sufficiently small, \hat{H}_{tot} flows between two near-CFT regions. For the theory (1.55) we have an intermediate region of near-dS₂ between the two near-AdS₂ regions close to the boundary and in the deep interior. It is likely that this will require adding an additional term to \hat{H}_{tot} , with a coupling that may have to take complex values. We leave the exploration of such constructions for future work.

Chapter 2

Correlation functions in de Sitter space

In this chapter, we study scalar correlation functions in a fixed de Sitter background in order to characterise the behaviour of such functions in the presence of the cosmological horizon. In doing so, we resolve a puzzle stemming from the fact that such correlation functions can be expressed as a sum over geodesics lengths, and yet real geodesics do not exist between arbitrary points in de Sitter.

2.1 The scalar two-point function in de Sitter

Consider the action for a free massive scalar field in dS_d ,

$$S_\phi = -\frac{1}{2} \int d^d x \sqrt{-g} [g^{\mu\nu} \partial_\mu \phi \partial_\nu \phi + m^2 \phi^2] , \quad (2.1)$$

where m is the mass of the scalar field and $g_{\mu\nu}$ is the d -dimensional de Sitter metric. We will study the Wightman two-point function in the Bunch-Davies (or Euclidean) vacuum state $|E\rangle$ [97,98]. This is denoted $G(X, Y) = \langle E | \phi(X) \phi(Y) | E \rangle$, where X and Y are arbitrary points on global de Sitter. This two-point function is a solution to the Klein-Gordon equation in dS_d ,

$$(\square - m^2)G(X, Y) = 0 . \quad (2.2)$$

Given that the Euclidean state is invariant under the de Sitter isometries, the two-point function can only depend on X and Y through their de Sitter invariant length $P_{X,Y}$. This

quantity is defined in embedding space as

$$P_{X,Y} \equiv \frac{1}{\ell^2} \eta_{IJ} X^I Y^J, \quad \eta_{IJ} = \text{diag} \left(\overbrace{-1, 1, \dots, 1}^{d+1} \right). \quad (2.3)$$

Note that in this expression X and Y are the coordinates describing the embedding of the d -dimensional de Sitter hyperboloid inside $(d+1)$ -dimensional Minkowski space, as in (3). For instance, if we choose to parameterise the hyperboloid with the global coordinates in equation (5), the de Sitter invariant length is given by

$$P_{X,Y} = -\sinh T_X \sinh T_Y + \cosh T_X \cosh T_Y \sum_{i=1}^d \omega_X^i \omega_Y^i, \quad (2.4)$$

where ω^i are coordinates on the $(d-1)$ -sphere and obey $\sum_{i=1}^d (\omega^i)^2 = 1$. It is useful to note that [97]

$$P_{X,Y} \begin{cases} > 1, & \text{for timelike separated points;} \\ = 1, & \text{for coincident or null separated points;} \\ < 1, & \text{for spacelike points.} \end{cases}$$

Additionally, for spacelike points

$$P_{X,Y} \begin{cases} > -1, & \text{when } X \text{ is spacelike separated from the antipodal point of } Y; \\ = -1, & \text{when } X \text{ is null separated from the antipodal point of } Y; \\ < -1, & \text{when } X \text{ is timelike separated from the antipodal point of } Y. \end{cases}$$

Going back to the two-point function, if we write $G(X, Y) = G(P_{X,Y})$, then the Klein-Gordon equation becomes

$$(1 - P_{X,Y}^2) \partial_{P_{X,Y}}^2 G(P_{X,Y}) - d P_{X,Y} \partial_{P_{X,Y}} G(P_{X,Y}) - m^2 \ell^2 G(P_{X,Y}) = 0. \quad (2.5)$$

This hypergeometric equation has two linearly independent solutions:

$$G(P_{X,Y}) = A {}_2F_1 \left(h_+, h_-; \frac{d}{2}; \frac{1 + P_{X,Y}}{2} \right) + B {}_2F_1 \left(h_+, h_-; \frac{d}{2}; \frac{1 - P_{X,Y}}{2} \right), \quad (2.6)$$

where

$$h_{\pm} = \frac{(d-1)}{2} \pm \sqrt{\left(\frac{d-1}{2} \right)^2 - m^2 \ell^2}. \quad (2.7)$$

The second of these solutions is singular when $P_{X,Y} = -1$, corresponding to antipodal points. We do not expect to see this behaviour in the two-point function, and therefore choose to set $B = 0$. The first solution, on the other hand, diverges at $P_{X,Y} = 1$, which mimics the expected short-distance behaviour of the two-point function. In order to fix the overall coefficient, we must match this solution to the short distance singularity in flat space [97, 102, 132], which for $d > 2$ takes the form

$$G(P_{X,Y} \sim 1) \approx \frac{\Gamma\left(\frac{d}{2}\right)}{(2\pi)^{\frac{d}{2}} \ell^{d-2} (d-2)} \frac{1}{(1 - P_{X,Y})^{\frac{d}{2}-1}}, \quad (2.8)$$

and is independent of m . Note that for $d = 2$ the correlator diverges logarithmically as

$$G(P_{X,Y} \sim 1) \approx -\frac{1}{4\pi} \log(1 - P_{X,Y}), \quad (2.9)$$

which is consistent with the expected QFT behaviour. Near $P_{X,Y} = 1$, the hypergeometric function behaves as

$${}_2F_1\left(h_+, h_-; \frac{d}{2}; \frac{1 + P_{X,Y}}{2}\right) \approx \left(\frac{2}{1 - P_{X,Y}}\right)^{\frac{d}{2}-1} \frac{\Gamma\left(\frac{d}{2}\right)\Gamma\left(\frac{d-2}{2}\right)}{\Gamma(h_+)\Gamma(h_-)}. \quad (2.10)$$

Matching the expansion of (2.6) to equation (2.8) thus shows that the solution that correctly reproduces the expected short distance behaviour of the two-point function (and does not have singularities at antipodal points) is given by [95, 133, 134]

$$G(P_{X,Y}) = \frac{\Gamma(h_+)\Gamma(h_-)}{\ell^{d-2}(4\pi)^{d/2}\Gamma\left(\frac{d}{2}\right)} {}_2F_1\left(h_+, h_-; \frac{d}{2}; \frac{1 + P_{X,Y}}{2}\right). \quad (2.11)$$

Note that, by definition, this is also the two-point function obtained from analytically continuing the two-point function on S^d to Lorentzian de Sitter spacetime. We are interested in the large mass expansion of the above correlator. The asymptotic form of the hypergeometric function when some of the parameters are large is non-trivial. The expansion of interest in our case is the one where the first two parameters become large in the imaginary direction (and with opposite signs). Asymptotic expressions in this limit were first found in [135]. See also [136] for the latest state of affairs. The form of the correlator in the large mass limit is thus given by

$$G(P_{X,Y}) \approx \frac{m^{\frac{d-3}{2}}}{2(2\pi\ell)^{\frac{d-1}{2}}} \left[\frac{e^{-m\ell \arccos P_{X,Y}}}{(1 - P_{X,Y}^2)^{\frac{d-1}{4}}} + \frac{(-1)^{\frac{d-1}{2}} e^{-m\ell(2\pi - \arccos P_{X,Y})}}{(1 - P_{X,Y}^2)^{\frac{d-1}{4}}} \right], \quad (2.12)$$

where this asymptotic form is valid for all points satisfying

$$|1 - P_{X,Y}^2| \gtrsim (m\ell)^{-2}. \quad (2.13)$$

For $P_{X,Y} < -1$, the correlator is manifestly real, consistent with the fact that the points are spacelike separated, and in our conventions spacelike separated points have real length between them:

$$G(P_{X,Y}) \approx \frac{m^{\frac{d-3}{2}}}{(2\pi\ell)^{\frac{d-1}{2}}} \operatorname{Re} \left[\frac{e^{-m\ell \arccos P_{X,Y}}}{(1 - P_{X,Y}^2)^{\frac{d-1}{4}}} \right], \quad P_{X,Y} < -1. \quad (2.14)$$

When $P_{X,Y} > -1$, the second term in (2.12) is always exponentially suppressed in the large mass limit, so the correlator takes the form

$$G(P_{X,Y}) \approx \frac{m^{\frac{d-3}{2}}}{2(2\pi\ell)^{\frac{d-1}{2}}} \frac{\exp(-m\ell \arccos P_{X,Y})}{(1 - P_{X,Y}^2)^{\frac{d-1}{4}}}, \quad P_{X,Y} > -1. \quad (2.15)$$

For $-1 < P_{X,Y} < 1$, it is straightforward to check that the correlator is real. When points become timelike separated, then $P_{X,Y} > 1$ and the expression becomes manifestly complex, consistent with the fact that, in our conventions, timelike separated points have an imaginary length between them.

Both (2.14) and (2.15), can be obtained by solving the Klein-Gordon equation (2.5) in a WKB expansion, which provides an independent check of these asymptotic expansions; see Appendix C. It is clear that both approximations break down when $P_{X,Y} \sim \pm 1$. As previously stated, when $P_{X,Y}$ is close to one, the correlator is chosen to mimic the short distance singularity in flat space (2.8). When $P_{X,Y} = -1$, the last argument in the hypergeometric function is zero, so in the large mass limit we obtain

$$G(P_{X,Y} = -1) \approx \frac{m^{d-2}}{\Gamma(\frac{d}{2})2^{d-1}\pi^{\frac{d}{2}-1}} e^{-m\ell\pi}. \quad (2.16)$$

This limit does not commute with taking the large mass limit first.

2.2 The geodesic approximation

In the worldline formalism [89, 90], one can schematically compute $G(X, Y)$, the correlator of a free massive scalar field between two points X and Y , as a path integral,

$$G(X, Y) = \int D\mathcal{P} e^{-mL[\mathcal{P}]}, \quad (2.17)$$

where m is the mass of the scalar field, \mathcal{P} is a path connecting X and Y , and $L[\mathcal{P}]$ is the length of that path. In the large mass limit, it is possible to take a saddle point approximation that reduces the path integral to a sum over geodesic lengths L_g ,

$$G(X, Y) \approx \sum_{g \in \text{geodesics}} e^{-mL_g}. \quad (2.18)$$

If there is more than one geodesic, we need to sum over them appropriately. These discussions go back to the seminal work by Bekenstein and Parker [91]. See also [92, 93]. So far, we have obtained the two-point correlator in the large mass limit by finding the asymptotic form of the relevant hypergeometric function. The main purpose of this chapter is to reconcile these results with the expression coming from the geodesic approximation (2.18), even when real geodesics do not exist. We start by reviewing how to compute geodesics in de Sitter in cases where real geodesics do exist. For simplicity, we demonstrate this in $d = 2$, but the results can be generalised to higher dimensions.

2.2.1 Review of geodesics in dS_2

The global metric of dS_2 is given by,

$$\frac{ds^2}{\ell^2} = -dT^2 + \cosh^2 T d\varphi^2, \quad (2.19)$$

with $\varphi \sim \varphi + 2\pi$ and $T \in \mathbb{R}$. The length functional is given by

$$L = \int ds = \int d\lambda \mathcal{L}(T, \dot{T}, \varphi, \dot{\varphi}, \lambda) = \ell \int d\lambda \sqrt{(-\dot{T}^2 + \cosh^2 T \dot{\varphi}^2)}, \quad (2.20)$$

where the dots represent derivatives with respect to the parameter λ along the geodesic. We are working in a slightly unusual convention where timelike geodesics will have a complex length. Often the length functional is redefined to be real for timelike geodesics, but we wish to use the same definition for both timelike and spacelike separated points. The Lagrangian

\mathcal{L} does not depend explicitly on φ , so we can define the following conserved quantity

$$\frac{\partial \mathcal{L}}{\partial \dot{\varphi}} \equiv Q = \frac{\ell \dot{\varphi} \cosh^2 T}{\sqrt{-\dot{T}^2 + \cosh^2 T \dot{\varphi}^2}}. \quad (2.21)$$

Since the length functional is invariant under reparametrisation, we may select λ such that it is an affine parameter,

$$\mathcal{L}^2 = \left(\frac{ds}{d\lambda} \right)^2 = \pm 1 = \ell^2 (-\dot{T}^2 + \cosh^2 T \dot{\varphi}^2), \quad (2.22)$$

where the \pm depends on whether the geodesic is spacelike or timelike, respectively. The first order equations (2.21) and (2.22) can be integrated to find the trajectories of the geodesics, which read

$$\tan(\varphi + \tilde{\varphi}) = \pm \frac{Q \sinh T}{\sqrt{Q^2 - \ell^2 \cosh^2 T}}, \quad (2.23)$$

where $\tilde{\varphi}$ is a constant of integration which, as well as Q , can be determined by the choice of the endpoints of the geodesic. The \pm in (2.23) depends on whether $T(\phi)$ is taken to be an increasing or decreasing function. Choosing the first endpoint of the geodesic to be at (T_1, φ_0) and taking $T(\phi)$ to be increasing at this point, we obtain

$$\tilde{\varphi} = \arctan \left(\frac{Q \sinh T_1}{\sqrt{Q^2 - \ell^2 \cosh^2 T_1}} \right) - \varphi_0. \quad (2.24)$$

Timelike geodesics. First, we consider timelike separated points at a fixed angle. Requiring that the geodesic passes through the point (T_2, φ_0) implies $Q = 0$. The result is the equation of motion $\varphi = \varphi_0$, and using (2.20) we find that these geodesics have length

$$L_g = i\ell |T_2 - T_1|. \quad (2.25)$$

Spacelike geodesics. We will consider points at opposite sides of the spatial circle by taking the second endpoint to be $(T_2, \varphi_0 + \pi)$. Plugging this into (2.23), we find that for any Q we have $T_1 = \pm T_2$. However, only one of these solutions is smooth. To see this, it is useful to invert the geodesic trajectory (2.23) to find the two possibilities

$$T(\phi) = \pm \operatorname{arccosh} \sqrt{\frac{Q^2 \sec^2(\varphi + \tilde{\varphi})}{Q^2 + \ell^2 \tan^2(\varphi + \tilde{\varphi})}}. \quad (2.26)$$

Choosing the positive sign for the entire geodesic gives the corresponding trajectory for $T_1 = T_2 > 0$, and the negative sign gives the trajectory $T_1 = T_2 < 0$, but neither of these solutions are continuous in their first derivatives, and so we discount them. Requiring a smooth trajectory necessitates gluing the two trajectories at the turning point of the function, leading to $T_1 = -T_2$. We therefore recover the result that spacelike geodesics between the poles of de Sitter only exist between times T_1 and $-T_1$ as shown in figures 2.1(a) and 2.1(b). This was explored in the context of holographic complexity in [66]. There is a one parameter family of such geodesics labelled by $|Q| > \ell^2 \cosh T$, and using equation (2.20), we find that all of these geodesics have the same length, $L_g = \ell\pi$ [66, 137]. Note that this result is completely different from the AdS₂ black hole case, where geodesics exist for arbitrarily long times and their length grows linearly with time [138].

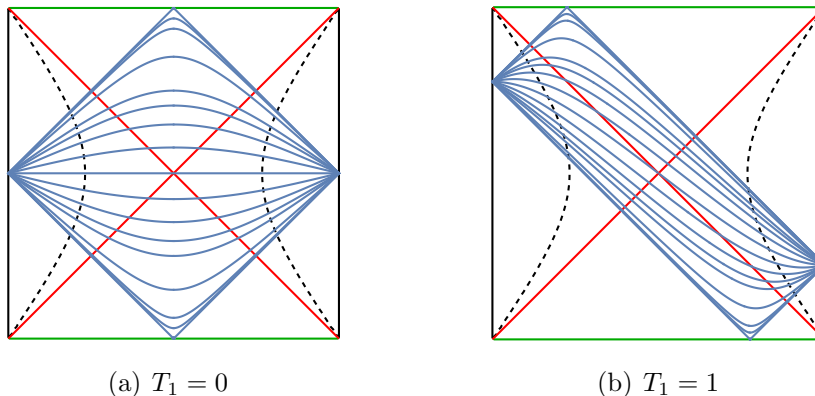


Figure 2.1: Penrose diagram for (half of) dS₂ with geodesics in blue, horizons in red, and past and future infinity in green. In dashed black, we also plot the position of stretched horizons.

2.2.2 From geodesics to two-point correlators

One would like to use the results obtained for the real geodesics in de Sitter to reproduce the form of the correlators studied in Section 2.1. However, it is clear from the result just shown for points on opposite sides of the spatial circle that real geodesics are not enough to reproduce the correlator for points such as $T_1 = T_2 \neq 0$, for example.

On the sphere geodesic distance between two points is given by $\ell \arccos P_{X,Y}$ with $P_{X,Y}$ defined similarly to (2.3) but with the metric replaced with the Euclidean one δ_{IJ} . Drawing inspiration from this, one can formally define $L_g = \ell \arccos P_{X,Y}$ to be the geodesic distance between the points X and Y in de Sitter. Timelike separated points have $P_{X,Y} > 1$, and for these points L_g reproduces the complex length (2.25). On the other hand, spacelike separated points have $P_{X,Y} < 1$, but real geodesics only exist for $-1 \leq P_{X,Y} < 1$. As an example,

consider points on opposite sides of the spatial circle, as in the previous section, for which $P_{X,Y} \leq -1$. Requiring L_g to be real then imposes that $P_{X,Y} = -1$. In this case, $L_g = \ell\pi$ in agreement with the result of the last section.

In terms of L_g , (2.12) becomes

$$G(L_g) \approx \frac{m^{\frac{d-3}{2}}}{2(2\pi\ell)^{\frac{d-1}{2}}} \left[\frac{e^{-mL_g}}{(\sin L_g)^{\frac{d-1}{2}}} + \frac{e^{-m(2\pi\ell-L_g)}}{(\sin(2\pi\ell-L_g))^{\frac{d-1}{2}}} \right]. \quad (2.27)$$

For any $P_{X,Y} > -1$, the second term is always exponentially suppressed, and so the propagator can be written in the form of the geodesic approximation (2.18). Moreover, we have seen that in those cases, the geodesic length is actually $L_g = \ell \arccos P_{X,Y}$, both for spacelike and timelike separated points. The only term that needs to be explained is the denominator, that will come from perturbations around the geodesic length.

If $P_{X,Y} < -1$, there seems to be more tension. In this case, we derived that there are no real geodesics connecting these points in de Sitter, and the naive continuation of L_g gives a complex geodesic length. Moreover, from the form of (2.27) it seems that there are two geodesics contributing to the correlator. As in the previous case, the denominator in each term needs to be explained. In the next section, we will show that the tension for $P_{X,Y} < -1$ can be cured by looking at geodesics on the sphere. In all cases, denominators will appear as one-loop corrections to the geodesic length.

Before moving on, let us comment on the special degenerate case of $P_{X,Y} = -1$. In this case, we showed that $L_g = \ell\pi$, which is consistent with $P_{X,Y} = -1$. But we found that there are infinitely many geodesics, which would naively yield an infinite correlator, unless properly regulated. Note also that equation (2.15) diverges in this limit, but that the correct large mass correlator is (2.16). In what follows, we will restrict to $P_{X,Y} \neq -1$.

2.3 Sphere two-point functions

In this section, we compute the two-point correlator on the sphere, where we know that any two points are connected by a geodesic with real (Euclidean) length. Considering the sphere is natural since, as we have seen previously, it is the Euclidean continuation of Lorentzian de Sitter spacetime. For simplicity, we will focus for now on two dimensions. Repeated here for

convenience, the round sphere metric (9) for $d = 2$ is

$$\frac{ds^2}{\ell^2} = d\theta^2 + \cos^2 \theta d\varphi^2, \quad (2.28)$$

where $\theta \in [-\pi/2, \pi/2]$ and $\varphi \sim \varphi + 2\pi$. It is known that, given two points on the sphere, there is always a great circle that passes through them. The great circle is defined by the intersection of the plane containing the two points and the origin with the sphere. The two segments of the great circle are geodesics connecting the two points.

It will be convenient to use a new set of coordinates $\{\Theta, \Phi\}$, where the Φ angle moves around the great circle between the two points, with $\Phi \in [0, 2\pi)$ and $\Theta \in [-\pi/2, \pi/2]$. The great circle lies at $\Theta = 0$. Note that you can always move to this coordinate frame for any two points X and Y on the sphere. The metric on this coordinate system is given by

$$\frac{ds^2}{\ell^2} = d\Theta^2 + \cos^2 \Theta d\Phi^2, \quad (2.29)$$

so the length functional becomes

$$\tilde{L}[\Phi_X, \Phi_Y, \Theta] = \ell \int_{\Phi_X}^{\Phi_Y} d\Phi \sqrt{\dot{\Theta}^2(\Phi) + \cos^2 \Theta(\Phi)}. \quad (2.30)$$

In this section, we use tildes to denote Euclidean quantities. We would like to compute the Euclidean two-point function on the sphere,

$$\tilde{\mathcal{G}}(\Phi_X, \Phi_Y) = \int_{\Theta(\Phi_X)=0}^{\Theta(\Phi_Y)=0} D\Theta(\Phi) \exp\left(-m\tilde{L}(\Phi_X, \Phi_Y, \Theta)\right), \quad (2.31)$$

using the geodesic approximation. We start by considering geodesics in $d = 2$ in Section 2.3.1. We then consider perturbations to the geodesic length in Section 2.3.2 and finally, we generalise our results to higher dimensions in Section 2.3.3.

2.3.1 Euclidean saddle points

In the large mass limit, (2.31) is dominated by its saddle points which are the geodesics connecting X and Y . To find these, we extremise the length (2.30). The equation of motion stemming from this length functional is

$$\ddot{\Theta} + 2\dot{\Theta}^2 \tan \Theta + \sin \Theta \cos \Theta = 0, \quad (2.32)$$

which is solved by

$$\Theta(\Phi) = \pm \arcsin \left[\frac{\sqrt{c_1 - 1} \tan(\Phi + c_2)}{\sqrt{1 + c_1 \tan^2(\Phi + c_2)}} \right], \quad (2.33)$$

where c_1 and c_2 are constants of integration. Boundary conditions at the endpoints of integration set $\Theta(\Phi_X) = \Theta(\Phi_Y) = 0$. A generic solution obeying the boundary conditions has $c_1 = 1$, reducing the solution to $\Theta_{\text{geodesic}} = 0$, *i.e.*, the geodesic goes through the great circle, as expected. Evaluating the action on-shell gives the length of the shorter geodesic,

$$\tilde{L}_g = \ell \int_{\Phi_X}^{\Phi_Y} d\Phi \sqrt{\dot{\Theta}_{\text{geodesic}}^2 + \cos^2 \Theta_{\text{geodesic}}} = (\Phi_Y - \Phi_X)\ell, \quad (2.34)$$

assuming, without loss of generality, that $0 < \Phi_Y - \Phi_X \leq \pi$. There is also another geodesic that goes around the other side of the great circle and has length

$$\tilde{L}_+ = \ell \int_{\Phi_Y}^{2\pi + \Phi_X} d\Phi \sqrt{\dot{\Theta}_{\text{geodesic}}^2 + \cos^2 \Theta_{\text{geodesic}}} = 2\pi\ell - (\Phi_Y - \Phi_X)\ell = 2\pi\ell - \tilde{L}_g. \quad (2.35)$$

Note that, generically, $\tilde{L}_g \leq \tilde{L}_+$, so only \tilde{L}_g will contribute to the Euclidean correlator in the large mass limit. However, as we will see in Section 2.4, we require both geodesics in certain cases to reproduce the correct Lorentzian correlator from analytic continuation of the Euclidean result.

There also exists another (infinite) set of geodesics that wrap multiple times around the great circle. Their lengths are given by $\pm\tilde{L}_g + 2\pi\ell n$ with $n \in \mathbb{N}$, and their contribution to the correlator will always be exponentially suppressed in the large mass expansion, even after analytic continuation to Lorentzian spacetime.¹

On the sphere, the only case where both \tilde{L}_g and \tilde{L}_+ will contribute corresponds to having $\Phi_Y - \Phi_X = \pi$. In this case, there is another set of solutions to (2.33) that satisfy the boundary conditions. These are a one-parameter family labelled by $c_1 \in \mathbb{R}^{\geq 1}$ and obtained by setting $c_2 = -\Phi_X$ in (2.33). These geodesics correspond to rotating the great circle around the sphere, while keeping Φ_Y and Φ_X fixed. Note that you can only do this when $\Phi_Y - \Phi_X = \pi$. The length of all these geodesics is the same and reads

$$\tilde{L}_g = \pi\ell, \quad (2.36)$$

independently of the choice of c_1 . In what follows, we will assume that $\Phi_Y - \Phi_X < \pi$.

¹With the exception of $-\tilde{L}_g + 2\pi\ell$, which is actually \tilde{L}_+ .

2.3.2 Quadratic perturbations

We have found geodesics that are saddle points of the Euclidean propagator (2.31). Now we can compute the corrections to the propagator stemming from quadratic perturbations to the geodesic length on the sphere. One-loop path integrals on the sphere have been computed in, for instance, [63, 64]. Recall that we are parameterising our paths as $\Theta(\Phi)$, so we want to consider perturbations to the geodesics of the form

$$\Theta(\Phi) = \Theta_{\text{geodesic}}(\Phi) + \delta\Theta(\Phi), \quad (2.37)$$

where the geodesic equation just gives $\Theta_{\text{geodesic}}(\Phi) = 0$. The variation of the Euclidean two-point function (2.31) is given by²

$$\tilde{\mathcal{G}}(\Phi_X, \Phi_Y) \approx \sum_{*=g,+} \left(e^{-m\tilde{L}_*(\Phi_X, \Phi_Y)} \int D\delta\Theta(\Phi) \exp \left(-m \delta\tilde{L}_*(\Phi_X, \Phi_Y, \delta\Theta, \delta\dot{\Theta}) \right) \right). \quad (2.38)$$

Evaluating the length functional (2.30) to second order around each geodesic, we obtain that,

$$\tilde{L}(\Phi_X, \Phi_Y, \delta\Theta) = \tilde{L}_*(\Phi_X, \Phi_Y) + \delta\tilde{L}_*(\Phi_X, \Phi_Y, \delta\Theta, \delta\dot{\Theta}), \quad (2.39)$$

with

$$\delta\tilde{L}_*(\Phi_X, \Phi_Y, \delta\Theta, \delta\dot{\Theta}) \equiv \frac{\ell}{2} \int d\Phi \left(\delta\dot{\Theta}(\Phi)^2 - \delta\Theta(\Phi)^2 \right), \quad (2.40)$$

where the integration limits in this integral depend on which geodesic we are expanding around and are the same as in equations (2.34) and (2.35). Given that $\delta\tilde{L}_*$ is quadratic in $\delta\Theta$, this path integral can be computed exactly. In general, consider the following quantum mechanical path integral,

$$Z(\Phi_0, \Phi_N) \equiv \int_{\delta\Theta(\Phi_0)=0}^{\delta\Theta(\Phi_N)=0} D\delta\Theta(\Phi) \exp \left(-\frac{m\ell}{2} \int_{\Phi_0}^{\Phi_N} d\Phi \left(\delta\dot{\Theta}^2 - \delta\Theta^2 \right) \right), \quad (2.41)$$

where the generic endpoints of the path integral are named Φ_0 and Φ_N , we assume $\Phi_N > \Phi_0$, and we require a vanishing variation of the trajectory at these points. In Appendix D, we show how to compute a more general class of quadratic path integrals in quantum mechanics,

²In principle, the measure in this path integral should include a factor of $\cos(\Theta)$ that comes from the determinant of the metric (2.29). The inclusion of this factor is needed for the path integral to be diffeomorphism invariant [91]. Note, however, that this term will not contribute to the path integral in the large mass expansion.

including this one. The final result is

$$Z(\Phi_0, \Phi_N) = \sqrt{\frac{m\ell}{2\pi \sin(\Phi_N - \Phi_0)}}. \quad (2.42)$$

Inserting this back into equation (2.38), we can write the correlator between any two points on the sphere, in the large mass limit, as a function of the geodesic length \tilde{L}_g between the two points. This yields,

$$\tilde{\mathcal{G}}(\tilde{L}_g) = \sqrt{\frac{m\ell}{2\pi \sin \tilde{L}_g}} e^{-m\tilde{L}_g} + \sqrt{\frac{m\ell}{2\pi \sin(2\pi\ell - \tilde{L}_g)}} e^{-m(2\pi\ell - \tilde{L}_g)}, \quad (2.43)$$

which looks suggestively similar to (2.27) with $d = 2$. We stress that this result is valid for any arbitrary two points on the sphere, as long as $\tilde{L}_g \gtrsim m^{-1}$ and $\pi\ell - \tilde{L}_g \gtrsim m^{-1}$. As previously mentioned, in Euclidean signature the second term in (2.43) will always be exponentially suppressed in the large mass limit. However, we will keep both saddle points, because interestingly, in some cases, after doing the analytic continuation back to Lorentzian signature, they will both contribute to the Lorentzian, large mass two-point correlator.

2.3.3 Generalising to higher dimensions

It is possible to extend the previous calculation on S^2 to higher dimensions. In this case, the analytic continuation of the global de Sitter metric is given by the round metric on S^d , equation (9). In any dimension, it is again true that geodesics between any two points are sections of the great circle connecting those two points. As in the case of two dimensions, it is convenient to rotate the coordinates to a frame where the Φ coordinate goes around the great circle between the two endpoints. We will call these coordinates $\{\Theta_1, \dots, \Theta_{d-1}, \Phi\}$. In this frame, the metric on S^d is given by

$$\frac{ds^2}{\ell^2} = d\Theta_1^2 + \cos^2 \Theta_1 d\Theta_2^2 + \cos^2 \Theta_1 \cos^2 \Theta_2 d\Theta_3^2 + \dots + \cos^2 \Theta_1 \cos^2 \Theta_2 \dots \cos^2 \Theta_{d-1} d\Phi^2, \quad (2.44)$$

so that the great circle lies at $\Theta_i = 0$. As in the two dimensional case, we can use Φ to parameterise the geodesic, which will follow a path $(\Theta_1(\Phi), \dots, \Theta_{d-1}(\Phi))$, that extremises the length functional,

$$\tilde{L} = \ell \int d\Phi \sqrt{\dot{\Theta}_1^2 + \cos^2 \Theta_1 \left(\dot{\Theta}_2^2 + \cos^2 \Theta_2 \dot{\Theta}_3^2 + \dots + \cos^2 \Theta_2 \dots \cos^2 \Theta_{d-1} \right)}. \quad (2.45)$$

In Appendix E, it is shown that the equations of motion imply that the saddle point is given by

$$\Theta_i^{(\text{geodesic})} = 0, \quad \text{for } 1 \leq i \leq d-1. \quad (2.46)$$

As in the case of two dimensions, this implies that there will be two geodesics leading the saddle point approximation. The one with minimal length is

$$\tilde{L}_g = \ell \int_{\Phi_X}^{\Phi_Y} d\Phi = (\Phi_Y - \Phi_X)\ell, \quad (2.47)$$

where again we assume that $0 < \Phi_Y - \Phi_X < \pi$. The other geodesic goes around the remainder of the great circle and has length

$$\tilde{L}_+ = \ell \int_{\Phi_Y}^{2\pi + \Phi_X} d\Phi = 2\pi\ell - (\Phi_Y - \Phi_X)\ell = 2\pi\ell - \tilde{L}_g. \quad (2.48)$$

The contributions from other geodesics that wrap around the great circle multiple times will be exponentially suppressed in the two-point function, so we neglect them. We can expand the length functional around each geodesic trajectory, $\Theta_i = 0 + \delta\Theta_i$, and this gives

$$\tilde{L} = \ell \int d\Phi \left(1 + \frac{1}{2} \sum_{i=1}^{d-1} (\delta\dot{\Theta}_i^2 - \delta\Theta_i^2) \right), \quad (2.49)$$

where each of the $(d-1)$ terms in the sum give the same contribution to the path integral, and this is exactly the same contribution as in the two-dimensional case. So, finally, we get that for most³ two points on the higher dimensional sphere, the Euclidean correlator in the large mass limit can be written as a function of the geodesic length between the two points. The Euclidean correlator, to this order, is given by

$$\tilde{\mathcal{G}}(\tilde{L}_g) = \left(\frac{m\ell}{2\pi \sin \tilde{L}_g} \right)^{\frac{d-1}{2}} e^{-m\tilde{L}_g} + \left(\frac{m\ell}{2\pi \sin(2\pi\ell - \tilde{L}_g)} \right)^{\frac{d-1}{2}} e^{-m(2\pi\ell - \tilde{L}_g)}. \quad (2.50)$$

2.4 Lorentzian two-point functions

We will now use the results of the last section to reproduce the Lorentzian two-point function for a free massive scalar field in the Euclidean state $|E\rangle$. For simplicity, let us consider $d = 2$. On the Euclidean sphere, the geodesic distance between any two points (θ_1, φ_1) and (θ_2, φ_2)

³The same restrictions as in the $d = 2$ case apply, *i.e.*, $\tilde{L}_g \gtrsim m^{-1}$ and $\pi\ell - \tilde{L}_g \gtrsim m^{-1}$.

is given by

$$\tilde{L}_g = \ell \arccos [\cos \theta_1 \cos \theta_2 \cos(\varphi_2 - \varphi_1) + \sin \theta_1 \sin \theta_2] . \quad (2.51)$$

Analytically continuing back to Lorentzian de Sitter space by taking $\theta \rightarrow iT$, we recover $L_g = \ell \arccos P_{X,Y}$, with $P_{X,Y}$ as in equation (2.4), even in the regime where Lorentzian geodesics do not exist. So it is straightforward to verify that Wick rotating (2.43) gives the large-mass expansion of the hypergeometric, up to a factor of $2m$. In fact, using (2.27) and (2.50), one can also verify that in higher d ,

$$\tilde{\mathcal{G}}(\tilde{L}_g) \Big|_{\theta \rightarrow iT} = 2m\ell^{d-1} G(L_g) . \quad (2.52)$$

The apparent tension in Section 2.2.2 is now resolved. For $P_{X,Y} < -1$, the complex nature of the Lorentzian geodesic length comes from analytic continuation of Euclidean geodesic lengths on the sphere. In this particular case, the Lorentzian geodesic length can be written as $L_g = \pi\ell - i\ell \operatorname{arccosh}|P_{X,Y}|$. The second saddle (corresponding to the Euclidean geodesic encircling the sphere from the opposite side) has length $2\pi\ell - L_g$ and so, in Lorentzian signature, they both have the same real part. Thus, neither of them can be neglected in the large mass limit. This explains the need for both terms in (2.27).

When $P_{X,Y} > -1$, it is always true that the second saddle is exponentially suppressed, as it will always have a larger real part than L_g , after analytically continuing back the Euclidean answer. For any $P_{X,Y}$, it is important to keep the next order correction to the saddle point answer in order to reproduce the large mass correlator. In the remainder of this section, we explore several choices of points that illustrate the different features of the correlator and the geodesics in the different regimes.

2.4.1 Timelike separated points

As a first example, consider a fixed point on the spatial S^{d-1} , at two different global times T_1 and T_2 . In this case, $P_{X,Y} = \cosh(T_2 - T_1) > 1$ and the relevant geodesics have a complex length $L_g = i\ell \operatorname{arccosh}|P_{X,Y}|$.

It follows from (2.15) that in the large mass limit the correlator is given by

$$G(P_{X,Y}) \approx \frac{m^{\frac{d-3}{2}}}{2^{\frac{d+1}{2}} (\pi\ell)^{\frac{d-1}{2}} \sinh^{\frac{d-1}{2}} |T_2 - T_1|} e^{-im|T_2 - T_1|} e^{-i\frac{\pi}{4}(d-1)} . \quad (2.53)$$

This correlator can be obtained from the geodesic approximation both in Lorentzian and in Euclidean signature. Given that L_g is purely imaginary, it is clear that the contribution coming from the geodesic with length $\tilde{L}_+ = 2\pi\ell - \tilde{L}_g$ will always have a larger real part when taken to Lorentzian signature, so it will be exponentially suppressed. To illustrate this case, consider the sphere for $d = 2$. We choose points with the same spatial angle $\varphi = \varphi_0$. On the sphere they will look as in Figure 2.2(a). The Euclidean geodesic length will be given by $\theta_Y - \theta_X$, with $\theta_Y > \theta_X$, and this is enough to reproduce (2.53) for $d = 2$.

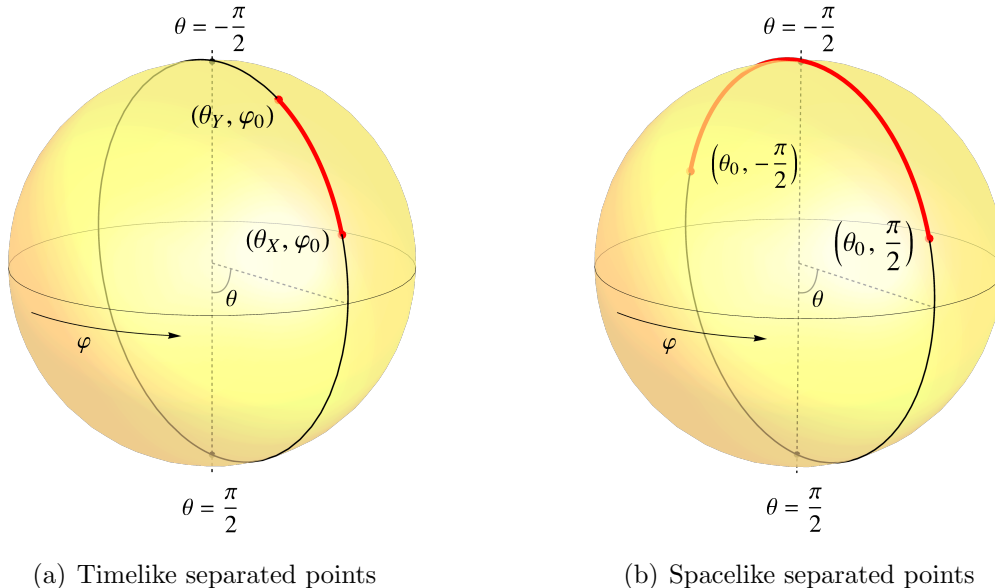


Figure 2.2: Upon analytic continuation to the Euclidean sphere, we look for two different types of geodesics, depending on the type of correlator under consideration. The geodesic with shorter length is shown in red, while the one going around the other side of the great circle is shown in black.

2.4.2 Spacelike separated points

Next, consider opposite points on the S^{d-1} at a given global time T . In this case, $P_{X,Y} = -\cosh 2T < -1$. In the large mass limit, it follows from equation (2.14) that,

$$G(P_{X,Y}) \approx \frac{m^{\frac{d-3}{2}}}{2^{\frac{d}{2}}(\pi\ell)^{\frac{d-1}{2}}} \frac{e^{-m\ell\pi}}{\sinh^{\frac{d-1}{2}} 2|T|} \left(\cos\left(2m\ell|T| - \frac{\pi d}{4}\right) - \sin\left(2m\ell|T| - \frac{\pi d}{4}\right) \right). \quad (2.54)$$

The correlator is real, but it oscillates with a frequency of $2m\ell$. Furthermore, it exponentially decays as a function of time and the decay rate does not depend on the mass. There do not exist real geodesics to account for this behaviour. This result for the two-point function was first found for $d = 2$ and $d = 4$ in [139] and [69], respectively.

Again, to illustrate this behaviour we focus on $d = 2$. On the sphere, it is natural to choose points opposite to each other at a given latitude $\theta = \theta_0$ (one at $\varphi = -\frac{\pi}{2}$ and the other one at $\varphi = \frac{\pi}{2}$), as in Figure 2.2(b). Then, the Euclidean geodesic lengths are given by

$$\tilde{L}_g(\theta_0) = (\pi - 2\theta_0)\ell, \quad \tilde{L}_+(\theta_0) = (\pi + 2\theta_0)\ell. \quad (2.55)$$

Note that, in this case, both will have the same real part when we analytically continue back to Lorentzian spacetime, and so neither can be neglected. Plugging this \tilde{L}_g into (2.43), it is straightforward to verify (2.52).

2.4.3 Spacelike separated points between stretched horizons

So far we have only considered points for which either $P_{X,Y} > 1$ or $P_{X,Y} < -1$. It is interesting to consider a case where $P_{X,Y}$ goes through the transition point $P_{X,Y} = -1$. A concrete example of this involves studying the form of the correlator between points anchored at opposite stretched horizons as a function of the static time; see Figure 2.3(a). For simplicity, we again restrict to $d = 2$. As discussed, all we need in order to find the correlator is $P_{X,Y}$ between these points. The stretched horizon r_{st} is defined as a constant r surface in the static patch metric (7). In order to get the position of the opposite stretched horizon, we need to relate static patch coordinates to global coordinates. Explicit expressions are shown in Appendix F.

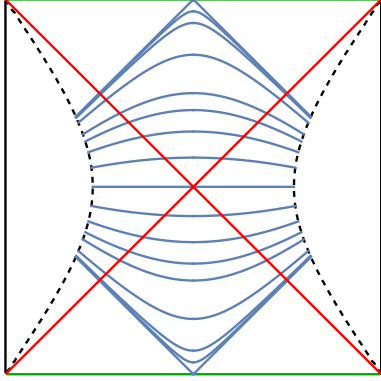
It is clear that opposite points on the Penrose diagram with a fixed $r = r_{st}$ will have the same T_0 and their angles will be at φ_0 and $-\varphi_0$. In this setup then, one point is at embedding coordinates X and the second one, Y , is at the same coordinates except for $Y_2 = -X_2$. This gives,

$$P_{X,Y}^{st} = \frac{1}{\ell^2} [-(X_0)^2 + (X_1)^2 - (X_2)^2] = (r_{st}^2 - 1) \cosh 2t + r_{st}^2. \quad (2.56)$$

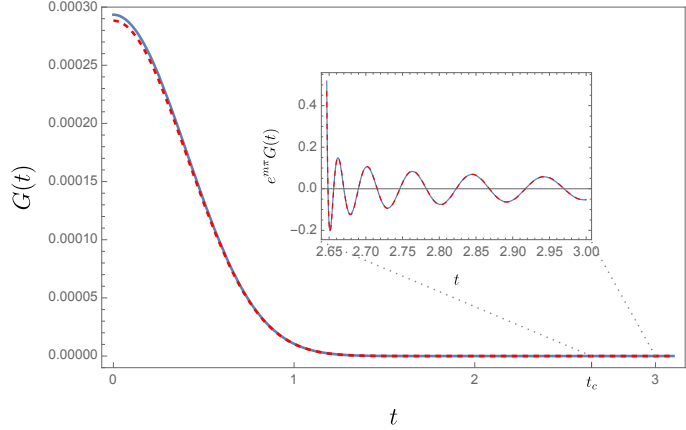
Note that $P_{X,Y}^{st} = -1$ at the critical time

$$t_c \equiv \frac{1}{2} \operatorname{arccosh} \left(\frac{1 + r_{st}^2}{1 - r_{st}^2} \right) = \frac{1}{2} \log \left(\frac{1 + r_{st}}{1 - r_{st}} \right). \quad (2.57)$$

For times between $0 < |t| < t_c$, the de Sitter invariant length has range $1 > P_{X,Y}^{st} > -1$, but for $|t| > t_c$, the range becomes $P_{X,Y}^{st} < -1$. The large mass correlator will then be given by (2.15) with $P_{X,Y}^{st}$ before t_c , and by (2.14), after. We plot the correlator in Figure 2.3(b). Before t_c the correlator decays monotonically, while afterwards it starts oscillating with frequency proportional to the mass. This differs from what happens to the correlator



(a) Penrose diagram



(b) Correlator

Figure 2.3: (a) Penrose diagram showing the geodesics (in blue) between two stretched horizons (in dashed black). The position of the stretched horizon is set to $r_{st} = 2/3$. (b) Exact (dashed red) and large mass (solid blue) correlator for two symmetric points on opposite stretched horizons as a function of the static patch time. At early times we observe a decay of the correlation function while at later times we observe an oscillatory behaviour. We multiply by $e^{m\pi}$ in the inset to make the oscillations apparent. In the plot, $m = 20$ and $r_{st} = 0.99$, so $t_c \sim 2.65$. Given the stretched horizon is very close to the actual horizon, at $t \sim 0$, the two points become very close to each other, and so the approximation breaks down.

for the black hole in AdS_2 , for which real geodesics exist at all times, and hence there is no oscillatory behaviour [66, 139]; see Figure 2.4(a).

We can easily obtain geodesics anchored at the stretched horizon by simply cutting parts of the geodesics obtained in Section 2.2.1. See Figure 2.3(a). Note that this breaks the degeneracy of geodesics at $T = 0$, and now there is at most one geodesic at each static time t . Their length is simply given by $L_g = \ell \arccos P_{X,Y}^{st}$, up to $|t| = t_c$. At these times, the last geodesics have length $L_g = \ell\pi$, as we are just removing two null pieces from the geodesics from Section 2.2.1 that have that same length.

After t_c , there are no more real geodesics. To find the complex geodesics, on the sphere we look for points at (θ_0, φ_0) and $(\theta_0, -\varphi_0)$. Using the geodesic length formula (2.51), we find that

$$\tilde{L}_g = \ell \arccos [\cos^2 \theta_0 \cos(2\varphi_0) + \sin^2 \theta_0] , \quad (2.58)$$

and for the longer geodesic, we have $\tilde{L}_+ = 2\pi\ell - \tilde{L}_g$. After analytic continuation, we can transform the global coordinates into static patch ones, and this Euclidean geodesic length recovers the Lorentzian two-point function, as in (2.52). For $|t| > t_c$, we do need the contri-

butions from both geodesics. It is interesting to note that the Euclidean length above works for both $P_{X,Y}^{st}$ smaller and larger than -1 , so it seems that the Euclidean computation does not know about t_c .

It is interesting to view these results from the perspective of the interpolating geometries that were introduced in Chapter 1. For such geometries, the presence of an asymptotic, timelike boundary permits us to interpret bulk correlators in terms of correlation functions of the boundary quantum mechanics. For heavy fields, we can employ a geodesic approximation to compute such correlators. In the two-sided geometries, the result is that geodesics between opposite boundaries only exist for a short period of time (of order of the inverse temperature), after which there are no more real geodesics [66, 139]. The last geodesic is almost null and goes all the way to the future (or past) infinity. This is reminiscent of what happens for the AdS double-sided black hole in dimensions higher than three. In that case, the singularity in the Penrose diagram bends inwards, and spacelike geodesics from the boundary are able to reach it [140, 141]. This is shown in Figure 2.4(b). However, the boundary correlator is not expected to have singularities of this type. The resolution is that there exist complex geodesics, whose contributions to the correlator are necessary to reproduce the correct answer for the boundary correlator. A similar story might hold for interpolating geometries where both the correlator and the geodesics can be computed in the bulk.

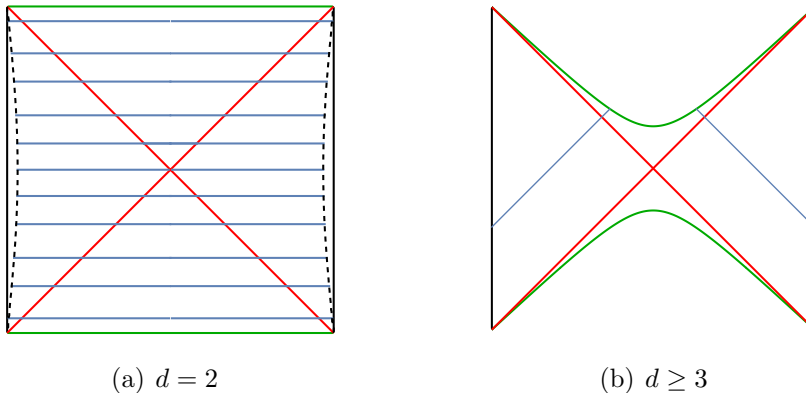


Figure 2.4: Penrose diagrams for an anti-de Sitter black hole in (a) $d = 2$ and in (b) $d \geq 3$. Geodesics are indicated in blue, horizons in red, and the singularities are in green. Figures adapted from those in [66].

One might worry that some of the effects shown here could be hard to observe, due to the exponential suppression in the large mass limit. However, the characteristic oscillations⁴ of

⁴As in the case of the AdS black hole [140, 142], these oscillations are probably related to the quasinormal mode frequencies of the cosmological horizon [143].

the two-point function will already be present for large separations in the exact correlator as soon as $m > (d-1)/2$. A harder question is whether there are signatures of the breakdown of the approximation in the exact correlator at $P_{X,Y} = -1$ in the large mass limit. As in [140], we see *subtle but distinct* signatures of this breakdown in the exact correlator that show up as an accumulation of zeroes near $P_{X,Y} = -1$ as we increase the mass; see Figure 2.5.

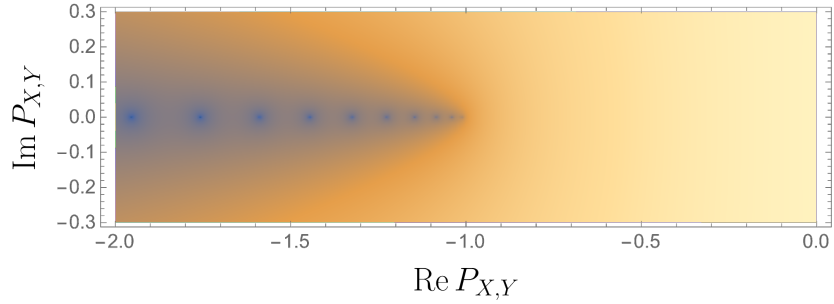


Figure 2.5: Density plot of $|G(P_{X,Y})|$ for $d = 4$ and $m = 25$. In the large- m limit zeroes (blue dots) accumulate near $P_{X,Y} = -1$.

Part II

Three spacetime dimensions

Introduction

Uncovering the microscopic origin of the cosmological horizon entropy is an important and intriguing pursuit. Essentially, one wishes to test the proposal of Gibbons and Hawking that the entropy is given by the logarithm of the Euclidean gravitational path integral, as in equation (12). The Euclidean path integral is somewhat of a black box - it seems to produce the correct answer for the horizon entropy, but how it does so is a bit mysterious given that we do not live in a Euclidean universe, but rather a Lorentzian one. Verifying the proposal, therefore, comes down to a search for an interpretation of this entropy in terms of a Hilbert space where we can count microstates explicitly, as this would constitute a more ‘Lorentzian’ picture of the thermodynamics. We have already noted that the sphere topology is the sensible saddle to compute the Euclidean gravitational path integral around, since both the global spacetime and the static patch metric Wick rotate to the round sphere metric. A more Lorentzian picture could be to consider quantum fields in a thermal density matrix within a single static patch. This can be achieved by placing them in a pure Hartle-Hawking state across the full S^{d-1} spatial slice at $T = 0$ and tracing out one of the two static patch regions. The Lorentzian topology that we will consider is therefore that of a single static patch, which is $D \times \mathbb{R}$ where D is a disc of appropriate dimension. This can be seen by taking constant time slices in the static patch metric (7). Thus, S^{d-1} timeslices in the global spacetime (6) get split into two static patch discs with a common S^{d-2} cosmological horizon.

In this part of the thesis, we conduct this search for a microscopic cosmological entropy in the context of three-dimensional gravity. The main reason we have chosen this setting is that three-dimensional gravity is semi-classically equivalent to a Chern-Simons gauge theory, where the choice of the gauge group determines the sign of the cosmological constant and the signature of the metric [34, 35]. This equivalence is beneficial as there already exists a plethora of results for Chern-Simons theory on both compact and bounded manifolds that will be useful for our purposes. For example, placing Chern-Simons theory on a manifold with a boundary, such as the $D \times \mathbb{R}$ topology of the static patch, induces an edge-mode theory at that boundary. One can also draw inspiration from literature on topological entanglement

entropy [58, 59, 144], which argues that upon quantising Chern-Simons theory on a spatial S^2 , dividing the space into two discs produces an entanglement entropy between the two regions. This entropy is given by the \mathcal{S}_0^0 component of the modular S -matrix \mathcal{S}_m^n of the edge-mode theory. Furthermore, as was shown in the seminal work [145], \mathcal{S}_0^0 also computes the partition function of Chern-Simons theory on an S^3 topology. One might therefore expect to see a match between the partition functions of the Euclidean theory evaluated on the three-sphere saddle and that of the edge-mode theory. However, the gauge group required to produce de Sitter in Lorentzian signature is $SL(2, \mathbb{C})$. Such complexified Chern-Simons theories have been the subject of various interesting works including [146–151]. The non-compact nature of this group makes it difficult to calculate the spectrum of the theory explicitly. We therefore tackle the problem by first considering the contributions to the thermodynamics of the cosmological horizon of massless Chern-Simons fields on a fixed de Sitter background. We proceed by studying analogous Abelian Chern-Simons theories that have a gauge group structure similar to that of the 3D gravity theory. For instance, for the Lorentzian theory we will take the gauge group to be $U_{\mathbb{C}}(1)$ to mimic the $SU_{\mathbb{C}}(2) \cong SL(2, \mathbb{C})$ of gravity. The possibility of using Chern-Simons theory to study three-dimensional gravity also appears in [103, 152–155].

In Chapter 3, we explore contributions from massless fields to the thermodynamic properties of the de Sitter horizon in three dimensions. In Section 3.1 we review and place several relevant results from the Chern-Simons literature into the context of three-dimensional de Sitter space. In Section 3.2 we describe in detail the relation between the edge-mode theory residing at the boundary of a spatial disc and the three-sphere partition function for Abelian Chern-Simons theory. The edge-mode theory introduced in this section serves as the basic template for the latter sections. In Section 3.3 we discuss an Abelian Chern-Simons theory with complexified $U(1)$ gauge group. This is meant to serve as an Abelian toy model for Lorentzian three-dimensional gravity expressed as a Chern-Simons theory with a complexified $SU(2)$ gauge group. In 3.4 we introduce an Abelian Chern-Simons theory with complexified level that is meant to act as a simplified toy model of Euclidean gravity expressed as a Chern-Simons theory with a complexified level. In Section 3.5 we briefly discuss how to extend the results of sections 3.3 and 3.4 to the non-Abelian case relevant to general relativity. In Section 3.6 we make some comments on AdS_4/CFT_3 in the case where AdS_4 has a three-dimensional de Sitter boundary. In Chapter 4, we consider a more general edge-mode theory to see whether specific boundary conditions may be able to tame the unboundedness that we saw in the original problem. Appendices G, H, and I provide further details on various computations presented in the main text of this section.

Chapter 3

Topological contributions to the de Sitter entropy

In three dimensions, for a theory of pure Einstein gravity with a positive cosmological constant $\Lambda = 1/\ell^2$, one has [63, 156–158]

$$\log \mathcal{Z}_{\text{grav}} = S_{\text{dS}} - 3 \log S_{\text{dS}} + 5 \log 2\pi + i\varphi_{\text{grav}} + \dots, \quad (3.1)$$

where $S_{\text{dS}} = \pi\ell/2G \gg 1$ is the tree-level Gibbons-Hawking entropy of the de Sitter horizon, which is parametrically large in the semiclassical limit. Unlike the leading term, the subleading terms in (3.1) stem from perturbative quantum corrections of the gravitational fluctuations. The logarithmic term is related to the residual $SO(4)$ subgroup of the diffeomorphism group preserved by the three-sphere saddle. The constant part is unambiguous in odd spacetime dimensions as it cannot be absorbed into a local counterterm, while the phase φ_{grav} can arise due to the unboundedness of the conformal mode. In the treatment of [159] one finds that $\varphi_{\text{grav}} = -5\pi/2$ to leading order at large S_{dS} . Although three-dimensional gravity carries no propagating degrees of freedom, the structure (3.1) is non-trivial, and a microscopic understanding is so far lacking (attempts include [160–164]).

Further corrections to (3.1) will appear as even inverse powers of S_{dS} . Upon coupling the theory to matter fields, the expansion (3.1) may receive additional contributions. Consider first matter fields that are parametrically heavy with respect to the de Sitter length ℓ . Integrating them out results in an effective gravitational theory that can be organised as a power series in the inverse mass, with coefficients that are functions of the metric [165]. In three dimensions these coefficients can only be built out of powers of the Ricci tensor. Since the mass is large, this theory will be perturbed, to high accuracy, by a local functional of the

metric containing higher derivative terms. Provided parity is preserved, due to the absence of local degrees of freedom in three-dimensional gravity, such a theory can always be brought back to an Einstein theory with a cosmological constant through local field redefinitions of the metric [63].¹ From this perspective, integrating out massless or light fields, or some more general conformal matter theory, is interesting in that one can affect the details of (3.1) which are of a more non-local nature. The two-dimensional version of this problem was recently explored in [121, 123]. In what follows we focus on the contribution to (3.1) from Chern-Simons gauge fields. These are massless gauge theories which are under solid theoretical control while producing various interesting modifications to (3.1). We will be interested in investigating the hypothesis that

$$\mathcal{Z}_{\text{grav}} \stackrel{?}{=} \lim_{\beta_T \rightarrow 0^+} Z_{\text{edge}}[\beta_T], \quad (3.2)$$

where β_T is the inverse Tolman temperature as defined in equation (1.12) and Z_{edge} is the thermal partition function of the proposed edge-mode theory, which is evaluated at high temperature due to the parametric proximity of the edge-modes to the de Sitter horizon. In this part of the thesis, we provide evidence that the subleading terms in equation (3.1) can be interpreted in terms of such edge-modes, but the interpretation of the leading term in terms of entanglement entropy of an edge-mode theory is left open.

As already mentioned, in much of what follows we will consider contributions to the thermal properties of a single static patch region from Chern-Simons and gravitational fields. With this in mind, we will repeat here the static patch metric. Here, it will be useful to make the coordinate transformation $r = \sin \rho$ in the static patch metric (7), which for $d = 3$ reads

$$\frac{ds^2}{\ell^2} = -\cos^2 \rho dt^2 + d\rho^2 + \sin^2 \rho d\varphi^2, \quad (3.3)$$

where $t \in \mathbb{R}$ and $0 \leq \rho \leq \pi/2$. The de Sitter horizon now resides at $\rho = \pi/2$ and has size $2\pi\ell$ in these coordinates. We note that the original global Cauchy surface at $T = 0$, which takes the form of a spatial S^2 , has been split into two discs whose common S^1 boundary comprises the dS_3 horizon. The induced metric on each disc at a constant t slice is given by

$$\frac{ds^2}{\ell^2} = d\rho^2 + \sin^2 \rho d\varphi^2. \quad (3.4)$$

¹Note that if the number of massive fields becomes large the coefficient of each term in the power series may be enhanced, and therefore this is only strictly true for a finite number of fields.

In three dimensions, the hypersurface (3) preserves an $SO(3, 1) \cong SL(2, \mathbb{C})/\mathbb{Z}_2$ subgroup of the Poincaré symmetries of $\mathbb{R}^{1,3}$, which constitutes the isometry group of dS_3 . As discussed in the introduction, analytically continuing equation (3) to Euclidean signature results in an S^3 embedded in \mathbb{R}^4 , and the isometries become $SO(4) \cong SU(2) \times SU(2)/\mathbb{Z}_2$. This reflects the fact that three-dimensional gravity with positive cosmological constant can be written as a combination of Chern-Simons theories with gauge group $SL(2, \mathbb{C})$ for Lorentzian signature and $SU(2) \times SU(2)$ for Euclidean signature.

Entanglement & gravitational entropy

It is generally a complicated problem to separate two regions of a gauge theory (including gravitational theories) in a strictly local way. In discussions of entanglement entropy for ordinary gauge theories there are various proposals for how to deal with the problem of the entangling surface [166–171]. For standard Yang-Mills theories, the possibilities are often labelled by a choice of ‘centre’ of the gauge invariant operator algebra. In Chern-Simons theories, which we will proceed to study, electric and magnetic fields do not commute. Consequently, it is not reasonable to classify choices in terms of electric and magnetic centres. Alternatively, [166, 168] one might extend the gauge invariant Hilbert space to admit non-trivial charges at the entangling surface. As overviewed in [171], the extended Hilbert space picture matches calculations of entanglement entropy employing Euclidean path integral techniques. Our considerations will be in line with this approach since we are interested in making contact with the manifestly gauge-invariant three-sphere partition function.

Consider Chern-Simons theory with gauge group \mathcal{G} and level k and whose three-sphere partition function we denote by $Z_{\mathcal{G}_k}[S^3]$. Although $Z_{\mathcal{G}_k}[S^3]$ is a manifestly gauge invariant object, it will be related to a Lorentzian edge-mode calculation, which we describe in sections 3.1 and 3.2, for which gauge invariance must be manifestly broken. Both the entanglement entropy of the edge-mode theory as well as $Z_{\mathcal{G}_k}[S^3]$ are ultraviolet divergent quantities. We will make sense [63] of the divergences of $Z_{\mathcal{G}_k}[S^3]$ by coupling the theory to three-dimensional gravity with cosmological constant $\Lambda = 1/\ell^2 > 0$, as in equation (14). The low energy effective theory in Euclidean signature is thus given by²

$$-S_E[g_{\mu\nu}, A_\mu] = \frac{1}{16\pi G} \int d^3x \sqrt{g} \left(R - \frac{2}{\ell^2} \right) + iS_{\text{CS}}[A_\mu], \quad (3.5)$$

²The Chern-Simons action (being insensitive to the metric) is insensitive to the signature and hence appears in the same form for both the Lorentzian and Euclidean path integral.

where $S_{\text{CS}}[A_\mu]$ is the Chern-Simons action. Unlike pure Chern-Simons theory, the above theory is no longer topological due to the explicit metric dependence in the gravitational sector. Here, we are distinguishing between a theory being topological, and a theory having no propagating degrees of freedom. These phrases are often used interchangeably but, specifically, we refer to a theory with no metric dependence as topological. When three-dimensional gravity is written as a Chern-Simons theory, the action depends explicitly on the metric through the gauge field. In this sense, the theory is no longer metric independent. The classical solution space for the metric remains that of three-dimensional gravity due to the metric independence of Chern-Simons theory. In three dimensions, this is nothing more than the round metric on the three-sphere or quotients thereof. The path integral of interest now becomes

$$\mathcal{Z}_{\text{grav+CS}} = Z_{\mathcal{G}_k}^{\text{reg}}[S^3] \times \mathcal{Z}_{\text{grav}}. \quad (3.6)$$

The pure gravitational path integral $\mathcal{Z}_{\text{grav}}$ is given by (3.1). Any ultraviolet divergences stemming from quantum fluctuations of the Chern-Simons sector can be absorbed into the cosmological constant Λ and Newton constant G , such that $Z_{\mathcal{G}_k}^{\text{reg}}[S^3]$ is the finite ultraviolet regularised part of the Chern-Simons partition function. The overall phase of $Z_{\mathcal{G}_k}^{\text{reg}}[S^3]$ is affected by the choice of framing and is given by $\varphi_{\text{CS}} = 2\pi n c_k / 24$ where c_k is the left-moving central charge of the WZW model with current algebra \mathcal{G}_k [145] — for $SU(2)_k$ this would be $c_k = 3k/(k+2)$ — and $n \in \mathbb{Z}$. We note that the total phase of $\mathcal{Z}_{\text{grav+CS}}$ is then given by

$$\varphi_{\text{grav+CS}} = \varphi_{\text{grav}} + \frac{2\pi n c_k}{24} + \dots \quad (3.7)$$

For the gravitational phase $\varphi_{\text{grav}} = -5\pi/2$ proposed in [159], special choices of n and k can lead to a vanishing $\varphi_{\text{grav+CS}}$ modulo 2π , at least to leading order in the large S_{dS} expansion.

At least for vanishing phase, $\log Z_{\mathcal{G}_k}^{\text{reg}}[S^3]$ can be viewed as a physical, ultraviolet finite correction to the tree-level Gibbons-Hawking de Sitter horizon entropy $S_{\text{dS}} = \pi\ell/2G$ [13]. So long as it is small compared to S_{dS} , there is no issue with the contribution to the entanglement entropy from the Chern-Simons sector being negative.

3.1 Chern-Simons theory on S^3 and dS_3

In this section, we consider Chern-Simons theory on the manifolds S^3 , $S^2 \times \mathbb{R}$, and $D \times \mathbb{R}$, where D denotes the two-dimensional disc. We frame the discussion in the language of Lorentzian and Euclidean three-dimensional de Sitter space. Chern-Simons theory with gauge

group \mathcal{G} and level $k \in \mathbb{Z}^+$ is described by the action

$$S_{\text{CS}}[A_\mu] = \frac{k}{4\pi} \int_M d^3x \varepsilon^{\mu\nu\rho} \text{Tr} \left(A_\mu \partial_\nu A_\rho + \frac{2}{3} A_\mu A_\nu A_\rho \right), \quad (3.8)$$

with $A_\mu = A_\mu^a T^a$, where T^a are the anti-Hermitian generators of \mathcal{G} satisfying the normalisation $\text{Tr}(T^a T^b) = -\frac{1}{2} \delta^{ab}$, and $a = 1, \dots, \dim \mathcal{G}$, while $\varepsilon^{\mu\nu\rho}$ is the Levi-Civita symbol. The non-Abelian field strength tensor is $F_{\mu\nu} = \partial_\mu A_\nu - \partial_\nu A_\mu + [A_\mu, A_\nu]$.

Our reason for studying Chern-Simons theories is threefold. Firstly, the topological nature of Chern-Simons theory ensures that all excitations have vanishing energy – all physics is ‘soft physics’. In particular, it contributes to the non-local structure of the de Sitter entropy (3.1). Secondly, we can draw from a host of exact results for Chern-Simons theory on compact manifolds, as well as on manifolds with boundaries. Both these features will prove to be particularly relevant to questions regarding de Sitter space. Thirdly, general relativity in three dimensions is equivalent, at least at the semiclassical level, to a Chern-Simons theory exhibiting certain unusual features such as a non-compact gauge group and/or a complexified value for the level [34, 35]. For now, we will steer clear of the third point, which we return to in Section 3.5, and focus on the first two.

3.1.1 Chern-Simons theory on S^3

We now consider the behaviour of Chern-Simons gauge fields on a fixed dS_3 or S^3 background. Pure Chern-Simons theory on a three-manifold \mathcal{M} will only perceive topological features, so one might wonder if there is any lesson to be learned specifically about de Sitter. Here, it is helpful to consider the more general setup whereby we couple Chern-Simons theory to three-dimensional gravity. The Lorentzian/Euclidean theory admits dS_3/S^3 solutions. Given that the metric is semiclassically fixed, the theory is no longer topological. In this context we can ask how the presence of a Chern-Simons gauge field contributes to the thermodynamic properties of the dS_3 horizon.

In the remainder of this section and the next our focus will be entirely on the case of a fixed background. We take the gauge group \mathcal{G} to be compact and semi-simple, and the level $k \in \mathbb{Z}^+$. Recall that Chern-Simons theory is topological, and hence only sensitive to the type of manifold on which it resides. From our discussion of the dS_3 geometry one is led to consider various three manifolds. These are S^3 , $S^2 \times \mathbb{R}$, and $D \times \mathbb{R}$.

Chern-Simons theory on S^3 . The first object we consider is the partition function of Chern-Simons theory on S^3 . Although naïvely this is nothing more than a number, and hence as good as our choice of normalisation, it turns out that Chern-Simons theory is sufficiently structured that one can make sense of this number in an essentially unambiguous way.³ The result [145] can be stated concisely in terms of the modular S -matrix \mathcal{S}_m^n associated to the WZW CFT with gauge group \mathcal{G} and level k , namely

$$Z_{\mathcal{G}_k}[S^3] = \mathcal{S}_0^0. \quad (3.9)$$

(An account of modular S -matrices and their properties can be found in the latter chapters of [172]. They encode the transformation of extended characters under inversion.) It should be emphasised that $Z_{\mathcal{G}_k}[S^3]$ is a gauge invariant object. As a concrete example, we can consider $\mathcal{G} = SU(5)$ for which

$$Z_{SU(5)_k}[S^3] = \frac{1}{\sqrt{5}(k+5)^2} \prod_{j=1}^4 \left[2 \sin \frac{\pi j}{k+5} \right]^{(5-j)}. \quad (3.10)$$

Notice that in the perturbative limit, where $k \rightarrow \infty$, the above expression is approximated by

$$\lim_{k \rightarrow \infty} Z_{SU(5)_k}[S^3] \approx \frac{9}{\pi^{14} 512 \sqrt{5}} \left(\frac{2\pi}{\sqrt{k+5}} \right)^{24}. \quad (3.11)$$

The above expression has some identifiable features. For instance the power of $\sqrt{k+5}$ corresponds to $\dim SU(5) = 24$. Whereas the numerical pre-factor is the reciprocal of the canonical group volume of $SU(5)$, given by (see for example [173, 174])

$$\text{vol } SU(N) = \frac{\sqrt{N} (2\pi)^{N(N+1)/2}}{2\pi G(N+1)}, \quad (3.12)$$

where $G(z)$ is the Barnes G -function. More generally, the large k limit of the sphere partition function of Chern-Simons theory with gauge group \mathcal{G} is given by

$$\lim_{k \rightarrow \infty} Z_{\mathcal{G}_k}[S^3] \approx \frac{1}{\text{vol } \mathcal{G}} \left(\frac{2\pi}{\sqrt{k+h}} \right)^{\dim \mathcal{G}}, \quad (3.13)$$

where h is the dual Coxeter number of \mathcal{G} . Schematically, we may view the above structure as stemming from the fact that the path integral requires division by the space of gauge transformations, of which all but the constant part are cancelled by redundancies in the

³There is an ambiguity in the overall phase of the S^3 partition function, which is fixed by a choice of framing. Unless otherwise stated, we will select a framing for which the overall phase vanishes.

local description of the theory. When a quantum field theory lives on a compact space, the constant part of a compact gauge group is finite and must be taken into account. Indeed, its contribution is responsible for the group theoretic factors exhibited by (3.13). The dependence on the level k is also sensible. The volume of the constant part of the gauge group must be normalised with respect to the size of the fluctuations of the theory, which are controlled by $1/\sqrt{k}$ in the perturbative limit. Such group theoretical factors have been recently explored in [63].

3.1.2 Chern-Simons on $S^2 \times \mathbb{R}$ and $D \times \mathbb{R}$

We now consider Chern-Simons theory on $S^2 \times \mathbb{R}$ and $D \times \mathbb{R}$. The first is topologically equivalent to the global geometry (6) of dS_3 , while the second is topologically equivalent to the static patch (3.3).

Chern-Simons theory on $S^2 \times \mathbb{R}$. We now proceed to consider Chern-Simons theory on $S^2 \times \mathbb{R}$. Here, we view \mathbb{R} as the global dS_3 time coordinate T , and the S^2 as the spatial Cauchy slice of global dS_3 . It is convenient to choose the following metric on S^2

$$ds^2 = \frac{4d\mathbf{x}^2}{(1 + \mathbf{x}^2)^2}, \quad \mathbf{x} = \{x, y\} \in \mathbb{R}^2. \quad (3.14)$$

We begin with a description of the Hilbert space. This is given by quantising the space of flat \mathcal{G} -connections on S^2 , modulo gauge transformations. But on $S^2 \times \mathbb{R}$, all flat connections are trivial. The Hilbert space is one-dimensional. The unique state of this peculiar world can be explicitly described in the Schrödinger picture. To describe it, it is convenient to work in the gauge $A_T = 0$. The gauge constraints that we must solve are then given by

$$F_{ij} = 0, \quad i, j \in \{x, y\}. \quad (3.15)$$

The following quantum state can be shown to solve the above equation [175]

$$\Psi_{S^2}[A_x(\mathbf{x})] = \mathcal{N} \exp \left\{ \left[\frac{ik}{4\pi} \text{Tr} \int_{S^2} d^2x [(g^{-1}\partial_x g)(g^{-1}\partial_y g)] - 2\pi ik \int_{S^2} d^2x w^0(g) \right] \right\}, \quad (3.16)$$

where \mathcal{N} is a normalisation constant, $g(\mathbf{x}) \in \mathcal{G}$, and w^0 is the time-component of the three-vector whose divergence gives the winding number density:

$$W(g) = \partial_\mu w^\mu = \frac{1}{24\pi^2} \text{Tr} \varepsilon^{\alpha\beta\gamma} (g^{-1}\partial_\alpha g g^{-1}\partial_\beta g g^{-1}\partial_\gamma g). \quad (3.17)$$

The gauge field is non-locally related to $g(\mathbf{x})$ as $A_x(\mathbf{x}) = g^{-1}\partial_x g$. Unlike what happens in standard Yang-Mills theory, the Chern-Simons wavefunctional $\Psi_{S^2}[A_x(\mathbf{x})]$ is not gauge invariant under the residual gauge freedom

$$A_i^h(\mathbf{x}) = h^{-1}(\partial_i + A_i(\mathbf{x}))h, \quad i \in \{x, y\}, \quad (3.18)$$

with $h(\mathbf{x}) \in \mathcal{G}$. Rather, under the residual gauge freedom $\Psi_{S^2}[A_x(\mathbf{x})]$ transforms as

$$\Psi_{S^2}[A_x(\mathbf{x})] = e^{2\pi i\alpha(A_x(\mathbf{x}); h)}\Psi_{S^2}[A_x(\mathbf{x})], \quad (3.19)$$

where

$$\alpha(A_x(\mathbf{x}); h) \equiv \frac{k}{8\pi^2} \text{Tr} \int d^2x [2A_x(\mathbf{x}) \partial_y h h^{-1} + h^{-1} \partial_x h h^{-1} \partial_y h] - k \int d^2x w^0(h). \quad (3.20)$$

As a function of the gauge field, the ground state $\Psi_{S^2}[A_x(\mathbf{x})]$ encodes non-local quantum correlations. The non-local correlations play an important role, for instance, if we are to trace out those degrees of freedom living in a certain spatial region. Our considerations of dS_3 suggest performing precisely such a trace if we are to consider the physics contained within a single dS_3 horizon, as depicted in Figure 3.1.

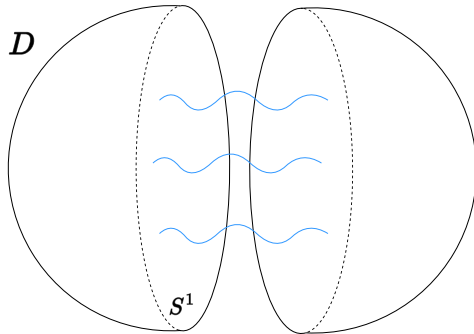


Figure 3.1: The $T = 0$ slice of global de Sitter split into two static patch hemispheres at the S^1 horizon. These hemispheres are topologically discs, and we can imagine ‘tracing out’ the degrees of freedom in one of the static patches that is behind the horizon of the other.

Chern-Simons theory on $D \times \mathbb{R}$. As already noted, the spatial section of a single static patch is given by the hemisphere metric on a two-dimensional disc D whose coordinates we denote by $\{\rho, \varphi\}$ with $\varphi \sim \varphi + 2\pi$. From this perspective, we are encouraged to consider the problem of Chern-Simons theory on $D \times \mathbb{R}$, where now \mathbb{R} is associated with the static patch time t . In this case, the Hilbert space of Chern-Simons theory is far richer [176] due to the presence of the spatial S^1 boundary.

We can construct the edge-mode theory as follows (see [177] for an overview). First, we must ensure that we have a well-defined variational problem in the presence of the S^1 boundary. We will not add further terms localised on the boundary $\partial\mathcal{M}$ of the disc. As such, the variational problem enforces us to impose boundary conditions on $\partial\mathcal{M}$:

$$(A_t - vA_\varphi)|_{\partial\mathcal{M}} = 0. \quad (3.21)$$

The parameter v is a real number which we take to be positive. We must further ensure that the gauge transformations do not disturb our boundary condition. This can be achieved by forcing the gauge parameter λ to vanish on the S^1 boundary. We can further impose (at least locally) that the gauge condition (3.21) holds away from the boundary of the disc as well. For that to be the case the bulk gauge parameter must satisfy

$$(\partial_t - v\partial_\varphi)\lambda = 0, \quad \lambda|_{S^1} = 0. \quad (3.22)$$

The above is solved by $\lambda = \bar{\lambda}(\varphi + vt, \rho)$ with $\bar{\lambda}|_{S^1} = 0$, which constitutes a residual gauge freedom. We can further specify a gauge fixing condition throughout the interior of the disc. The constraint arising from extending the gauge condition (3.21) into the disc interior is solved by the following configurations

$$A_\rho = U^{-1}\partial_\rho U, \quad A_\varphi = U^{-1}\partial_\varphi U, \quad (3.23)$$

with $U \in \mathcal{G}$. The residual gauge freedom transforms the group valued function $U \rightarrow e^{i\varepsilon\bar{\lambda}}U$, where ε is a small parameter. Consequently, the residual gauge parameter can be entirely fixed upon fixing the form of U . Unless otherwise specified, we impose that A_μ remains smooth throughout the interior of the disc. To do so, we must ensure that the holonomy of the gauge field vanishes around any closed loop in the interior of the disc. Non-vanishing holonomy would indicate the presence of external charge puncturing the disc. The resulting theory at the boundary of the disc, upon taking everything into account, becomes a chiral WZW model with group \mathcal{G} and level k built from the boundary values of U [176]. Upon quantisation, this theory has an infinite number of states. We now study the Abelian case in detail.

3.2 Abelian example

In this section, we construct and explore the edge-mode theory associated to Abelian Chern-Simons theory with gauge group $U(1)$ at level k quantised on a spatial disc D . The purpose of the section is to provide a detailed discussion of this edge-mode theory and its relation to the three-sphere partition function $Z_{U(1)_k}[S^3]$. This is meant to serve as the basic template for the discussion of edge-mode theories in the latter sections. The Abelian theory on a three-manifold \mathcal{M} is governed by the action

$$S_{U(1)_k}[A_\mu] = \frac{k}{4\pi} \int_{\mathcal{M}} d^3x \varepsilon^{\mu\nu\rho} A_\mu \partial_\nu A_\rho, \quad (3.24)$$

where A_μ is a real-valued Abelian gauge field. So long as the three-manifold \mathcal{M} has no boundary, the above is gauge invariant under $A_\mu \rightarrow A_\mu - \partial_\mu \lambda$, where λ is a smooth function on \mathcal{M} . If it is further assumed that $U(1)$ is compact, and moreover that $S_{U(1)_k}$ is the low energy limit of a theory containing both electric and magnetic monopoles, then the standard Dirac argument enforces $k \in \mathbb{Z}$. For the sake of simplicity, we take $k \in 2 \times \mathbb{Z}^+$ in what follows.⁴

3.2.1 Three-sphere partition function

We begin by computing the S^3 partition function. We have

$$Z_{U(1)_k}[S^3] = (\text{vol } \mathcal{G})^{-1} \int \mathcal{D}A_\mu e^{iS_{U(1)_k}[A_\mu]}, \quad (3.25)$$

where we have manifestly divided by the volume of the gauge group, which is generated by the space of smooth real functions on S^3 . Given that S^3 is compact, we must also consider the constant part of the gauge group which is generated by the constant function λ_c on S^3 . We take the group elements generated by λ_c to be given by

$$U(\lambda_c) = e^{i\lambda_c}, \quad (3.26)$$

such that λ_c is compact with radius 2π . It is convenient to rescale the gauge field by $\sqrt{2\pi/k}$, to remove the k dependence from the action. In doing so, we change the volume of the constant part of the gauge group to $\sqrt{2\pi k}$. Whenever we evaluate path integrals, we will assume this normalisation for the action. To get a feel for the structure of the result [178],

⁴This is, in part, to avoid subtleties associated to fermionic states in the edge-mode theory.

we can parameterise A_μ as

$$A_\mu = A_\mu^T + \partial_\mu \mathcal{B}, \quad \nabla^\mu A_\mu^T = 0, \quad (3.27)$$

where we exclude the constant part of the scalar field \mathcal{B} as it does not contribute to the configuration space of the A_μ . We thus find

$$Z_{U(1)_k}[S^3] = (\text{vol } \mathcal{G})^{-1} \times \sqrt{\det'(-\nabla^2)} \times \int \mathcal{D}'\mathcal{B} \int \mathcal{D}A_\mu^T e^{iS_{U(1)_k}[A_\mu^T]}. \quad (3.28)$$

The prime indicates we are dropping the zero-mode. Although the above expression is still rather schematic, one can already note that the path-integral over \mathcal{B} will mostly cancel the volume of \mathcal{G} . The difference lies in the zero-mode sector which is absent in the space of functions \mathcal{B} . Since no other term in the partition function depends on k , we can already conclude that

$$Z_{U(1)_k}[S^3] \propto \sqrt{\frac{1}{k}}. \quad (3.29)$$

We now fix the remaining proportionality constant. One way to do so involves calculating and regularising the divergent functional determinants stemming from the Gaussian path integral. Generally speaking, a local quantum field theory in three dimensions on a compact space with metric $g_{\mu\nu}$ will have a partition function of the form

$$\log Z[g_{\mu\nu}] = c_0 \ell_{\text{uv}}^{-3} \int d^3x \sqrt{g} + c_1 \ell_{\text{uv}}^{-1} \int d^3x \sqrt{g} R + \text{finite}, \quad (3.30)$$

where ℓ_{uv} is an ultraviolet length scale. The finite piece will encode some non-local functional of $g_{\mu\nu}$. If the theory is not parity invariant, as is the case for Chern-Simons theory, one will generally have a local contribution proportional to the gravitational Chern-Simons term contributing to the Λ -independent part. In certain circumstances, due to the presence of additional symmetries or structures, such as supersymmetry, some of the divergences can be argued to be absent. As we discuss in Appendix G, applying the Fadeev-Popov procedure in the Lorenz gauge to the Abelian Chern-Simons theory yields the following contribution to the sphere partition function

$$Z_{U(1)_k}[S_3] = e^{i\varphi_{\text{CS}}} (\text{vol } S^3 \ell_{\text{uv}}^{-3})^{-1/2} \sqrt{\frac{1}{k}} \times \frac{(\det'(-\nabla^2/\ell_{\text{uv}}^{-2}))^{1/2}}{(\det LL^\dagger/\ell_{\text{uv}}^{-2})^{1/4}}, \quad (3.31)$$

where L is the operator $i\varepsilon^{\mu\nu\rho}\partial_\rho$ acting on the space of transverse vector fields, and the numerator stems from path integration over the ghost fields. The prime in the determinant means we are omitting any zero modes, which must be dealt with separately. Any of the

local ultraviolet divergences in (3.30) come from evaluating the functional determinants in (3.31).

To assess the nature to the leading cubic divergence, it is sufficient to consider the problem on \mathbb{R}^3 (or a large enough box). In this case the spectra are straightforward to obtain, and one finds that the eigenvalues of both LL^\dagger and $-\nabla^2$ are given by $\mathbf{k} \cdot \mathbf{k}$ with LL^\dagger having twice the multiplicity due to the two polarisations of A_μ^T . Consequently, at least the absolute value of $Z_{U(1)_k}[S_3]$ is free of cubic ultraviolet divergences. This resonates well with the absence of local degrees of freedom in Chern-Simons theory. So far, our arguments do not suffice to conclude anything about the linear divergence of $Z_{U(1)_k}[S_3]$. As we discuss in Appendix G, a linear divergence is indeed present in the heat kernel regularisation scheme. We find

$$|Z_{U(1)_k}[S^3]| = \sqrt{\frac{1}{k}} e^{-\frac{3\pi}{4\varepsilon}}, \quad \varepsilon \equiv \frac{2e^{-\gamma}\ell_{\text{uv}}}{\ell}. \quad (3.32)$$

The phase φ_{CS} of $Z_{U(1)_k}[S_3]$ requires a careful treatment. We can heuristically argue that it will not contribute to the cubic divergence either. Indeed, given that the phase is associated to the parity non-invariance of the theory, we might expect any associated divergence to also be parity non-invariant such as the gravitational Chern-Simons term.⁵

A more sophisticated approach to compute the sphere partition function, and its phase, follows [145]. Since this approach will be of use more generally, we now discuss it. Consider two solid tori, $\mathbf{T}_L^2 = D_L \times S^1$ and $\mathbf{T}_R^2 = D_R \times S^1$, with boundary tori T_L^2 and T_R^2 . If we glue these together by identifying the points on T_L^2 with those on an oppositely oriented T_R^2 , we obtain an $S^2 \times S^1$. The partition function $Z_{\mathcal{G}_k}[S^2 \times S^1]$ counts the number of states of Chern-Simons theory with gauge group \mathcal{G} at level k quantised on a spatial S^2 , that is to say

$$Z_{\mathcal{G}_k}[S^2 \times S^1] \equiv 1. \quad (3.33)$$

That the above equation holds, regardless of the gauge group and level (so long as there are no punctures on the S^2) is simply the statement that Chern-Simons theory on a spatial S^2 has a unique state in its Hilbert space. What is perhaps less immediate is that by identifying the points on T_L^2 with a particular modular transformation τ_R of the points on T_R^2 , we instead get an S^3 . This is true for a variety of τ_R . For our immediate purpose we will consider an

⁵Alternatively, we could consider adding two Chern-Simons terms with equal and opposite level and regularise in such a way that the phase of the sphere partition function vanishes.

inversion $\tilde{\tau}_R = -1/\tau_R$. Finally, we must now take into account the general relation

$$Z_{\mathcal{G}_k}[\tilde{\mathbf{T}}^2] = \mathcal{S}_0^0 \times Z_{\mathcal{G}_k}[\mathbf{T}^2], \quad (3.34)$$

where $\tilde{\mathbf{T}}^2$ is a solid torus, whose boundary is given by that of \mathbf{T}^2 upon performing the inversion $\tilde{\tau} = -1/\tau$. The above formula follows from a careful consideration of the solid torus Hilbert space [145], but we will not attempt to derive it here. If we can view the partition functions on the left- and right-hand sides of (3.34) as quantum wavefunctions in the Hilbert space of the theory quantised on a spatial T^2 , we can take an inner product of both sides with the state on the right hand side to get

$$Z_{U(1)_k}[S^3] = \mathcal{S}_0^0 \times Z_{U(1)_k}[S^2 \times S^1]. \quad (3.35)$$

Using the modular S -matrix for $U(1)_k$, it is concluded that

$$Z_{U(1)_k}[S^3] = \sqrt{\frac{1}{k}}. \quad (3.36)$$

In such a way, we can fix the overall constant and phase in (3.28). We now proceed to consider the above expressions from the perspective of the theory quantised on a spatial disc.

3.2.2 Classical edge-mode theory

Quantisation of Chern-Simons theory on a spatial disc requires a careful consideration of boundary conditions on the S^1 boundary. As already mentioned, a well-posed variational problem with Dirichlet conditions on the gauge field enforces the boundary condition (3.21). Imposing this condition throughout the remainder of space fixes our gauge entirely. The resulting constraints impose that the spatial components of the gauge field take the following form

$$A_\rho = i e^{i\Xi(t,\varphi,\rho)} \partial_\rho e^{-i\Xi(t,\varphi,\rho)}, \quad A_\varphi = i e^{i\Xi(t,\varphi,\rho)} \partial_\varphi e^{-i\Xi(t,\varphi,\rho)}, \quad (3.37)$$

where we recall that $\rho \in [0, \pi/2]$ and $\varphi \sim \varphi + 2\pi$ are coordinates on the disc (3.4). The edge-mode theory residing at the boundary of the disc where $\rho = \pi/2$ in the case of $\mathcal{G} = U(1)$ is described by the Floreanini-Jackiw action [179]

$$S_{\text{edge}} = \frac{k}{4\pi} \int dt d\varphi \partial_\varphi \zeta (\partial_t - v \partial_\varphi) \zeta, \quad (3.38)$$

where the field $\zeta(t, \varphi) = \Xi(t, \varphi, \rho)|_{\rho=\pi/2}$ is a compact scalar field with periodicity $\zeta \sim \zeta + 2\pi$ mapping $\mathbb{R} \times S^1 \rightarrow S^1$. The above theory is that of a compact chiral boson. Classically, the

solution space is given by

$$\zeta(t, \varphi) = g(\varphi + vt) + m\varphi + f(t). \quad (3.39)$$

The first term corresponds to a chiral excitation moving at angular velocity v [180]. The second term, which arises due to the compactness of ζ , provides a winding number $m \in \mathbb{Z}$ counting the number of times ζ wraps around the spatial S^1 . The third term does not contribute to the classical energy of the solution, as can be seen from the classical Hamiltonian

$$H = \frac{kv}{4\pi} \int d\varphi (\partial_\varphi \zeta)^2. \quad (3.40)$$

As can be seen from (3.37), $f(t)$ carries no physical information and can be dropped all together. The global $U(1)$ symmetry of the edge-mode theory corresponds to shifts of ζ (modulo integer multiples of 2π), and is generated by the following charge

$$\mathcal{Q} = \int \frac{d\varphi}{2\pi} \partial_\varphi \zeta. \quad (3.41)$$

It is convenient to expand the non-winding mode sector in a Fourier expansion

$$\zeta(t, \varphi) = \frac{1}{\sqrt{2\pi}} \sum_{n \in \mathbb{Z}^+} (\alpha_n(t) e^{-in\varphi} + \bar{\alpha}_n(t) e^{in\varphi}). \quad (3.42)$$

3.2.3 Quantum edge-mode theory

Upon quantisation, the complex functions $\alpha_n(t)$ are promoted to operators satisfying the equal-time commutation relations

$$[\hat{\alpha}_n, \hat{\alpha}_m] = [\hat{\alpha}_n^\dagger, \hat{\alpha}_m^\dagger] = 0, \quad [\hat{\alpha}_n, \hat{\alpha}_m^\dagger] = \frac{2\pi}{kn} \delta_{m,n}. \quad (3.43)$$

To derive the above, we should keep in mind that this problem involves a constrained phase space. It follows from the commutation relations (3.43) that the edge-mode theory contains a level k $\mathfrak{u}(1)$ Kac-Moody algebra. The periodicity $\zeta \sim \zeta + 2\pi$ leads us to consider the vertex operators

$$\hat{\mathcal{O}}_n = : e^{in\hat{\zeta}} :, \quad n = 1, 2, \dots, k-1. \quad (3.44)$$

Acting with the $\hat{\mathcal{O}}_n$ inserts a timelike Wilson line piercing the interior of the disc. The operator carries fractional charge $\mathcal{Q}_n = n/k$ under the $U(1)$ shift symmetry (3.41) of the edge-mode theory. We view such anyonic insertions as external data to the edge-mode theory, and consequently not part of the edge-mode Hilbert space. For $n = mk$, with $m \in \mathbb{Z}$, the

above operators are no longer singular in the disc interior. Indeed, the closed-loop integral $\oint A_\varphi d\varphi$ from a single winding mode evaluates to $2\pi m$. Instead, for $n = mk$ these correspond to winding mode excitations which indeed reside in the edge-mode Hilbert space.

The quantum Hamiltonian for a given winding sector m is given by

$$\hat{H}_m = k v \frac{m^2}{2} \hat{\mathbb{I}}_m + \frac{vk}{2\pi} \sum_{n \in \mathbb{Z}^+} n^2 \hat{\alpha}_n^\dagger \hat{\alpha}_n, \quad (3.45)$$

where $\hat{\mathbb{I}}_m$ is the identify operator in a given winding sector. The ground state is given by the state carrying vanishing winding and annihilated by all the $\hat{\alpha}_n$. In a given winding sector the eigenstates of the Hamiltonian are given by

$$|n_1, d_1; n_2, d_2; \dots, n_p, d_p\rangle_m = \prod_{i=1}^p \sqrt{\frac{1}{d_i!} \left(\frac{kn_i}{2\pi}\right)^{d_i}} (\hat{\alpha}_{n_i}^\dagger)^{d_i} |0\rangle, \quad d_i, p \in \mathbb{N}, \quad (3.46)$$

and their corresponding energy is

$$E_{\{n_i, d_i\}; m} = k v \frac{m^2}{2} - v \left(\epsilon_0 + \frac{1}{24} \right) + v \sum_{i=1}^p d_i n_i. \quad (3.47)$$

The degeneracy of those states for fixed $\sum_i d_i n_i = N$ is given by the integer partition number $p(N)$. We have allowed for an overall shift in the energy $v\epsilon_0$ to account for normal ordering ambiguities. The thermal partition function of the edge-mode theory is thus given by

$$Z_{\text{edge}}[\beta_T] = \text{tr} e^{-\beta_T \hat{H}} = q^{-\epsilon_0} \times \frac{\vartheta_3(0, q^{k/2})}{\eta(q)}, \quad (3.48)$$

where $q = e^{-v\beta_T}$, and $\vartheta_3(0, q)$ is the elliptic theta function

$$\vartheta_3(z, q) \equiv \sum_{n \in \mathbb{Z}} q^{n^2} e^{2niz}. \quad (3.49)$$

In the coordinates (3.3), the inverse Tolamn temperature is $\beta_T = 2\pi \cos \rho$. Equation (3.48) is reproduced from the perspective of a Euclidean partition function in Appendix H.

We now imagine that our edge-modes are located parametrically close to the dS_3 horizon. One might argue, in such a case, that the edge-mode theory should be placed at a parametrically high temperature (in units measured by the inertial clock at $\rho = 0$). Let us discuss this from a Euclidean perspective. Recall that Euclidean continuation of the de Sitter horizon

becomes a circle in S^3 . Removing a small region near the horizon corresponds to excising a thin solid torus \mathbf{T}^2 from the S^3 , as shown in Figure 3.2. The two cycles of the boundary of \mathbf{T}^2 correspond to a spatial cycle and a thermal cycle. As we take the region to vanishing size, the size of the thermal cycle shrinks to zero, which is the Euclidean picture of a high temperature limit. This is, to some extent, similar to the brick-wall regularisation considered by 't Hooft [181] (see also [182–184]). Thus, to make contact with the dS_3 picture, we would like to study the edge-mode theory (3.38) at high temperature.

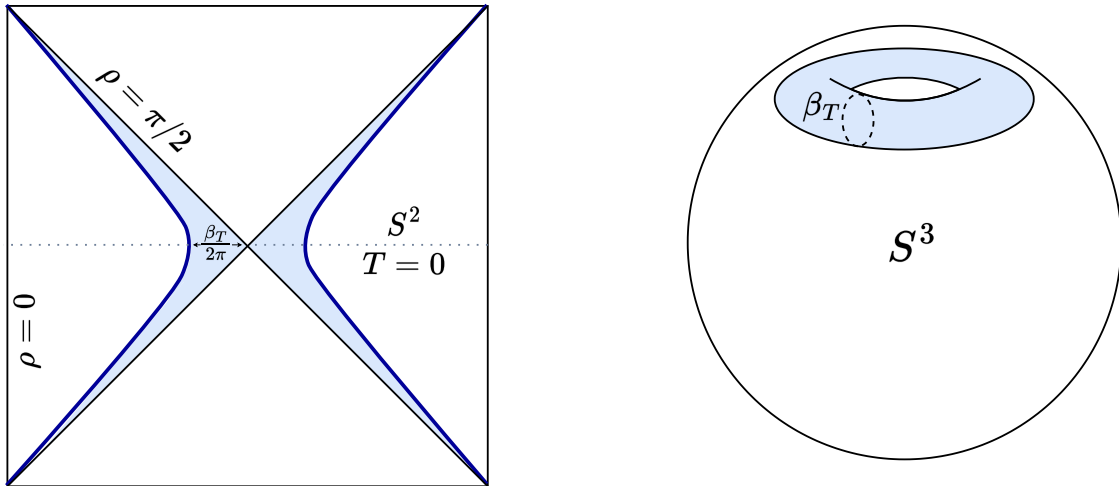


Figure 3.2: The Penrose diagram on the left shows the Lorentzian picture of the edge-modes, which live on the thick, blue line at a distance $\beta_T/2\pi \ll 1$ from the horizon. On the right is the Euclidean picture, where the edge-modes live on the surface of a solid torus with thermal cycle β_T . Shrinking the thermal cycle is the same as taking the high temperature limit, or taking the edge-modes to live very close to the horizon.

In the high temperature limit, we can exploit the modular properties of $\vartheta(0, q^{k/2})$ and $\eta(q)$ to find

$$\lim_{\beta_T \rightarrow 0^+} \log Z_{\text{edge}}[\beta_T] = \frac{\pi^2}{6\nu\beta_T} - \frac{1}{2} \log k \dots \quad (3.50)$$

The first term encodes the contribution from the high energy sector of the theory and is proportional to the temperature. The finite term is temperature independent, and moreover it is independent of our choice of ν . In fact, it is equal to the three-sphere partition function (3.36). The entropy S_e of the edge-modes at high temperature can similarly be computed and reads

$$S_e = \frac{\pi^2}{3\nu\beta_T} - \frac{1}{2} \log k \dots \quad (3.51)$$

Thus, we can relate the regularised expression for $Z_{U(1)_k}[S_3]$ (3.36) to the finite part of the entropy of the edge-mode theory in the high temperature limit. The divergent high temperature contribution is most naturally accommodated by a linearly divergent ultraviolet

piece of the three-sphere partition function, indicating that

$$Z_{U(1)_k}[S_3] = \lim_{\beta_T \rightarrow 0^+} Z_{\text{edge}}[\beta_T], \quad (3.52)$$

in a regularisation scheme where the linear divergence of $Z_{U(1)_k}[S_3]$ in (3.32) is tuned accordingly. We note that there are no cubic divergences appearing on either side.

It has been argued [58, 59] that the temperature independent term in (3.50) is a universal contribution to the entanglement entropy, independent of any of the detailed features associated to the cutoff surface. Here, in view of our discussion in Section 3, we can interpret $-\log \sqrt{k}$ as a contribution to the dS_3 horizon entropy. From this perspective, the fact that this is negative is immaterial.

3.2.4 Edge-mode symmetries.

It is worth pausing momentarily here and noting that the edge-mode theory, which is nothing more than a chiral compact boson theory, has a large symmetry group containing an affine extension of the Virasoro algebra.⁶ The Virasoro generators are constructed in the usual way

$$\hat{L}_0 = \frac{k}{2\pi} \sum_{n \in \mathbb{Z}^+} n^2 \hat{\alpha}_n^\dagger \hat{\alpha}_n, \quad \hat{L}_m = \frac{k}{2\pi} \sum_{n=1}^{\infty} (m+n)n \hat{\alpha}_n^\dagger \hat{\alpha}_{n+m} + \frac{k}{4\pi} \sum_{n=1}^{m-1} (m-n)n \hat{\alpha}_{m-n} \hat{\alpha}_n, \quad (3.53)$$

giving rise to the corresponding Virasoro algebra

$$[\hat{L}_m, \hat{L}_n^\dagger] = \begin{cases} (m+n)\hat{L}_{m-n} + \frac{1}{12}m(m^2-1)\delta_{n,m}, & m \geq n, \\ (m+n)\hat{L}_{n-m}^\dagger, & m < n. \end{cases} \quad (3.54)$$

We notice that the edge-mode Hamiltonian in (3.45) obeys $\hat{H}_0 = v\hat{L}_0$. We can further compute the commutation relations between the \hat{L}_n and $\hat{\alpha}_n$,

$$[\hat{L}_n, \hat{\alpha}_m] = -(n+m)\hat{\alpha}_{n+m}, \quad [\hat{L}_n, \hat{\alpha}_m^\dagger] = \begin{cases} (m-n)\hat{\alpha}_{m-n}^\dagger, & m > n \\ (n-m)\hat{\alpha}_{n-m}, & m < n. \end{cases} \quad (3.55)$$

The presence of the vertex operators (3.44) allows the algebra to be extended beyond the Virasoro- $\mathfrak{u}(1)$ Kac-Moody algebra. The generators additionally include the vertex operators $\hat{\mathcal{J}}_\pm^{(k)} =: e^{\pm ik\hat{\zeta}}$. Recalling that k is even, it follows that the conformal dimension of the

⁶The dS_3/CFT_2 literature discusses a Virasoro symmetry associated to the future/past boundary [20]. Here we see the appearance of a Virasoro symmetry within a single static patch.

generators, $\Delta_{\pm} = k/2$, is also an integer. The extended algebra has a finite number, k , of highest weight irreducible representations (see [172] for a pedagogical discussion). We can organise the Hilbert space of the edge-mode theory in terms of these. The different representations are labelled by a parameter $s = 0, 1, \dots, k-1$, denoting the representation carried by the Wilson line inserted in the interior of the disc [145]. Their corresponding character is given by

$$\chi_s(q) = \frac{1}{\eta(q)} \sum_{m \in \mathbb{Z}} q^{\frac{k}{2}(m + \frac{s}{k})^2}, \quad s = 0, 1, \dots, k-1. \quad (3.56)$$

We observe that upon fixing $\epsilon_0 = 0$ and $q = e^{-v\beta_T}$, the above character for $s = 0$ is equivalent to the thermal partition (3.48). The modular S -matrix for the extended $\mathfrak{u}(1)$ character at level k is given by (see for example [185, 186])

$$\mathcal{S}_m^n = \sqrt{\frac{1}{k}} e^{2\pi i m n / k}, \quad m, n = 0, 1, \dots, k-1. \quad (3.57)$$

Using that \mathcal{S}_m^n relates the $\chi_s(q)$ under $\beta_T \rightarrow 1/\beta_T$, we can re-derive the high temperature behaviour (3.50).

Odd values of k & $\mathcal{N} = 2$ supersymmetry, briefly

Before moving on to the non-Abelian case, we briefly comment that for odd k much of the above discussion carries through. The essential difference is that the generators $\hat{\mathcal{J}}_{\pm}^{(k)} =: e^{\pm i k \hat{\zeta}}$: will carry half-integer conformal dimensions and obey fermionic anti-commutation relations.

Let us focus on the case $k = 3$, which is studied for example in [144]. In this case the generators $\hat{\mathcal{J}}_{\pm}^{(3)} =: e^{\pm 3i\hat{\zeta}}$: have weight $\Delta_{\pm} = 3/2$. Decomposing the generators into their respective Fourier modes $\hat{\mathcal{J}}_{\pm, n}^{(3)}$ on the cylinder, one finds the anti-commutation relations

$$\begin{aligned} \{\hat{\mathcal{J}}_{\pm, n}^{(3)}, \hat{\mathcal{J}}_{\pm, m}^{(3)}\} &= 0, \\ \{\hat{\mathcal{J}}_{+, n}^{(3)}, \hat{\mathcal{J}}_{-, m}^{(3)}\} &= \frac{1}{2} \left(n^2 - \frac{1}{4} \right) \delta_{n+m, 0} + 3\hat{L}_{n+m} + \frac{3i}{2} (m^2 - n^2) \hat{a}_{n+m}. \end{aligned} \quad (3.58)$$

We can also compute the commutation relations between the $\hat{\mathcal{J}}_{\pm}^{(3)}$, the Virasoro generators (3.53), and the Kac-Moody generators (3.43) leading to an $\mathcal{N} = 2$ superconformal algebra.

This has been explored, for example, in [144, 187].⁷ The operators $: e^{\pm i\zeta} :$ correspond to insertions of fractional charge $\pm 1/3$ inside the spatial disc, and are primaries under the $\mathcal{N} = 2$ superconformal algebra.

Supersymmetry is not often associated to physics in de Sitter space [188], but the usual arguments do not preclude the possibility of a supersymmetric edge-mode theory (or a superconformal theory more generally [189]).

3.2.5 Comments on the non-Abelian case

From the modular S -matrix (3.57) we observe that inserting a single Wilson line in the interior of the disc will not affect the constant part of the partition function because $\mathcal{S}_m^0 = \mathcal{S}_0^0$. This is no longer true for the non-Abelian case. For instance, if we take Chern-Simons theory with gauge group $SU(2)$ at level k the relevant modular S -matrix is (see for example [172])

$$\mathcal{S}_m^n = \sqrt{\frac{2}{k+2}} \sin\left(\frac{(m+1)(n+1)\pi}{k+2}\right), \quad m, n = 0, 1, \dots, k. \quad (3.59)$$

As mentioned earlier, \mathcal{S}_0^0 is equal to the regularised partition function $Z_{SU(2)_k}[S^3]$ for the choice of framing leading to vanishing phase. Explicitly,

$$Z_{SU(2)_k}[S^3] = \sqrt{\frac{2}{k+2}} \sin\left(\frac{\pi}{k+2}\right). \quad (3.60)$$

When considering the theory on the disc, the thermal partition function of the edge-mode theory is again given by a character of the $\widehat{\mathfrak{su}}(2)_k$ extended algebra. These are known from the rational CFT literature. For an insertion of the spin- $s/2$ integrable highest weight representation of level k in the interior of the disc, we have (see for example [172])

$$Z_{\text{edge}}[\beta_T; s] = \frac{\vartheta_{s+1}^{k+2} - \vartheta_{-s-1}^{k+2}}{\vartheta_1^2 - \vartheta_{-1}^2}, \quad s = 0, 1, \dots, k, \quad (3.61)$$

where the generalised ϑ -functions are

$$\vartheta_s^k(q, z) \equiv \sum_{p \in \frac{s}{2k} + \mathbb{Z}} q^{kp^2} e^{2\pi ipkz}. \quad (3.62)$$

⁷The edge-mode theory of Chern-Simons theory with an $SU(2)$ gauge group at level $k = 2$ also enjoys an $\mathcal{N} = 2$ superconformal symmetry.

As in the Abelian case, $q = e^{-\beta_T v}$ and $z = 0$ in (3.61) gives the thermal partition function of the edge-mode theory. The entropy in the high temperature limit of the edge-mode theory, which is now an $SU(2)_k$ chiral WZW model, will be given by

$$S_e^{(s)} = \frac{3k}{k+2} \frac{\pi^2}{3\beta_T v} + \log \left(\sqrt{\frac{2}{k+2}} \sin \left(\frac{(s+1)\pi}{k+2} \right) \right) \dots \quad (3.63)$$

The above is an increasing function of s in the range $s = 0, 1, \dots, k$.⁸ For vanishing s , the temperature independent piece of S_e is the S^3 partition function (3.60) of Chern-Simons theory with $SU(2)$ gauge group at level k . For non-vanishing s , it is the S^3 partition function including the insertion of a closed unknotted Wilson loop carrying the spin- $s/2$ integrable representation of level k . The large k expansion makes clear that in this case, horizon thermodynamics will receive contributions at all loop orders. In the weakly coupled limit, one finds

$$\lim_{k \rightarrow \infty} \exp \{ S_e^{(s)} \} \approx (1+s) \times \frac{1}{\text{vol } SU(2)} \left(\frac{4\pi^2}{k} \right)^{3/2} \times e^{\frac{\pi^2}{\beta_T v}}, \quad s = 0, 1, \dots, k. \quad (3.65)$$

We see that the exponential of the entropy receives a multiplicative factor of $(1+s)$ in the weakly coupled limit. The factor $(1+s)$ is nothing more than the dimension of the Hilbert space attached to the puncture, and hence the entropy increases by this amount if the state is not measured with further precision.

Finally, we can also consider the phase of $Z_{SU(2)_k}[S^3]$ from the perspective of the edge-mode theory, again following [145]. Usually, when we consider a two-dimensional conformal field theory on the torus, the partition function is invariant under shifts $\tau \rightarrow \tau + 1$. This is simply the statement that the angular momentum is quantised. However, our edge-mode theory is chiral, and transforms anomalously upon shifting $\tau \rightarrow \tau + 1$. The integrable character of weight h transforms as

$$\chi_h(\tau + 1) = e^{2\pi i(h - c_k/24)} \chi_h(\tau), \quad (3.66)$$

⁸It is also customary to express the entropy in terms of the quantum dimensions $d_s^{(k)}$ of $SU(2)_k$. The numbers encode the multiplicity of various operators appearing upon fusion. They are given by

$$d_s^{(k)} = \sin \left(\frac{\pi(s+1)}{k+2} \right) \arcsin \left(\frac{\pi}{k+2} \right), \quad s = 0, 1, 2, \dots, k, \quad (3.64)$$

such that the temperature independent part of the entropy is given by $S_e^{(s)} = -\frac{1}{2} \log \sum_s d_s^{(k)} d_s^{(k)}$. In the large k limit the quantum dimensions are approximately given by the usual degeneracy formula for $SU(2)$ spin- $s/2$ irreducible representations $d_s^{(k)} \approx s + 1$.

where for the $SU(2)_k$ theory under consideration the weights of the spin- $s/2$ primaries are given by $h = s(s+2)/4(k+2)$ and $c_k = 3k/(k+2)$. In particular, under $\tau \rightarrow \tau + n$ the identity character transforms by a phase given by $e^{2\pi i n c_k/24}$ where n is an integer. This agrees with the set of admissible phases for $Z_{SU(2)_k}[S^3]$ stemming from the framing anomaly.

3.3 Complexified Abelian Chern-Simons: Lorentzian model

In this section, we proceed to consider a complexified version of the Abelian Chern-Simons theory. This theory is introduced as a simple and calculable toy model with a complexified gauge group, a property common to three-dimensional gravity with Lorentzian signature and $\Lambda > 0$ expressed as a Chern-Simons theory.

3.3.1 Lorentzian model

The Lorentzian model is built from a complexified gauge field $\mathcal{A}_\mu = A_\mu + iB_\mu$, where A_μ and B_μ are real Abelian gauge fields. Our action is given by

$$S_L[\mathcal{A}_\mu] = \frac{k+i\lambda}{8\pi} \int_{\mathcal{M}} d^3x \varepsilon^{\mu\nu\rho} \mathcal{A}_\mu \partial_\nu \mathcal{A}_\rho + \frac{k-i\lambda}{8\pi} \int_{\mathcal{M}} d^3x \varepsilon^{\mu\nu\rho} \bar{\mathcal{A}}_\mu \partial_\nu \bar{\mathcal{A}}_\rho, \quad (3.67)$$

and is real-valued. The parameters k and λ are taken to be real-valued. We denote the Lie algebra of our theory by $\mathfrak{u}_{\mathbb{C}}(1)$. The gauge transformations act in the following way

$$\mathcal{A}_\mu \rightarrow \mathcal{A}_\mu + \partial_\mu \vartheta, \quad (3.68)$$

where the gauge parameter ϑ is a complex-valued function. In terms of A_μ and B_μ the action is given by

$$S_L[\mathcal{A}_\mu] = \frac{1}{4\pi} \int_{\mathcal{M}} d^3x \varepsilon^{\mu\nu\rho} [k(A_\mu \partial_\nu A_\rho - B_\mu \partial_\nu B_\rho) - \lambda(A_\mu \partial_\nu B_\rho + B_\mu \partial_\nu A_\rho)]. \quad (3.69)$$

At $\lambda = 0$, the real and imaginary parts of the gauge field \mathcal{A} decouple. Setting either $\lambda = 0$ or $k = 0$ reduces the model to an Abelian BF model with $U(1)$ gauge group (see [190, 191] for an overview). In addition to being real-valued, we will impose that k takes integer values upon quantisation of the theory. This follows from taking A_μ as the generator of a compact $\mathfrak{u}(1)$ gauge algebra. The parameter λ is not constrained to be an integer. Unless otherwise specified, we will take $k \in \mathbb{Z}^+$ and $\lambda \in \mathbb{R}/\{0\}$ in what follows.

The classical equations of motion for (3.69) are given by

$$\varepsilon^{\mu\nu\rho}\partial_\nu A_\rho = \varepsilon^{\mu\nu\rho}\partial_\nu B_\rho = 0. \quad (3.70)$$

They are satisfied when the field strengths associated to A_μ and B_μ vanish. The classical solution space is the space of flat connections modulo gauge transformations. Assuming the theory resides on a three-manifold with topology $\mathbb{R} \times S^2$, we can canonically quantise the theory in the $A_t = B_t = 0$ gauge. States must then satisfy the constraints

$$F_{ij}^A = F_{ij}^B = 0, \quad i, j \in S^2. \quad (3.71)$$

The equal time commutation relations are given by

$$[A_i(\mathbf{x}), A_j(\mathbf{y})] = -[B_i(\mathbf{x}), B_j(\mathbf{y})] = \frac{2\pi i}{k} \varepsilon_{ij} \delta(\mathbf{x} - \mathbf{y}). \quad (3.72)$$

It follows that on a spatial S^2 the Hilbert space has a unique state.

As a final remark before embarking onto the edge-mode theory, it is worth noting that the volume of $U_{\mathbb{C}}(1)$ is infinite, making it difficult to interpret the perturbative formula (3.13) for the S^3 partition function of the Lorentzian model.

3.3.2 Lorentzian edge-mode theory & quantisation

Following the discussion in Section 3.2.2, we can construct an edge-mode theory at the S^1 boundary of the spatial disc. As before, we consider fixing the following gauge⁹

$$\mathcal{A}_t - v\mathcal{A}_\varphi = 0, \quad (3.73)$$

where $v = v_{re} + iv_{im}$ is now a complex parameter. The gauge constraint that follows from imposing the above condition is

$$\mathcal{A}_i(t, \rho, \varphi) = ie^{i\Xi(t, \rho, \varphi)} \partial_i e^{-i\Xi(t, \rho, \varphi)}, \quad i \in \{\rho, \varphi\}, \quad (3.74)$$

⁹More general boundary conditions will be considered in the next chapter.

where now the boundary value of $\Xi(t, \rho, \varphi)|_{\rho=\pi/2}$ is denoted by $\zeta = \zeta_{re} + i\zeta_{im}$ and has compact real part. The action governing our edge-mode theory is given by

$$S_{\text{edge}} = \frac{k+i\lambda}{8\pi} \int dt d\varphi (\partial_t \zeta - v \partial_\varphi \zeta) \partial_\varphi \zeta + \frac{k-i\lambda}{8\pi} \int dt d\varphi (\partial_t \bar{\zeta} - \bar{v} \partial_\varphi \bar{\zeta}) \partial_\varphi \bar{\zeta}. \quad (3.75)$$

Once again, the classical solutions are given by complexified chiral excitations of both the real and imaginary parts of ζ . We find

$$\zeta = f(\varphi + vt) + m\varphi + g(t), \quad (3.76)$$

where $f(z)$ is a complex valued function. We note that $\zeta_{im} = (\zeta - \bar{\zeta})/2i$ does not contain winding modes around the S^1 . The classical Hamiltonian is given by

$$\mathcal{Q}_t = \frac{(k+i\lambda)v}{8\pi} \int d\varphi (\partial_\varphi \zeta)^2 + \frac{(k-i\lambda)\bar{v}}{8\pi} \int d\varphi (\partial_\varphi \bar{\zeta})^2, \quad (3.77)$$

which generates time translations. We note that \mathcal{Q}_t is real. The generator of φ -translations is given by

$$\mathcal{Q}_\varphi = \frac{(k+i\lambda)}{8\pi} \int d\varphi \partial_\varphi \zeta \partial_t \zeta + \frac{(k-i\lambda)}{8\pi} \int d\varphi \partial_\varphi \bar{\zeta} \partial_t \bar{\zeta}. \quad (3.78)$$

On-shell, \mathcal{Q}_t and \mathcal{Q}_φ are equivalent within the sector with vanishing winding number. The classical theory (3.75) is also invariant under shifts $\zeta \rightarrow \zeta + \delta$ of the field ζ by some $\delta \in \mathbb{C}$. The generators of the shift symmetries are

$$\mathcal{Q}_\zeta = \frac{1}{2\pi} \int d\varphi \partial_\varphi \zeta, \quad \mathcal{Q}_{\bar{\zeta}} = \frac{1}{2\pi} \int d\varphi \partial_\varphi \bar{\zeta}. \quad (3.79)$$

Quantisation. In order to quantise the theory, it is convenient to express ζ in terms of Fourier modes. For the non-winding mode sector, we have

$$\zeta(t, \varphi) = \frac{1}{\sqrt{2\pi}} \sum_{n \in \mathbb{Z}/\{0\}} \alpha_n(t) e^{in\varphi}. \quad (3.80)$$

The $\alpha_n(t) \equiv a_n(t) + ib_n(t)$ are independent complex functions of t for all n , and we take $a_n(t)$ and $b_n(t)$ to be real-valued. To quantise the theory, it is convenient to follow the procedure outlined in [192]. For a given n , we can define the vector with components ξ_n^i by $\xi_n \equiv (a_{-n}, b_{-n}, a_n, b_n)$. One finds the commutator

$$[\hat{\xi}_n^i, \hat{\xi}_n^j] = \frac{i}{n} M^{ij}, \quad (3.81)$$

with

$$M^{-1} = \frac{2\pi}{k^2 + \lambda^2} \begin{pmatrix} 0 & -1 \\ 1 & 0 \end{pmatrix} \otimes \begin{pmatrix} \lambda & k \\ k & -\lambda \end{pmatrix}. \quad (3.82)$$

The eigenvalues of M^{-1} are $\pm 2\pi i/\sqrt{k^2 + \lambda^2}$, each doubly degenerate. In terms of the $\hat{\xi}_n$, the quantum Hamiltonian for the vanishing winding mode sector is given by

$$\hat{Q}_t = \frac{1}{4\pi} \sum_{n \in \mathbb{Z}/\{0\}} n^2 \left(\omega \left(\hat{\xi}_n^3 \hat{\xi}_n^1 - \hat{\xi}_n^4 \hat{\xi}_n^2 \right) - \psi \left(\hat{\xi}_n^3 \hat{\xi}_n^2 + \hat{\xi}_n^4 \hat{\xi}_n^1 \right) \right). \quad (3.83)$$

Here we have defined $\omega \equiv kv_{re} - \lambda v_{im}$ and $\psi \equiv \lambda v_{re} + kv_{im}$. We can construct operators obeying the more standard creation/annihilation algebra. We find that

$$\begin{aligned} \hat{A}_n^\pm &\equiv \hat{\xi}_n^4 \pm i\hat{\xi}_n^3 \pm \frac{(ik \mp \lambda)}{\sqrt{k^2 + \lambda^2}} \left(\hat{\xi}_n^1 \pm i\hat{\xi}_n^2 \right), \\ \hat{B}_n^\pm &\equiv \hat{\xi}_n^4 \mp i\hat{\xi}_n^3 \pm \frac{(ik \pm \lambda)}{\sqrt{k^2 + \lambda^2}} \left(\hat{\xi}_n^1 \mp i\hat{\xi}_n^2 \right), \end{aligned} \quad (3.84)$$

obey the commutation relations

$$[\hat{A}_n^+, \hat{A}_m^-] = [\hat{B}_n^+, \hat{B}_m^-] = \frac{8\pi}{n\sqrt{k^2 + \lambda^2}} \delta_{n,m}, \quad (3.85)$$

with all others vanishing. The Hamiltonian can then be put into the following form

$$\hat{Q}_t = \frac{\sqrt{k^2 + \lambda^2}}{16\pi} \sum_{n \in \mathbb{Z}/\{0\}} n^2 \left(v_{re} \left(\hat{A}_n^+ \hat{A}_n^- - \hat{B}_n^+ \hat{B}_n^- \right) + iv_{im} \left(\hat{A}_n^+ \hat{B}_n^+ - \hat{A}_n^- \hat{B}_n^- \right) \right). \quad (3.86)$$

Consequently, uncovering the spectrum of \hat{Q}_t reduces to a two-site hopping type problem, where the sites are labelled by A and B .

3.3.3 Lorentzian edge-mode spectrum

At this stage, we are confronted with diagonalising the Lorentzian edge-mode Hamiltonian (3.86). Since each Fourier mode decouples, it is sufficient to discuss the problem for a single mode number n . It is convenient to represent the creation and annihilation operators satisfying (3.85) in the following way

$$\hat{A}_n^\pm = \left(\frac{4\pi}{n\sqrt{k^2 + \lambda^2}} \right)^{1/2} \left(x_n \pm \frac{d}{dx_n} \right), \quad \hat{B}_n^\pm = \left(\frac{4\pi}{n\sqrt{k^2 + \lambda^2}} \right)^{1/2} \left(y_n \pm \frac{d}{dy_n} \right). \quad (3.87)$$

As detailed in Appendix I, it is straightforward to put the single mode Hamiltonian $\hat{Q}_t^{(n)}$ problem into the Schrödinger problem

$$\frac{\text{sign } w_n}{2} \left(-\frac{d^2}{dw_n^2} + w_n^2 - \frac{1/4 + p_n^2}{w_n^2} \right) \psi_n = \frac{1}{v_{re}} \left(\frac{E_n}{n} + v_{im} p_n \right) \psi_n, \quad (3.88)$$

where $x_n = w_n \cosh t_n$, $y_n = w_n \sinh t_n$ and $p_n \in \mathbb{R}$ is the Fourier momentum associated to the $t_n \in \mathbb{R}$ coordinate. The E_n are the eigenvalues of $\hat{Q}_t^{(n)}$. The operator on the left-hand side of (3.88) is precisely that of a conformal quantum mechanics, as studied for example in [193–196], whose $sl(2, \mathbb{R})$ generators are given by

$$\hat{K}_n = \frac{\text{sign } w_n}{2} w_n^2, \quad \hat{D}_n = -\frac{i}{2} \left[w_n \frac{d}{dw_n} + \frac{1}{2} \right], \quad \hat{H}_n = -\frac{\text{sign } w_n}{2} \left[\frac{d^2}{dw_n^2} + \frac{1/4 + p^2}{w_n^2} \right], \quad (3.89)$$

satisfying

$$[\hat{D}_n, \hat{H}_n] = i\hat{H}_n, \quad [\hat{D}_n, \hat{K}_n] = -i\hat{K}_n, \quad [\hat{K}_n, \hat{H}_n] = 2i\hat{D}_n. \quad (3.90)$$

The generators (3.89) furnish the principal series representation with weight $\Delta = 1/2 + ip_n/2$. It is known that the spectrum of $\hat{H}_n + \hat{K}_n$ is given by the even integers and is thus unbounded [194–196]. Consequently, the single mode energy spectrum is given by

$$E_n(m, p_n) = 2v_{re}nm - v_{im}np_n, \quad m \in \mathbb{Z}, \quad p_n \in \mathbb{R}. \quad (3.91)$$

The unboundedness and continuity of the edge-mode Hamiltonian reflects the fact that the Lorentzian Chern-Simons theory has a complexified gauge group. It also implies that the thermal partition function of the edge-mode theory is no longer a sensible quantity to compute. (Sensible quantities to compute might involve [197, 198] imposing additional constraints on the state-space or modifying the boundary conditions on the Chern-Simons gauge field at the boundary of the disc, which we will examine in Chapter 4.) To sharpen this issue, we consider the edge-mode theory on a torus.

3.3.4 Lorentzian model in Euclidean signature?

The Euclidean continuation of the complexified edge-mode theory (3.75) can be achieved by taking $t = -i\xi$. If we are to place the system at a finite inverse temperature β_T , we further impose that $\xi \sim \xi + \beta_T$, such that the theory resides on a torus. Upon continuing to Euclidean time, we end up with the Euclidean edge-mode action

$$S_{\text{edge}}^{(E)} = \frac{k + i\lambda}{8\pi} \int d\xi d\varphi (-i\partial_\xi \zeta + v\partial_\varphi \zeta) \partial_\varphi \zeta + \frac{k - i\lambda}{8\pi} \int d\xi d\varphi (-i\partial_\xi \bar{\zeta} + \bar{v}\partial_\varphi \bar{\zeta}) \partial_\varphi \bar{\zeta}. \quad (3.92)$$

It is convenient to further express the action in terms of the modes on the torus

$$\zeta(\xi, \varphi) = \frac{1}{\sqrt{2\pi}} \sum_{(m,n) \in \mathbb{Z}^2} e^{2\pi i m \xi / \beta_T + i n \varphi} \zeta_{m,n}, \quad \bar{\zeta}(\xi, \varphi) = \frac{1}{\sqrt{2\pi}} \sum_{(m,n) \in \mathbb{Z}^2} e^{-2\pi i m \xi / \beta_T - i n \varphi} \bar{\zeta}_{m,n}, \quad (3.93)$$

such that

$$S_{\text{edge}}^{(E)} = \sum_{(m,n) \in \mathbb{Z}^2} \frac{k + i\lambda}{8\pi} (\beta_T v n^2 - 2\pi i m n) \zeta_{m,n} \bar{\zeta}_{-m,-n} + \frac{k - i\lambda}{8\pi} (\beta_T \bar{v} n^2 - 2\pi i m n) \bar{\zeta}_{m,n} \zeta_{-m,-n}. \quad (3.94)$$

Here $\zeta_{m,n} \in \mathbb{C}$ and $\bar{\zeta}_{m,n}$ is the complex conjugate of $\zeta_{m,n}$. As discussed in Appendix H, in the Abelian case a Euclidean continuation that preserves the reality conditions of the Chern-Simons gauge field would further require the continuation $v = -iv_E$. In the complexified case, this is no longer necessitated as v is allowed to take complex values. Instead, given the unboundedness of the spectrum we must confront a Gaussian unsuppressed Euclidean path integral

$$\mathcal{Z}_{\text{edge}}[\beta_T] = \int \mathcal{D}\zeta \mathcal{D}\bar{\zeta} e^{-S_{\text{edge}}^{(E)}[\zeta, \bar{\zeta}]}. \quad (3.95)$$

In order to render $\mathcal{Z}_{\text{edge}}[\beta_T]$ better defined, we can complexify the contour of path integration [147]. For simplicity, we take $v_{re} > 0$ and $\lambda = 0$ while recalling $k \in \mathbb{Z}^+$. It is then clear that taking a contour where $\zeta(\xi, \varphi)$ and $\bar{\zeta}(\xi, \varphi)$ are independent real fields will render $\mathcal{Z}_{\text{edge}}[\beta_T]$ well-defined.¹⁰ Upon continuing the contour of ζ and $\bar{\zeta}$, the symmetry group of the edge-mode theory becomes $U(1) \times U(1)$. As we will see in the following section, the price to pay in curing the unboundedness of the Hamiltonian is unitarity of the edge-mode theory. For $\lambda \neq 0$, we must consider a more elaborate contour to render $\mathcal{Z}_{\text{edge}}[\beta_T]$ better defined. This is discussed in the next section where we view the $\lambda \neq 0$ case as a continuation of the $\lambda = 0$ case with $k \in \mathbb{Z}^+$.

From the perspective of the original Chern-Simons gauge theory (3.67) with complexified gauge group $U_{\mathbb{C}}(1)$, the analytic continuation rendering $\zeta(\xi, \varphi)$ and $\bar{\zeta}(\xi, \varphi)$ as independent

¹⁰Expressing $\mathcal{Z}_{\text{edge}}[\beta_T]$ in terms of the Fourier modes (3.93), we can view the problem as an infinite-dimensional version of the complex integral

$$\mathcal{I}_{\sigma} = \int_{\mathbb{C} \times \mathbb{C}} dz d\bar{z} dw d\bar{w} e^{-\sigma zw - \sigma \bar{z} \bar{w}}, \quad (3.96)$$

where $\sigma \in \mathbb{C}$ with positive real part. To define \mathcal{I}_{σ} we first take z and \bar{z} as well as w and \bar{w} to be independent complex variables, and then integrate over the contour $w = \bar{z}$ and $\bar{w} = z$. In this sense, we have that $\mathcal{I}_{\sigma} = \pi^2 / \sigma^2$.

real fields can be achieved by continuing the complexified Chern-Simons gauge fields \mathcal{A}_μ and $\bar{\mathcal{A}}_\mu$ to two independent real-valued $U(1)$ gauge fields, whilst maintaining a complexified level.

3.4 Complexified Abelian Chern-Simons: Euclidean model

In this section, we proceed to consider a different complexified version of the Abelian Chern-Simons theory. This theory is introduced as a simple and calculable toy model with a complexified level, a property common to three-dimensional gravity with Euclidean signature and $\Lambda > 0$ viewed as a Chern-Simons theory.

3.4.1 Euclidean model on S^3

The action for the Euclidean model is given by

$$S_E[A_\mu^\pm] = \frac{\kappa + i\gamma}{4\pi} \int_{\mathcal{M}} d^3x \varepsilon^{\mu\nu\rho} A_\mu^+ \partial_\nu A_\rho^+ + \frac{\kappa - i\gamma}{4\pi} \int_{\mathcal{M}} d^3x \varepsilon^{\mu\nu\rho} A_\mu^- \partial_\nu A_\rho^-, \quad (3.97)$$

where now A^+ and A^- are two real-valued $\mathfrak{u}(1)$ gauge fields. We assume that both $U(1)$ groups are compact and take the parameter $\kappa \in \mathbb{Z}^+$. There is no restriction on γ so we take $\gamma \in \mathbb{R}^+$. The S^3 partition function must be carefully defined since $iS_E[A_\mu^\pm]$ is no longer purely oscillatory but rather an unbounded functional rendering the path integral over e^{iS_E} problematic. To make sense of it we can again consider a complexification of the original path integration contour. On S^3 the only $U(1)$ flat connection (modulo gauge transformations) is the trivial one. Moreover, given that the action is quadratic in the fields the choice of contour can be reduced to a problem of Gaussian integration. The Gaussian integral we are interested in is of the form

$$\mathcal{I}_\sigma = \int_{\mathcal{C}} dx e^{-\sigma x^2/2}, \quad (3.98)$$

with $\sigma = e^{i\vartheta}|\sigma| \in \mathbb{C}$. We take \mathcal{C} to be along a path $e^{i\varphi}\tilde{x}$ with $\tilde{x} \in \mathbb{R}$ and $\vartheta + 2\varphi \in (-\pi/2, \pi/2)$ such that

$$\mathcal{I}_\sigma = \sqrt{\frac{2\pi}{|\sigma|}} e^{-i\vartheta/2}. \quad (3.99)$$

We further take that $\mathcal{I}_{\bar{\sigma}} \equiv (\mathcal{I}_\sigma)^*$ such that the corresponding contour is $e^{-i\varphi}\tilde{x}$, and the product $\mathcal{I}_{\bar{\sigma}}\mathcal{I}_\sigma$ is positive and real. Applying the same reasoning to the Chern-Simons case, we arrive at

$$Z_{\kappa,\gamma}[S^3] = \left(\frac{1}{\text{vol } U(1)} \right)^2 \times \left| \frac{4\pi^2}{\kappa + i\gamma} \right| = \frac{1}{\sqrt{\kappa^2 + \gamma^2}}. \quad (3.100)$$

The above result is invariant under complex conjugation, in other words $\gamma \rightarrow -\gamma$. For $\gamma = 0$ we retrieve the standard result (3.36) with a choice of framing leading to a vanishing phase. For $\kappa = 0$, the result makes sense for $\gamma \in \mathbb{R}^+$ but becomes non-analytic if one tries to continue to the whole complex- γ plane.¹¹

3.4.2 Euclidean edge-mode theory on the torus

Since A^\pm are now compact $\mathfrak{u}(1)$ gauge fields the boundary chiral bosons, which we denote as ζ^\pm , are now compact. Following the procedure outlined in previous sections, and imposing the boundary condition

$$A_\xi^\pm - v^\pm A_\varphi^\pm|_{\partial\mathcal{M}} = 0, \quad (3.101)$$

with $v^\pm \in \mathbb{R}$, we end up with an edge-mode theory governed by the action

$$S_{\text{edge}} = \frac{\kappa + i\gamma}{4\pi} \int d\xi d\varphi \partial_\varphi \zeta^+ (\partial_\xi - v^+ \partial_\varphi) \zeta^+ + \frac{\kappa - i\gamma}{4\pi} \int d\xi d\varphi \partial_\varphi \zeta^- (\partial_\xi - v^- \partial_\varphi) \zeta^-. \quad (3.102)$$

The above theory, which we take to be in Euclidean signature, is non-unitary. Consequently, a Hilbert space interpretation of the theory is unclear. Nevertheless, we can try to compute the Euclidean torus partition function of S_{edge} . We take the periodicity of Euclidean time to be $\xi \sim \xi + \beta_T$, and we recall that $\varphi \sim \varphi + 2\pi$. It is convenient to express the non-winding sector in terms of their respective Fourier modes, namely

$$\zeta^\pm(\xi, \varphi) = \frac{1}{\sqrt{2\pi}} \sum_{(m,n) \in \mathbb{Z}^2} \zeta_{m,n}^\pm e^{2\pi i m \xi / \beta_T + i n \varphi}. \quad (3.103)$$

The reality condition is $\zeta_{-m,-n}^\pm = (\zeta_{m,n}^\pm)^*$. The edge-mode action now reads

$$S_{\text{edge}} = \sum_{(m,n) \in \mathbb{Z}^2} \frac{\kappa + i\gamma}{4\pi} (2\pi m n - \beta_T v^+ n^2) |\zeta_{m,n}^+|^2 + \frac{\kappa - i\gamma}{4\pi} (2\pi m n - \beta_T v^- n^2) |\zeta_{m,n}^-|^2, \quad (3.104)$$

and the path integral becomes an integral over all the $\zeta_{m,n}^\pm$. We can compare the edge-mode action iS_{edge} to the one stemming from Lorentzian edge-mode theory, i.e. $-S_{\text{edge}}^{(E)}$ in (3.94), discussed in the previous section. If we map $(k, \lambda) = (2\kappa, 2\gamma)$ and $(v, \bar{v}) = i(v^+, v^-)$, it follows that the deformed contour discussed below (3.95) indeed leads to the Euclidean edge-mode theory (3.104).

¹¹Although our treatment leads to a real valued $Z_{\kappa,\gamma}[S^3]$, it seems feasible that a more general regularization can lead to an overall phase that depends on the choice of framing of S^3 . It would be interesting to explore this both for the Abelian case and the non-Abelian extension that will be discussed in Section 3.5.1.

In order to render the path integral over iS_{edge} convergent, we must again alter the integration contour \mathcal{C} of $\zeta_{n,m}^{\pm}$. The path integration over the non-winding mode sector of ζ^{\pm} yields a functional determinant proportional to the Dedekind η -function (see Appendix H). The sum over the winding sector must be similarly defined. The winding modes are given by $\zeta^{\pm}(t, \varphi) = m_{\pm}\varphi$ where m_{\pm} are integers.¹² Consequently, we must perform the sum

$$\mathcal{S}_w = \sum_{m_{\pm} \in \mathbb{Z}} e^{-i\frac{\kappa+i\gamma}{2}v^+\beta_T m_+^2 - i\frac{\kappa-i\gamma}{2}v^-\beta_T m_-^2} = \vartheta_3\left(0, q_+^{(\kappa+i\gamma)/2}\right) \vartheta_3\left(0, q_-^{(\kappa-i\gamma)/2}\right). \quad (3.105)$$

The above sum exists provided $-(\kappa \pm i\gamma)\beta_T v^{\pm}/2\pi$ is in the upper-half plane. In the last equality, we have defined $q_{\pm} \equiv e^{-iv^{\pm}\beta_T}$. Putting it all together, upon path integrating over $e^{iS_{\text{edge}}}$ we end up with the torus partition function

$$Z_{\text{edge}}[\beta_T] = \frac{\vartheta_3\left(0, q_+^{(\kappa+i\gamma)/2}\right) \vartheta_3\left(0, q_-^{(\kappa-i\gamma)/2}\right)}{\eta(q_+)\eta(q_-)}. \quad (3.106)$$

To render the Dedekind η -functions well-defined, we take v^{\pm} to have a small negative imaginary part. Taking the $\beta_T \rightarrow 0^+$ limit we have

$$\lim_{\beta_T \rightarrow 0^+} \log Z_{\text{edge}}[\beta_T] = \frac{\pi^2}{6\beta_T i v^+} + \frac{\pi^2}{6\beta_T i v^-} - \log |\kappa + i\gamma| \dots \quad (3.107)$$

The finite part agrees with the S^3 partition function (3.100). We further note that the above expression can be obtained from the Abelian edge-mode expression (3.50) by a simple analytic continuation.

3.5 Remarks on gravitation in three dimensions

The classical action of general relativity in three dimensions can be expressed as a Chern-Simons theory [34,35]. The gauge group depends on the signature and sign of the cosmological constant Λ . We restrict to $\Lambda = +1/\ell^2 > 0$. In Euclidean signature the gauge group is $SU(2) \times SU(2)$ and the level is complex. In Lorentzian signature the gauge group becomes $SL(2, \mathbb{C})$, which can be viewed as the complexification of $SU(2)$ (or $SL(2, \mathbb{R})$). These Chern-Simons theories are natural non-Abelian extensions of the complexified Abelian theories

¹²Given the periodicity of ζ^{\pm} , one is also tempted to consider the vertex operators $\hat{\mathcal{O}}_n^{\pm} =: e^{in\hat{\zeta}^{\pm}}$: carrying $U(1)$ charge (3.41) $\mathcal{Q}_n^{\pm} = n/(\kappa \pm i\gamma)$. Although \mathcal{O}_n^{\pm} bear some similarity to the anyonic operators (3.44) of ordinary Abelian Chern-Simons theory, their physical meaning is more obscure at complex level. For instance, in the ordinary Abelian case $k \in \mathbb{Z}^+$ corresponds to the number of anyonic species, something hard to understand when the level is complex.

explored in sections 3.3 and 3.4. The purpose of this section is to comment briefly on how the properties of the complexified Abelian theories generalise, leaving a more detailed analysis to future work.

3.5.1 Euclidean signature

We begin by considering the Euclidean theory whose action is given by $S_E = S_E^+ + S_E^-$, where

$$S_E^\pm[A_\mu^\pm] = \frac{\kappa \pm i\gamma}{4\pi} \int_{\mathcal{M}} d^3x \varepsilon^{\mu\nu\rho} \text{Tr} \left(A_\mu^\pm \partial_\nu A_\rho^\pm + \frac{2}{3} A_\mu^\pm A_\nu^\pm A_\rho^\pm \right). \quad (3.108)$$

The A_μ^\pm are $SU(2)$ gauge fields. In terms of the vielbein e_μ^i and spin-connection $\omega_{ij,\mu} = \varepsilon_{ijk} \omega_\mu^k$, where ε_{ijk} is the Levi-Civita symbol, one has

$$A_\mu^\pm = \left(\omega_\mu^i \pm \frac{1}{\ell} e_\mu^i \right) T_i, \quad T_i = \frac{1}{2} i \sigma_i, \quad (3.109)$$

where the σ_i are the Pauli matrices. Substituting A^\pm into (3.108) leads to Einstein gravity in three dimensions plus a parity-odd Chern-Simons type term for the spin connection. The imaginary part of the level, $\gamma \in \mathbb{R}^+$, is given by $\gamma = \ell/4G$, while $\kappa \in \mathbb{Z}$ is the coupling of a parity-odd gravitational Chern-Simons term.

The equations of motion stemming from (3.108) are the flat connection equations, and the solutions are the space of flat connections modulo gauge transformations. For standard $SU(2)$ Chern-Simons theory on an S^3 we would discard the presence of multiple possible saddles due to the absence of non-trivial flat connections. However, when the Chern-Simons coupling is taken away from the integers one must exercise further caution. In particular, gauge transformations changing the winding number will no longer be trivial. So, the spaces of flat connections with differing winding number have different on-shell actions. Of these, most will not have a clear interpretation from the perspective of the gravitational theory since they will lead to non-invertible or otherwise non-standard vielbeins. This is a feature we did not have to confront in the Abelian toy models of the previous sections. We consider perturbative effects around the flat-connection $A^+ = g^{-1} dg$ and $A^- = 0$, where $g \in SU(2)$. Recalling that the group geometry of $SU(2)$ under the Haar metric is the three-sphere, this flat connection corresponds to the round S^3 in the gravitational theory as can be explicitly checked. Following reasoning analogous to the Euclidean $U(1)$ model with complexified levels, it has been

argued that [63, 148]

$$\mathcal{Z}_{\text{grav}} = e^{2\pi\gamma} \times e^{i\varphi_{\text{grav}}} \left| \sqrt{\frac{2}{\kappa + i\gamma + 2}} \sin \frac{\pi}{\kappa + i\gamma + 2} \right|^2, \quad (3.110)$$

to all orders in a large- γ perturbative expansion, and this expansion reproduces (3.1). According to Gibbons and Hawking [13], $S_{\text{dS}} = \log \mathcal{Z}_{\text{grav}}$ calculates the quantum corrected entropy of the dS_3 horizon. To leading order in the large γ expansion, $S_{\text{dS}} = 2\pi\gamma = \pi\ell/2G$. The one-loop correction is given by the analytic continuation of the expression at integer level:

$$e^{S_{\text{dS}}^{(1)}} = \left(\frac{1}{\text{vol } SU(2)} \right)^2 \times \left| \frac{4\pi^2}{\kappa + i\gamma + 2} \right|^3. \quad (3.111)$$

This is the natural non-Abelian extension of (3.100). It is challenging to reproduce the leading contribution S_{dS} directly from the gravitational perspective (attempts include [161–163]). In line with our discussion so far, we now consider the possibility of an edge-mode theory which may reproduce the subleading corrections to S_{dS} from a Lorentzian perspective.

3.5.2 Lorentzian signature

We now turn to the Lorentzian theory

$$S_L[\mathcal{A}_\mu] = \frac{k + i\lambda}{8\pi} \int_{\mathcal{M}} d^3x \varepsilon^{\mu\nu\rho} \text{Tr} \left(\mathcal{A}_\mu \partial_\nu \mathcal{A}_\rho + \frac{2}{3} \mathcal{A}_\mu \mathcal{A}_\nu \mathcal{A}_\rho \right) + \text{c.c.}, \quad (3.112)$$

where \mathcal{A}_μ is an $SL(2, \mathbb{C})$ gauge field related to the vielbein and spin connection as

$$\mathcal{A}_\mu = \left(\omega_\mu^i + \frac{i}{\ell} e_\mu^i \right) T_i, \quad \bar{\mathcal{A}}_\mu = \left(\omega_\mu^i - \frac{i}{\ell} e_\mu^i \right) T_i, \quad (3.113)$$

where $(T_1, T_2, T_3) = \frac{1}{2}(i\sigma_2, \sigma_1, \sigma_3)$ are the real generators of $SL(2, \mathbb{R})$ obeying $\text{Tr}(T_i T_j) = \frac{1}{2}\eta_{ij}$ and $[T_i, T_j] = \varepsilon_{ijk} T^k$, with $T^i = \eta^{ij} T_j$. We further have that $k \in \mathbb{Z}^+$ and $\lambda \in \mathbb{R}$.

As for the Abelian theory with $U_{\mathbb{C}}(1)$ gauge group, we would like to understand the edge-mode theory. We must pick a boundary condition for the $SL(2, \mathbb{C})$ gauge field. Any choice will break the full diffeomorphism group, for the same reason that boundary conditions break the gauge-symmetries of the Chern-Simons theory. Various proposals for boundary conditions have appeared in the literature [197–199]. Our interest is to understand the diffeomorphism invariant one-loop correction $S_{\text{dS}}^{(1)}$ (3.111), and more generally the subleading corrections to the tree-level de Sitter entropy S_{dS} encoded in (3.110), from a Lorentzian perspective. In line

with our previous discussions, we choose boundary conditions (3.21), namely

$$(\mathcal{A}_t - v\mathcal{A}_\varphi)|_{\partial\mathcal{M}} = 0, \quad (3.114)$$

with $v \in \mathbb{C}$. Going through the same steps, the Lorentzian edge-mode theory is then described by a chiral $SL(2, \mathbb{C})$ WZW theory at level $k + i\lambda$ [146, 161, 199]

$$S_{\text{edge}}[g] = \frac{k + i\lambda}{8\pi} \text{Tr} \int dt d\varphi (g\partial_\varphi g^{-1}) (g(\partial_t - v\partial_\varphi)g^{-1}) + \pi(k + i\lambda)S^{\text{WZ}}[g] + \text{c.c.}, \quad (3.115)$$

where $g(t, \varphi)$ is an $SL(2, \mathbb{C})$ valued function, and

$$S^{\text{WZ}}[g] = \frac{1}{24\pi^2} \int_{\mathcal{B}} d^3y \varepsilon^{\mu\nu\rho} \text{Tr} (g^{-1}\partial_\mu g g^{-1}\partial_\nu g g^{-1}\partial_\rho g), \quad (3.116)$$

where \mathcal{B} is a three-manifold whose boundary is the $t\varphi$ -cylinder. As for the Abelian Lorentzian model, the Hamiltonian stemming from (3.115) is real but unbounded from below. The theory satisfies an $SL(2, \mathbb{C})$ current algebra given by (see for instance [161])

$$\begin{aligned} [J_n^a, J_m^b] &= \frac{1}{2}(k + i\lambda)n\delta_{ab}\delta_{n+m,0} - if_{abc}J_{n+m}^c, \\ [\tilde{J}_n^a, \tilde{J}_m^b] &= \frac{1}{2}(k - i\lambda)n\delta_{ab}\delta_{n+m,0} - if_{abc}\tilde{J}_{n+m}^c, \end{aligned} \quad (3.117)$$

where the $SL(2, \mathbb{C})$ structure constants are $f_{abc} = \varepsilon_{abc}$, and ε_{abc} is the Levi-Civita symbol. Using the above currents, the Sugawara construction yields a Virasoro algebra with central charge

$$c_{SL(2,\mathbb{C})} = \frac{3(k + i\lambda)}{(k + i\lambda + 2)} + \frac{3(k - i\lambda)}{(k - i\lambda + 2)} = \frac{6(k(k + 2) + \lambda^2)}{(k + 2)^2 + \lambda^2}. \quad (3.118)$$

Some details of the derivation for $c_{SL(2,\mathbb{C})}$ are provided in Appendix J. Notice that in the semiclassical limit $k \rightarrow \infty$, we have that $c_{SL(2,\mathbb{C})} \approx 6$ which is the number of field theoretic degrees of freedom in (3.115). Interestingly, upon analytically continuing $k = -2$, the central charge is exactly $c_{SL(2,\mathbb{C})} = 6$, which might suggest that the theory is very simple at this point. Moreover, we see that c_{WZW} is given by complexifying the level k for the central charge $c_{SU(2)} = 3k/(k + 2)$ of the $SU(2)$ WZW model. It also appears that the vacuum ($s = 0$) $\widehat{\mathfrak{su}}(2)_k$ character (3.61) can be analytically continued to complex level, giving the thermal partition function of this theory.

As for the case of the Lorentzian complexified $U(1)$ model studied in Section 3.3, upon continuing the Lorentzian edge-mode theory (3.112) to Euclidean signature, one can consider complexifying the $SL(2, \mathbb{C})$ contour leading to that of a WZW model with two copies

of $SU(2)$ at complex level. In particular, to render the path integral better defined it is natural to pursue the same avenue as in Section 3.3.4. Upon complexifying the contour of g to one where it is valued in $SU(2) \times SU(2)$ we can make contact with (3.111) much like (3.63) connects to the three-sphere partition function of $SU(2)$ Chern-Simons theory (3.60). A detailed treatment of the putative gravitational edge-mode theory (3.115) and its thermodynamic properties is left for future work.

As a final remark, we note that timelike Wilson lines piercing the origin of the spatial disc carry unitary irreducible representations of $SL(2, \mathbb{C})$ which, when non-trivial, contain an infinite number of states.¹³ This is another indication of the non-compactness of $SL(2, \mathbb{C})$. It would be interesting to generalise the discussion in Section 3.2.5 to this case.

3.6 AdS_4/CFT_3 and S^3

In this final section we would like to consider the AdS_4/CFT_3 correspondence for an AdS_4 spacetime whose asymptotic boundary is given by a Euclidean or Lorentzian three-dimensional de Sitter space. This allows us to explore the thermodynamic properties of strongly coupled conformal matter theories on a fixed de Sitter background and their geometrisation in the bulk of AdS_4 .

The metric of Euclidean AdS_4 is given by

$$\frac{ds^2}{\ell_A^2} = d\vartheta^2 + \sinh^2 \vartheta d\Omega_3^2, \quad (3.119)$$

with $\vartheta \in [0, \infty)$ and $d\Omega_3^2$ describing the round metric on a unit S^3 . The four-dimensional cosmological constant is $\Lambda = -3/\ell_A^2$. The asymptotic boundary resides at $\vartheta_\infty = \infty$ and the induced metric at the boundary is the round metric on S^3 . Recalling our previous discussion, we can consider a Lorentzian continuation of (3.119) to the following static spacetime

$$\frac{ds^2}{\ell_A^2} = d\vartheta^2 + \sinh^2 \vartheta (-dt^2 \cos^2 \rho + d\rho^2 + \sin^2 \rho d\varphi^2). \quad (3.120)$$

This is a static Lorentzian anti-de Sitter universe whose constant- ϑ surfaces are given by the static patch of dS_3 . A constant- t slice of this geometry is shown in Figure 3.3. The global geometry is given by replacing the three-dimensional static patch metric in (3.120) with the global one. The static geometry (3.120) has a horizon at $\rho = \pi/2$. The topology of the

¹³See [102] for a related discussion.

horizon is $S^1 \times \mathbb{R}^+$. The Bekenstein-Hawking entropy of the horizon is given by

$$S_{\text{BH}} = \frac{\pi \ell_A^2}{2 \ell_{\text{pl}}^2} \int_0^{-\log \varepsilon} d\vartheta \sinh \vartheta \approx \frac{\pi \ell_A^2}{2 \ell_{\text{pl}}^2} \left(\frac{1}{2\varepsilon} - 1 + \dots \right), \quad (3.121)$$

where ℓ_{pl} is the four-dimensional Planck length (such that $G = \ell_{\text{pl}}^2$) and ε is a small number cutting off $z = e^{-\vartheta}$. From the perspective of AdS/CFT the entropy S_{BH} corresponds to the entropy across the dS_3 horizon of the dual CFT, and the $1/\varepsilon$ divergence corresponds to a local divergence in the CFT due to entanglement of modes localised on the S^1 horizon.

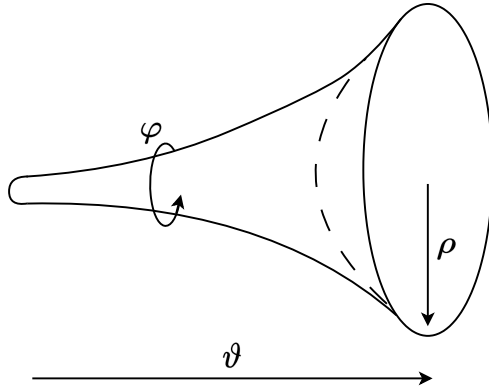


Figure 3.3: A constant t slice of the geometry (3.120). The space is foliated by static patch hemispheres with exponentially increasing radius in the ϑ direction and the horizon at $\rho = \pi/2$ is the surface of this shape.

It is useful to expand the geometry in small z

$$\frac{ds^2}{\ell_A^2} = \frac{dz^2}{z^2} + \frac{1}{4} \left(\frac{1}{z^2} - 2 + z^2 \right) d\Omega_3^2. \quad (3.122)$$

From the above expansion it follows that the solution has vanishing boundary Brown-York stress tensor. Since the energy vanishes, we have that the logarithm of the thermal partition function is given entirely by the entropy. The thermal partition function is given by the Euclidean gravity path integral with an S^3 boundary, such that

$$\log Z[\text{EAdS}_4] \stackrel{?}{=} S_{\text{BH}}. \quad (3.123)$$

In the semiclassical limit, we can calculate $\log Z[\text{EAdS}_4]$ by evaluating the on-shell Einstein action

$$S_E[g_{ij}] = -\frac{1}{16\pi \ell_{\text{pl}}^2} \int_{\mathcal{M}} d^4x \sqrt{g} \left(R + \frac{6}{\ell_A^2} \right) - \frac{1}{8\pi \ell_{\text{pl}}^2} \int_{\partial \mathcal{M}} d^3x \sqrt{h} K, \quad (3.124)$$

on the solution (3.119). The second term is the Gibbons-Hawking-York boundary term,

where K is the extrinsic curvature at the boundary $\partial\mathcal{M}$, and h_{ij} is the induced metric at the boundary:

$$ds_{\text{bdy}}^2 = \ell_A^2 \sinh^2 \vartheta_\infty d\Omega_3^2. \quad (3.125)$$

Using a similar regularisation prescription as in (3.121), the on-shell action (3.124) evaluates to

$$S_E = \frac{\pi\ell_A^2}{2\ell_{pl}^2} - \frac{\pi\ell_A^2}{16\ell_{pl}^2\varepsilon^3} - \frac{3\pi\ell_A^2}{16\ell_{pl}^2\varepsilon}. \quad (3.126)$$

In general, we can also add boundary counterterms which are built locally from the boundary metric h_{ij} . These will not affect the bulk equations of motion:

$$S_{CT} = \frac{a_0}{\varepsilon^3} \int_{S^3} d^3x \sqrt{\tilde{h}} + \frac{a_1}{\varepsilon} \int_{S^3} d^3x \sqrt{\tilde{h}} R[\tilde{h}], \quad (3.127)$$

where \tilde{h} is the boundary CFT metric in units of ε with the conformal factor stripped off,

$$ds_{\text{CFT}}^2 = \frac{\ell_A^2}{4} d\Omega_3^2. \quad (3.128)$$

The coefficients a_0 and a_1 are ambiguous and depend on our choice of terms localised at the boundary. In the dual quantum field theory these are related to ultraviolet divergences (3.30) renormalising the boundary cosmological constant and Newton constant. One may choose the coefficients such as to cancel the UV divergences stemming from the on-shell action [200]. Indeed, if our theory is supersymmetric, we expect that the cubic divergences associated to the cosmological constant term should vanish, and we therefore choose $a_0 = 1/4\pi\ell_A\ell_{pl}^2$. Thus, in the semiclassical limit we have

$$\log Z[\text{EAdS}_4] = -\frac{\pi\ell_A^2}{2\ell_{pl}^2} + \frac{3\pi\ell_A^2}{16\ell_{pl}^2\varepsilon} - \frac{6\pi^2\ell_A a_1}{\varepsilon}. \quad (3.129)$$

We see that the finite term indeed matches (3.121). Rather than choosing a_1 to cancel the linear divergence in (3.129), if we instead tune $a_1 = 7\ell_A/96\pi\ell_{pl}^2$, we can also match the linearly divergent term in equation (3.121).¹⁴

For ABJM theory with $SU(N)_k \times SU(N)_{-k}$ gauge group, the partition function (3.129) has been calculated exactly in [202] and matched to the bulk in [203]. The finite part, in

¹⁴Entanglement entropy in de Sitter was also studied holographically in [201]. There, the entropy of quantum fields cuts over many horizons at the late time boundary, whereas we consider the entanglement of gravitational fields within a single static patch.

terms of the ABJM data, reads

$$\log Z_{\text{ABJM}}[S^3] = -N^2 \frac{\pi\sqrt{2}}{3} \lambda^{-1/2}, \quad (3.130)$$

where $\lambda = N/k$ is the 't Hooft parameter which is kept fixed and large in the large N limit. The fact that $\log Z_{\text{ABJM}}[S^3]$ goes as $\sim N^2$ suggests that the theory is in a deconfined phase, reminiscent of the discussion in [204]. From our perspective, the calculations of [202, 203] are a microscopic derivation of the Bekenstein-Hawking entropy of the horizon in (3.120). The Bekenstein-Hawking entropy (3.121) predicts only linear ultraviolet divergences in the partition function. In fact, this is also true for the S^3 partition function calculated in [202], since they regularise the theory in a way that preserves supersymmetry. The ultraviolet divergent piece of their calculation comes from the one-loop determinants of a transverse vector field and a gaugino on S^3 . The absence of a cubic divergence is a result of the spectrum alone and is insensitive to any mass terms.

Recalling (3.30), the only other allowed divergence in a parity invariant three-dimensional quantum field theory is linear in ℓ_{uv}^{-1} and is indeed implicitly present in the localisation treatment of [202]. This is in agreement with (3.121). Interestingly, the calculations of [202, 203] can be done for any value of the Chern-Simons level k and rank N . They can be viewed as predicting string and loop corrections of the Bekenstein-Hawking entropy from the bulk perspective. In the perturbative limit, where $\lambda \ll 1$, it is found that

$$\log Z_{\text{ABJM}}[S^3] \approx -N^2 \log \lambda^{-1} + \dots, \quad (3.131)$$

which is in agreement with the pure Chern-Simons partition function result (3.13) in the perturbative limit.¹⁵

One can also consider adding Wilson loops [202, 203]. In the Euclidean picture, the simplest case is a Wilson loop that goes around the equator of the S^3 . To preserve supersymmetry, in addition to the gauge field, one also has additional matter fields on the loop. For instance, in ABJM, the partition function endowed with a 1/2-BPS preserving Wilson loop in the fundamental representation is given as follows

$$\frac{Z_{\text{ABJM}}[S^3; W_C]}{Z_{\text{ABJM}}[S^3]} = \frac{e^{i\pi/2}}{2} e^{\pi\sqrt{2\lambda}}, \quad (3.132)$$

¹⁵The relation between topological entanglement entropy and black holes in AdS/CFT was also studied in [205].

where the expression is given to leading order in the large N limit at fixed and large 't Hooft coupling $\lambda = N/k$. From the bulk perspective, the above is computed by a string whose worldsheet intersects the S^3 boundary at the equatorial S^1 . The phase is due to a type IIA B-field. We can Wick rotate to a Lorentzian picture (3.120), where the equatorial S^1 at $\rho = 0$ is now parameterised by the Lorentzian coordinate t . The worldsheet now intersects the boundary along t at $\rho = 0$ and goes all the way to the horizon. In the thermodynamic field picture, we can continue the worldsheet across the horizon such that the worldsheet intersects the second boundary static patch. As in our discussion of pure Chern-Simons theory, we might view the partition function with the insertion of the Wilson loop as computing a part of the entanglement entropy between the two static patches in the presence of an insertion at the origin of the two spatial discs. From the bulk perspective this is the contribution to the Bekenstein-Hawking entropy (3.121) due to a worldsheet crossing the bulk horizon.

Chapter 4

An alternative edge-mode theory

One might ask if the boundary conditions we have chosen for the disc (3.21) are the most general we could consider. It might be possible that with an alternative choice of boundary conditions, we could engineer the Lorentzian edge-mode theory with complexified gauge group to have a spectrum which is bounded from below, hence avoiding the need to complexify the integration contour. In this chapter, we explore this possibility and show that the boundary condition (3.21) does in fact lead to the most general edge-mode theory. This chapter is based on unpublished work that was done with Dionysios Anninos and Kévin Nguyen.

4.1 General boundary conditions

We will be interested again in the Lorentzian action (3.69), which is repeated here for convenience:

$$S_L = \frac{k}{4\pi} \int_{\mathcal{M}} d^3x \varepsilon^{\mu\nu\rho} (A_\mu \partial_\nu A_\rho - B_\mu \partial_\nu B_\rho) - \frac{\lambda}{4\pi} \int_{\mathcal{M}} d^3x \varepsilon^{\mu\nu\rho} (A_\mu \partial_\nu B_\rho + B_\mu \partial_\nu A_\rho), \quad (4.1)$$

where $\mathcal{M} = D \times \mathbb{R}$. This action has a discrete symmetry under $A_\mu \leftrightarrow B_\mu$ and $k \rightarrow -k$. Instead of the condition (3.73), we would like to impose the more general gauge condition

$$\begin{aligned} A_t &= \gamma_1 A_\varphi + \gamma_2 B_\varphi, \\ B_t &= \gamma_3 A_\varphi + \gamma_4 B_\varphi, \end{aligned} \quad (4.2)$$

where $\gamma_i \in \mathbb{R}$. If we take

$$\begin{aligned} \gamma_1 &= \gamma_4 = v_{re}, \\ -\gamma_2 &= \gamma_3 = v_{im}, \end{aligned} \quad (4.3)$$

then this is equivalent to the original gauge choice (3.73). Upon imposing the boundary conditions, the discrete symmetry also requires us to map $\gamma_1 \leftrightarrow \gamma_4$ and $\gamma_2 \leftrightarrow \gamma_3$. Varying the action, we find

$$\begin{aligned} \delta S_L = & \frac{k}{4\pi} \int_{\mathcal{M}} d^3x \varepsilon^{\mu\nu\rho} (\delta A_\mu F_{\nu\rho}^A - \delta B_\mu F_{\nu\rho}^B + \partial_\nu (A_\mu \delta A_\rho - B_\mu \delta B_\rho)) \\ & - \frac{\lambda}{4\pi} \int_{\mathcal{M}} d^3x \varepsilon^{\mu\nu\rho} (\delta A_\mu F_{\nu\rho}^B + \delta B_\mu F_{\nu\rho}^A + \partial_\nu (A_\mu \delta B_\rho + B_\mu \delta A_\rho)), \end{aligned} \quad (4.4)$$

where $F_{\mu\nu}^A$ and $F_{\mu\nu}^B$ are the field strength tensors for A_μ and B_μ respectively. Requiring the total derivative boundary term to vanish leads us to

$$k(A_t \delta A_\phi - A_\phi \delta A_t - B_t \delta B_\phi + B_\phi \delta B_t) - \lambda(A_t \delta B_\phi - A_\phi \delta B_t + B_t \delta A_\phi - B_\phi \delta A_t) \stackrel{!}{=} 0. \quad (4.5)$$

Upon imposing (4.2), this is equivalent to the condition

$$k(\gamma_2 + \gamma_3) + \lambda(\gamma_1 - \gamma_4) = 0. \quad (4.6)$$

We can therefore replace, for example, γ_4 in terms of the other γ_i in order for the boundary term to vanish, and we will proceed to do this. It is interesting to note though that the condition is also satisfied at the fine tuned point

$$k = -\frac{\lambda(\gamma_1 - \gamma_4)}{\gamma_2 + \gamma_3}. \quad (4.7)$$

The associated gauge constraints are

$$\begin{aligned} F_{ij}^A = 0 & \implies A_i = \partial_i \zeta_{re}, \\ F_{ij}^B = 0 & \implies B_i = \partial_i \zeta_{im}, \quad i \in (r, \phi), \end{aligned} \quad (4.8)$$

where $\zeta = \zeta_{re} + i\zeta_{im}$. Imposing the gauge and the gauge constraints on the action leads to the edge-mode theory

$$\begin{aligned} S_{\text{edge}} = & \frac{1}{4\pi} \int dt d\phi (\lambda\gamma_3 - k\gamma_1) (\partial_\phi \zeta_{re})^2 + (k\gamma_4 + \lambda\gamma_2) (\partial_\phi \zeta_{im})^2 - 2\lambda \partial_t \zeta_{re} \partial_\phi \zeta_{im} \\ & + (k(\gamma_3 - \gamma_2) + \lambda(\gamma_1 + \gamma_4)) \partial_\phi \zeta_{re} \partial_\phi \zeta_{im} + k(\partial_t \zeta_{re} \partial_\phi \zeta_{re} - \partial_t \zeta_{im} \partial_\phi \zeta_{im}). \end{aligned} \quad (4.9)$$

Plugging in the values (4.3), this becomes the edge-mode theory that we considered Section 3.3 of Chapter 3. The discrete symmetry of (4.1) is mapped to $\zeta_{re} \leftrightarrow \zeta_{im}$, $k \rightarrow -k$, $\gamma_1 \leftrightarrow \gamma_4$

and $\gamma_2 \leftrightarrow \gamma_3$ in the edge-mode theory. In terms of ζ and $\bar{\zeta}$, the action is

$$S_{\text{edge}} = \frac{1}{16\pi} \int dt d\phi (\lambda\gamma_3 - k\gamma_1)(\partial_\phi\zeta + \partial_\phi\bar{\zeta})^2 - (k\gamma_4 + \lambda\gamma_2)(\partial_\phi\zeta - \partial_\phi\bar{\zeta})^2 - 2i(k\gamma_3 + \lambda\gamma_1)((\partial_\phi\zeta)^2 - (\partial_\phi\bar{\zeta})^2) + 2(k + i\lambda)\partial_t\zeta\partial_\phi\zeta + 2(k - i\lambda)\partial_t\bar{\zeta}\partial_\phi\bar{\zeta}. \quad (4.10)$$

We can then express the fields in terms of the mode expansions

$$\begin{aligned} \zeta(t, \phi) &= \frac{1}{\sqrt{2\pi}} \sum_{n \in \mathbb{Z}/\{0\}} \alpha_n(t) e^{in\phi}, \\ \bar{\zeta}(t, \phi) &= \frac{1}{\sqrt{2\pi}} \sum_{n \in \mathbb{Z}/\{0\}} \bar{\alpha}_n(t) e^{-in\phi}, \end{aligned} \quad (4.11)$$

where $\alpha_n = a_n + ib_n$, with a_n and b_n real-valued. The Hamiltonian is then

$$\begin{aligned} \hat{H} &= \frac{1}{16\pi} \sum_{n \in \mathbb{Z}/\{0\}} n^2 \left[(k\gamma_1 - \lambda\gamma_3)(\alpha_n\alpha_{-n} + 2\alpha_n\bar{\alpha}_{-n} + \bar{\alpha}_n\bar{\alpha}_{-n}) \right. \\ &\quad \left. + (k\gamma_4 + \lambda\gamma_2)(\alpha_n\alpha_{-n} - 2\alpha_n\bar{\alpha}_{-n} + \bar{\alpha}_n\bar{\alpha}_{-n}) + 2i(k\gamma_3 + \lambda\gamma_1)(\alpha_n\alpha_{-n} - \bar{\alpha}_n\bar{\alpha}_{-n}) \right]. \end{aligned} \quad (4.12)$$

Since the kinetic term in (4.10) is unchanged by the new boundary conditions, we can use the same coordinate transformation as in (3.84) in the previous chapter to bring the Hamiltonian to the form

$$\begin{aligned} \hat{H} &= -\frac{\sqrt{k^2 + \lambda^2}}{32\pi\lambda} \sum_{n \in \mathbb{Z}/\{0\}} n^2 \left[(\gamma_2 + \gamma_3)\sqrt{k^2 + \lambda^2}(\hat{A}_n^+\hat{B}_n^+ + \hat{A}_n^-\hat{B}_n^- + \hat{A}_n^+\hat{A}_n^- + \hat{B}_n^+\hat{B}_n^-) \right. \\ &\quad \left. + (k(\gamma_2 + \gamma_3) + 2\lambda\gamma_1)(\hat{B}_n^+\hat{B}_n^- - \hat{A}_n^+\hat{A}_n^-) + i(\gamma_2 - \gamma_3)\lambda(\hat{A}_n^+\hat{B}_n^+ - \hat{A}_n^-\hat{B}_n^-) \right], \end{aligned} \quad (4.13)$$

where the final term comes from a normal ordering ambiguity from using the commutators. Note here that the Hamiltonian does not contain structures like $\hat{A}_n^+\hat{B}_n^-$ or $\hat{A}_n^-\hat{B}_n^+$. The discrete symmetry in these variables is

$$\begin{aligned} \hat{A}_n^+ &\leftrightarrow i\hat{A}_n^-, \\ \hat{B}_n^+ &\leftrightarrow -i\hat{B}_n^-, \\ k &\rightarrow -k, \quad \gamma_1 \leftrightarrow \gamma_4, \quad \gamma_2 \leftrightarrow \gamma_3. \end{aligned} \quad (4.14)$$

If we take (4.3) for the γ_i in equation (4.13), the first term drops out and this reverts back to the Hamiltonian that we considered in the previous chapter, which comprised of

the remaining two terms. Therefore, we should investigate whether diagonalising these new terms can produce an energy spectrum that is bounded from below, such that if we switch off the remaining terms, we might have a sensible edge-mode theory.

4.2 Bogoliubov transformation

We will employ the Bogoliubov transformation to diagonalise the Hamiltonian. We will begin by applying this technique, as reviewed in [206], for our original Hamiltonian from Section 3.3.

4.2.1 Original edge-mode theory

First, focus on the Hamiltonian (4.13) with (4.3):

$$\hat{H} = \frac{\sqrt{k^2 + \lambda^2}}{16\pi} \sum_{n \in \mathbb{Z}/\{0\}} n^2 \left[v_{re} (\hat{A}_n^+ \hat{A}_n^- - \hat{B}_n^+ \hat{B}_n^-) + i v_{im} (\hat{A}_n^+ \hat{B}_n^+ - \hat{A}_n^- \hat{B}_n^-) \right]. \quad (4.15)$$

In matrix form, this reads

$$\hat{H} = \frac{\sqrt{k^2 + \lambda^2}}{16\pi} \sum_{n \in \mathbb{Z}/\{0\}} \frac{n^2}{2} (\hat{A}_n^+ \hat{B}_n^- \hat{A}_n^- \hat{B}_n^+) \begin{pmatrix} v_{re} & i v_{im} & 0 & 0 \\ -i v_{im} & -v_{re} & 0 & 0 \\ 0 & 0 & v_{re} & -i v_{im} \\ 0 & 0 & i v_{im} & -v_{re} \end{pmatrix} \begin{pmatrix} \hat{A}_n^- \\ \hat{B}_n^+ \\ \hat{A}_n^+ \\ \hat{B}_n^- \end{pmatrix}. \quad (4.16)$$

We will take the transformation

$$\begin{pmatrix} \hat{A}_n^- \\ \hat{B}_n^+ \end{pmatrix} = \begin{pmatrix} u_1 & v_1 \\ v_2 & u_2 \end{pmatrix} \begin{pmatrix} \hat{C}_n^- \\ \hat{D}_n^+ \end{pmatrix}, \quad (4.17)$$

where $u_1, u_2, v_1, v_2 \in \mathbb{C}$. Given the commutation relations

$$[\hat{A}_n^+, \hat{A}_n^-] = [\hat{B}_n^+, \hat{B}_n^-] = \frac{8\pi}{n\sqrt{k^2 + \lambda^2}}, \quad (4.18)$$

and imposing that

$$\begin{aligned} [\hat{C}_n^+, \hat{C}_n^-] &= [\hat{D}_n^+, \hat{D}_n^-] = \frac{8\pi}{n\sqrt{k^2 + \lambda^2}}, \\ [\hat{C}_n^\pm, \hat{D}_n^\pm] &= 0 \end{aligned} \quad (4.19)$$

we have that

$$|u_i|^2 - |v_i|^2 = 1, \quad i \in \{1, 2\}. \quad (4.20)$$

In order to have $[\hat{A}_n^\pm, \hat{B}_n^\pm] = 0$, we also require

$$v_1 u_2^* - u_1 v_2^* = 0. \quad (4.21)$$

We can therefore parametrise the matrix coefficients as

$$\begin{aligned} u_i &= e^{i\theta_i} \cosh r_i, \\ v_i &= e^{i\phi_i} \sinh r_i, \end{aligned} \quad (4.22)$$

with $\{\theta_i, \phi_i, r_i\} \in \mathbb{R}$. Then the condition (4.21) reads

$$\tanh r_1 e^{i(\phi_1 - \theta_2)} = \tanh r_2 e^{i(\theta_1 - \phi_2)}. \quad (4.23)$$

Therefore, we must have

$$r_1 = r_2, \quad \theta_1 + \theta_2 = \phi_1 + \phi_2 + 2n\pi, \quad n \in \mathbb{Z}. \quad (4.24)$$

Focusing on the top left block of the Hamiltonian,

$$\left(\hat{C}_n^+, \hat{D}_n^- \right) \begin{pmatrix} u_1^* & v_2^* \\ v_1^* & u_2^* \end{pmatrix} \begin{pmatrix} v_{re} & i v_{im} \\ -i v_{im} & -v_{re} \end{pmatrix} \begin{pmatrix} u_1 & v_1 \\ v_2 & u_2 \end{pmatrix} \begin{pmatrix} \hat{C}_n^- \\ \hat{D}_n^+ \end{pmatrix}, \quad (4.25)$$

and expanding out the matrices, we find that the off-diagonal terms are complex conjugates of each other. After imposing (4.24), in order for the transformation to produce a diagonal Hamiltonian we must have

$$e^{2i\phi_1} \sinh^2 r = e^{2i\theta_2} \cosh^2 r. \quad (4.26)$$

Thus,

$$\phi_1 = \theta_2, \quad \tanh^2 r = 1, \quad (4.27)$$

which requires $r \rightarrow \infty$. This solution is singular, and therefore our Hamiltonian represents a system at an unstable equilibrium, which is reflected in the fact that the spectrum (3.91) found in the previous chapter is unbounded from below.

4.2.2 Diagonalising the new term

We may simplify our general Hamiltonian (4.13) to just comprise of the term not seen with the previous choice of boundary conditions by choosing the coefficients

$$\gamma_2 = \gamma_3 \equiv \gamma, \quad \gamma_1 = -\frac{k}{\lambda}\gamma. \quad (4.28)$$

Then in matrix form, the Hamiltonian is

$$\hat{H} = -\frac{(k^2 + \lambda^2)\gamma}{32\pi\lambda} \sum_{n \in \mathbb{Z}/\{0\}} n^2 (\hat{A}_n^+ \hat{B}_n^- \hat{A}_n^- \hat{B}_n^+) \begin{pmatrix} 1 & 1 & 0 & 0 \\ 1 & 1 & 0 & 0 \\ 0 & 0 & 1 & 1 \\ 0 & 0 & 1 & 1 \end{pmatrix} \begin{pmatrix} \hat{A}_n^- \\ \hat{B}_n^+ \\ \hat{A}_n^+ \\ \hat{B}_n^- \end{pmatrix}. \quad (4.29)$$

We can attempt to diagonalise this term by taking the same transformation as in equation (4.17), which requires us to again impose the constraints (4.22) and thus (4.24). Then by following the same steps as before, we find that the condition required for the Hamiltonian to be diagonal is

$$0 = e^{i\theta_2} \sinh r + e^{i\phi_1} \cosh r. \quad (4.30)$$

The solution of this is given by

$$\tanh r = -e^{i(\phi_1 - \theta_2)}. \quad (4.31)$$

Since $r \in \mathbb{R}$, this can only be satisfied if $\tanh r = \pm 1$, where $r \rightarrow \pm\infty$. We see that this solution is again singular, and hence does not represent a sensible Bogoliubov transformation. The Hamiltonian (4.29) will also represent a system in an unstable equilibrium, and so including this term in our theory does will not result in a bounded energy spectrum. We have therefore shown that the edge-mode theory considered in Section 3.3 is, in fact, of the most general form for our purposes, and that considering more general boundary conditions for the disc does not provide a richer edge-mode theory.

Conclusion

In this thesis we have delved into various approaches for characterising quantum physics in de Sitter space, often by making use of the topological nature of low-dimensional gravity. In Part I we found that in two-dimensional gravity, it is possible to have thermodynamically stable geometries that interpolate between de Sitter and anti-de Sitter regions. Specifically, for geometries that interpolate to an asymptotically AdS boundary, we postulated the existence of boundary theories whose microscopic degrees of freedom should describe the expanding region in the interior holographically. We suggested two such possible dual theories; a matrix model with a density of eigenstates that dips slightly downwards in comparison to the pure AdS energy density, and an SYK-like theory that includes relevant deformations and, at least naïvely, may have to be non-unitary [67, 131]. We then changed tact and investigated the behaviour of correlation functions in a fixed de Sitter background, working for the most part in two dimensions, but ultimately extending our results to general spacetime dimensions. We showed that in order to reproduce the correct asymptotic form of the two-point function of a massive scalar field, it is crucial to include saddles of complex length in the geodesic approximation. This became evident after analytically continuing the relevant geodesics from the sphere and resulted in an oscillatory behaviour in the two-point function.

In Part II, we explored contributions to the entropy of the de Sitter horizon stemming from topological entanglement entropy. We studied de Sitter in three dimensions, where the Euclidean Chern-Simons path integral produces the exact, all-loop quantum corrected de Sitter entropy. There ought to be an intrinsically Lorentzian Hilbert space interpretation for this entropy as a counting of microscopic states. We proposed that this should take the form of an edge-mode theory living close to the de Sitter horizon and found that, after complexifying the contour of integration in the edge-mode theory, it was possible to reproduce the form of the entropy in an Abelian toy model. Difficulty arises for the full three-dimensional gravity theory due to the non-compactness of the gauge group. We then attempted to tame this unboundedness by exploring more general boundary conditions for the near-horizon region, but found that the theory considered was in fact of the most general type.

Future directions

Having proposed dual matrix model theories to the interpolating geometries in two dimensions, in the future it would be valuable to test these proposals. Recently, much interesting work has been done on generalising the matrix model description to incorporate dilaton gravity theories away from the pure AdS₂ limit [85–87]. It would therefore be fruitful to try and use such methods to pin down the precise form that the matrix model with density of states (1.61) takes. Another way to test this duality would be to incorporate matter in the theory and compare correlation functions of such matter in the bulk and boundary theories [88]. For correlators in the bulk theory, one can use the geodesic approximation discussed in Chapter 2 to reduce the problem to one of computing geodesic lengths, and in the same way that we saw for pure de Sitter, it will likely become crucial to include saddles of complex length in order to do so. Ultimately, one would hope to isolate the de Sitter piece of the ultraviolet theory, and it may be possible to do so by taking a $T\bar{T}$ -like deformation [78, 79].

Furthermore, geodesics are not the only interesting extended extremal objects that are used in holography. For instance, co-dimension 2 surfaces are related to entanglement entropy [207], and co-dimension 1 (or zero), to holographic complexity [208, 209]. It is reasonable to expect the existence of complex surfaces in the context of de Sitter [101]; see also [137]. However, it would be hard to interpret complex areas or volumes as measures of these naturally real quantities. As we have seen, in the case of the two-point function, the complex geodesics combine such that the final answer is real. It would be interesting to understand the more general role that complex surfaces might play in holography. It may also be interesting to study the role of complex geodesics in interacting quantum field theories in de Sitter, perhaps along the lines of the Källén-Lehmann representation [210], or in other backgrounds with positive cosmological constant, such as de Sitter black holes.

As previously mentioned, it has been advocated that the dual theory to de Sitter might live on a stretched horizon [29, 30, 211]. The microscopic candidate theory is an SYK model in a particular double-scaled limit [28, 212–214]. We computed correlation functions of bulk scalar fields anchored at opposite stretched horizons in Section 2.4. The conclusion is that real geodesics exist only up to some critical time t_c , that depends on the position of the stretched horizon. After this time, the correlator starts exhibiting oscillations, and the geodesic length becomes complex. Using holography, we would expect the boundary theory to know about this time scale. It looks hard to envision how a standard SYK model would incorporate this scale. Other proposals relating non-Hermitian SYK models to de Sitter include [67, 131, 215].

From the three-dimensional perspective, in future work it would be interesting to attempt to converge on the full, non-Abelian three-dimensional gravity theory from the perspective of a large- N limit. Chern-Simons theory with gauge group $SU(N)$ describes higher spin gravity and, upon taking a 't Hooft limit with $N \rightarrow \infty$ and large level, admits a description in terms of a topological string theory [216]. Presumably, this must be related to a corresponding Lorentzian picture by way of a large- N Wess-Zumino-Witten model with gauge group $SU(N)_k$. It has been suggested that this theory reduces to one consisting of free fermions [217]. Therefore, one hopes this will provide another simplified environment in which to study contributions to the de Sitter horizon entropy stemming from topological entanglement entropy. Furthermore, given that JT gravity can be rewritten in the first order formalism as a BF theory, which in turn can be found as a dimensional reduction from Chern-Simons theory in three dimensions, it may be worthwhile to explore combining the 2D and 3D perspectives described in this work. One can ask if there is a notion of topological entanglement entropy in 2D gravity [218,219], and therefore whether it is possible to replicate the setup explored in Part II in the lower dimensional theory. It would be interesting to use such a setup to see if there might be an entanglement nature to the quantum entropy of the de Sitter horizon in two dimensions as well.

One of the major motivations for pursuing a quantum theory of de Sitter in low-dimensional gravity was the hope that our findings would elucidate some features of the more physical, four-dimensional theory. This could occur quite directly in the two-dimensional case, due to the fact that the near-horizon limit of the Nariai black hole is $dS_2 \times S^2$. Thus, if one could successfully isolate the ultraviolet theory that describes dS_2 , then it may be possible to use this to describe the microscopic degrees of freedom of the four-dimensional black hole in de Sitter, at least in some limit. The influence of our three-dimensional results on the 4D case may be somewhat more philosophical, in the sense that if it is possible to converge on a Lorentzian edge-mode theory that correctly reproduces the exact Gibbons-Hawking entropy, then this suggests that we should take seriously the proposal that the de Sitter horizon entropy is counting microstates. We saw in three dimensions that entanglement entropy was a key contribution to this entropy, stemming from the fact that we can rewrite gravity as a gauge theory precisely in this case. However, diffeomorphisms act as gauge symmetries in gravity in any dimensions, and so this implies that there should be some entanglement nature of the entropy in higher dimensional theories as well.

Appendices

Appendix A

Thermodynamics of finite boundary geometries

In this appendix we consider pure JT gravity and the dilaton-gravity model arising from the dimensional reduction of four-dimensional Einstein gravity in the presence of a Dirichlet boundary.

A.1 AdS₂ JT gravity

The dilaton potential that gives rise to an AdS₂ geometry is $V(\phi) = 2\phi$. We can see that this potential results in the Euclidean AdS₂ black hole metric (which is the Poincaré disc) by using equation (1.10):

$$\frac{ds^2}{\ell^2} = (r^2 - r_h^2)d\tau^2 + \frac{dr^2}{(r^2 - r_h^2)}, \quad r \in [r_h, \infty), \quad (\text{A.1})$$

where $r_h > 0$ and $\tau \sim \tau + \beta$. The on-shell action is

$$\log Z_{\text{AdS}_2} = 2\pi\phi_0 + \beta\phi_b^2, \quad (\text{A.2})$$

with the Euclidean time periodicity $\beta = 2\pi/r_h$. The Tolman temperature is

$$\beta_T = \frac{2\pi}{\phi_h} \sqrt{r_b^2 - \phi_h^2}, \quad (\text{A.3})$$

where, as previously, $\phi_h = r_h$. One thus finds [220]

$$-\beta_T F_{\text{AdS}_2} = 2\pi\phi_0 + \phi_b \sqrt{4\pi^2 + \beta_T^2}. \quad (\text{A.4})$$

Using the expressions (1.17), (1.18), and (1.19), we find the following thermodynamic quantities

$$E_{\text{AdS}_2} = -\sqrt{\phi_b^2 - \phi_h^2}, \quad S_{\text{AdS}_2} = 2\pi\phi_0 + 2\pi\phi_h, \quad C_{\text{AdS}_2} = \frac{4\pi^2\phi_b\beta_T^2}{(\beta_T^2 + 4\pi^2)^{3/2}}. \quad (\text{A.5})$$

We note that C_{AdS_2} is manifestly positive since $\phi_b > 0$. If we take $\phi_b \gg 1$, we find the leading order expressions

$$E_\infty = -\phi_b + \frac{2\pi^2}{\phi_b\beta^2}, \quad S_\infty = 2\pi\phi_0 + \frac{4\pi^2}{\beta}, \quad C_\infty = \frac{4\pi^2}{\beta}, \quad (\text{A.6})$$

in agreement with the known expressions (see, for example, [119]) for asymptotically near-AdS₂, up to a physically inconsequential shift in E_∞ . We note that in this limit thermodynamical variations are with respect to β which is defined entirely at the horizon.

A.2 Schwarzschild dilaton gravity

The dilaton potential that appears in the dimensional reduction of the four-dimensional Schwarzschild solution is [221]

$$V(\phi) = \frac{1}{2\sqrt{\phi}}, \quad \phi \geq 0. \quad (\text{A.7})$$

Using (1.10) we find the two-dimensional Euclidean metric

$$\frac{ds^2}{\ell^2} = (\sqrt{r} - \sqrt{r_h}) d\tau^2 + \frac{dr^2}{(\sqrt{r} - \sqrt{r_h})}. \quad (\text{A.8})$$

The on-shell Euclidean action yields

$$\log Z_{\text{flat}} = 2\pi\phi_0 + \beta \left(\sqrt{\phi_b} - \frac{3}{4}\sqrt{\phi_h} \right), \quad (\text{A.9})$$

where $\beta = 8\pi\sqrt{r_h}$ is the periodicity in Euclidean time and $\phi_h = r_h$. The Tolman temperature is

$$\beta_T = 8\pi\sqrt{\phi_h}\sqrt{\sqrt{r_b} - \sqrt{\phi_h}}. \quad (\text{A.10})$$

The thermodynamic properties of Schwarzschild in two dimensions with a finite boundary are found to be

$$E_{\text{flat}} = -\sqrt{\sqrt{\phi_b} - \sqrt{\phi_h}}, \quad S_{\text{flat}} = 2\pi(\phi_0 + \phi_h), \quad C_{\text{flat}} = \frac{8\pi\phi_h(\sqrt{\phi_b} - \sqrt{\phi_h})}{3\sqrt{\phi_h} - 2\sqrt{\phi_b}}. \quad (\text{A.11})$$

Here we see further evidence of a finite boundary resulting in a transition from positive to negative heat capacity. Since $\phi_b > \phi_h > 0$, the numerator of C_{flat} in (A.11) is always positive, but the sign of the denominator depends on the location of the wall with respect to ϕ_h . This is the phenomenon observed by York for Schwarzschild black holes in a Dirichlet box [72, 84].

Appendix B

Double interpolating geometry with finite boundary

In this appendix, we consider the Dirichlet problem, with β_T and ϕ_b fixed, for the dilaton-gravity theory with potential (1.55).

For $\phi_b > 0$, the temperatures of each saddle are

$$\beta_T^1 = \frac{4\pi}{|2\phi_1 + \tilde{\phi} - 4x|} \sqrt{r_b^2 + \tilde{\phi} r_b - 2x^2 + \phi_1(4x - \phi_1 - \tilde{\phi})}, \quad (\text{B.1})$$

$$\beta_T^2 = \frac{4\pi}{|\tilde{\phi} - 2\phi_2|} \sqrt{r_b^2 + \phi_2^2 + \tilde{\phi}(r_b - \phi_2)}, \quad (\text{B.2})$$

$$\beta_T^3 = \frac{4\pi}{|\tilde{\phi} + 2\phi_3|} \sqrt{r_b^2 - \phi_3^2 + \tilde{\phi}(r_b - \phi_3)}. \quad (\text{B.3})$$

Case 1: $\tilde{\phi} \geq 0$

We require $\phi_b > 0$ in order to have a geometry containing the full, double interpolating solution (1.56). The free energy of the first saddle at ϕ_1 is

$$-\beta_T F_1 = 2\pi \left(\phi_0 + 2x - \frac{\tilde{\phi}}{2} \right) + \frac{1}{2} \sqrt{(\beta_T^2 + 4\pi^2) \left((2\phi_b + \tilde{\phi})^2 + 8x^2 - 8x\tilde{\phi} \right)}. \quad (\text{B.4})$$

The properties of the second and third saddles have been described in Section 1.3.2, with their free energies given by (1.48) and (1.46) respectively. From equation (1.19), the heat

capacity of the double interpolating saddle is

$$C_1 = \frac{2\pi^2\beta_T^2\sqrt{(2\phi_b + \tilde{\phi})^2 + 8x^2 - 8x\tilde{\phi}}}{(\beta_T^2 + 4\pi^2)^{3/2}} > 0, \quad (\text{B.5})$$

and hence the saddle is stable, similarly to the case with an asymptotic AdS₂ boundary. The heat capacity of the second saddle C_2 will be either (1.49) or (1.50) depending on the ranges of β_T and ϕ_b as described in Section 1.3.2. The third saddle C_3 will have specific heat (1.47).

First take the case $\frac{4\pi}{\tilde{\phi}}\sqrt{\phi_b(\phi_b + \tilde{\phi})} \geq \beta_T \geq 2\pi$ and $\phi_b \geq \chi_-$ such that the second saddle has heat capacity (1.49) and is unstable. Then comparing the free energies of the first and third saddle we find

$$\begin{aligned} \Delta F &= F_3 - F_1 \\ &= \frac{1}{2\beta_T} \left(8\pi x - \sqrt{\beta_T^2 + 4\pi^2} (2\phi_b + \tilde{\phi}) + \sqrt{(\beta_T^2 + 4\pi^2) \left((2\phi_b + \tilde{\phi})^2 + 8x^2 - 8x\tilde{\phi} \right)} \right). \end{aligned} \quad (\text{B.6})$$

This can either be positive or negative depending on the range of x . The difference is positive if

$$x < \frac{1}{\beta_T^2 - 4\pi^2} \left((\beta_T^2 + 4\pi^2)\tilde{\phi} - 2\pi\sqrt{(\beta_T^2 + 4\pi^2)(4\phi_b^2 + 4\phi_b\tilde{\phi} + \tilde{\phi}^2)} \right), \quad (\text{B.7})$$

and negative otherwise. For example, take $\tilde{\phi} = 1$, $\phi_b = 1$ and $\beta_T = 4\pi$ to satisfy the conditions on ϕ_b and β_T . Then if $x < \frac{5}{3} - \sqrt{5}$ then (B.6) will be positive and otherwise it will be negative. Thus, for certain temperatures, the double interpolating saddle will be dominant.

When instead we take $\frac{4\pi}{\tilde{\phi}}\sqrt{\phi_b(\phi_b + \tilde{\phi})} < \beta_T < 2\pi$ and $\phi_b < \chi_-$, we have a stable saddle at ϕ_2 and no longer have a saddle at ϕ_3 . In this case the difference in free energies is

$$\begin{aligned} \Delta F &= F_2 - F_1 = \frac{1}{2\beta_T} \left(4\pi(2x - \tilde{\phi}) + \right. \\ &\quad \left. \sqrt{(\beta_T^2 + 4\pi^2)(8x^2 - 8x\tilde{\phi} + (2\phi_b + \tilde{\phi})^2)} + \sqrt{(4\pi^2 - \beta_T^2)(\tilde{\phi}^2 - 4\phi_b\tilde{\phi} - 4\phi_b^2)} \right), \end{aligned} \quad (\text{B.8})$$

which is negative for this range of β_T . Therefore, the interpolating saddle will dominate over the double interpolating one.

Case 2: $\tilde{\phi} < 0$

In this case, the free energy and heat capacity will still be given by (B.4) and (B.5) respectively. To ensure that these expressions are real, we must have $(2\phi_b + \tilde{\phi})^2 > 8x(\tilde{\phi} - x)$. As in the case $\tilde{\phi} < 0$ in Section 1.3.2, the change in sign of $\tilde{\phi}$ restricts the possible ranges of β_T . Again, the first case is when $\sqrt{2\pi} \left| \frac{2\phi_b + \tilde{\phi}}{\tilde{\phi}} \right| \geq \beta_T \geq 2\pi$ and $\phi_b \geq -\chi_+$ where the ϕ_2 saddle is again unstable. The difference between the free energies of the third and first saddle is (B.6). For $\tilde{\phi} < 0$ this can again be either positive if the condition (B.7) is satisfied, or negative otherwise.

If instead, $\sqrt{2\pi} \left| \frac{2\phi_b + \tilde{\phi}}{\tilde{\phi}} \right| < \beta_T < 2\pi$ and $|\tilde{\phi}|/2 < \phi_b < -\chi_+$, then all three saddles at ϕ_1 , ϕ_2 and ϕ_3 are stable. As seen in equation (1.53), in this case the AdS₂ saddle at ϕ_3 is thermodynamically favoured over the interpolating one at ϕ_2 . The difference in the free energies between ϕ_3 and ϕ_1 is again given by (B.6), which in this case will be negative, and so the AdS₂ saddle at ϕ_3 is favoured. However, if $0 < \phi_b < |\tilde{\phi}|/2$ then there is no ϕ_3 saddle and the difference between the ϕ_1 and ϕ_2 saddles is given by (B.8), which again is negative under the assumptions we have here. Therefore, the interpolating saddle will again dominate over the double interpolating one.

Appendix C

WKB approximation

The Klein-Gordon equation as a function of $P \equiv P_{X,Y}$ can be solved systematically, order by order in the large mass expansion, through a WKB approach. A similar procedure is followed in Appendix B of [222] for the case of timelike geodesics in AdS.

To start, we recall here equation (2.5),

$$(1 - P^2)\partial_P^2 G(P) - dP\partial_P G(P) - m^2\ell^2 G(P) = 0. \quad (\text{C.1})$$

We take the ansatz,

$$G(P) \propto \exp(-m\ell X(P)), \quad (\text{C.2})$$

where X is assumed to be independent of m . At leading order in the large mass limit, it satisfies the equation,

$$(P^2 - 1) X'(P)^2 + 1 = 0. \quad (\text{C.3})$$

This equation is solved by

$$X_{\pm}^{(1)}(P) = c_{\pm}^{(1)} \pm \arccos P, \quad \text{for } P < -1, \quad (\text{C.4})$$

$$X_{\pm}^{(2)}(P) = c_{\pm}^{(2)} \pm \arccos P, \quad \text{for } -1 < P < 1, \quad (\text{C.5})$$

$$X_{\pm}^{(3)}(P) = c_{\pm}^{(3)} \pm \arccos P, \quad \text{for } P > 1. \quad (\text{C.6})$$

The six constants $c_{\pm}^{(i)}$ will be fixed later. To next order, we add functions $A_{\pm}^{(i)}(P)$, such that now,

$$G^{(j)}(P) = m^{\alpha} \sum_{i=\pm} A_i^{(j)}(P) \exp\left(-m\ell X_i^{(j)}(P)\right), \quad (\text{C.7})$$

where α is an arbitrary constant, and we again assume that the functions $A_{\pm}^{(i)}(P)$ are independent of m . Plugging this back in the Klein-Gordon equation, we obtain

$$(d-1)PA_i^{(j)} + 2(P^2 - 1)\partial_P A_i^{(j)} = 0, \quad (\text{C.8})$$

which is solved by

$$A_i^{(j)}(P) = a_i^{(j)}(1 - P^2)^{\frac{1-d}{4}}, \quad (\text{C.9})$$

where $a_i^{(j)}$ are constant factors. Although $a_i^{(j)}$ and $c_{\pm}^{(i)}$ are a priori not independent, they represent multiplicative factors with different powers of m , and thus they have to be treated separately. The general solution we obtain for the propagator at this order is given by

$$G^{(j)}(P) = \frac{m^{\alpha}}{(1 - P^2)^{\frac{d-1}{4}}} \left[a_+^{(j)} e^{-m\ell(c_+^{(j)} + \arccos P)} + a_-^{(j)} e^{-m\ell(c_-^{(j)} - \arccos P)} \right]. \quad (\text{C.10})$$

The solutions (C.4)-(C.6) break down near $P = \pm 1$ when $1 - P^2 \sim (m\ell)^{-2}$. In order to connect the solutions in the three disjoint domains, we need to solve (C.1) exactly near $P = \pm 1$ and then match the solution to the adjacent WKB solutions.

Let us start with $P = -1$. In the vicinity of this point, (C.1) simplifies to

$$2(P+1)\partial_P^2 G(P) + d\partial_P G(P) - m^2\ell^2 G(P) = 0, \quad (\text{C.11})$$

which is solved by

$$G(P) = (P+1)^{\frac{2-d}{4}} \left[aI_{\frac{d}{2}-1} \left(m\ell\sqrt{2P+2} \right) + bK_{\frac{d}{2}-1} \left(m\ell\sqrt{2P+2} \right) \right], \quad (\text{C.12})$$

where a and b are two constants and I and K are modified Bessel functions. In order to recover (2.16), we need to set

$$a = 2^{\frac{1}{2} - \frac{3d}{4}} \left(\frac{\pi\ell}{m} \right)^{1 - \frac{d}{2}} e^{-m\ell\pi}, \quad b = 0. \quad (\text{C.13})$$

This completely fixes the form of the correlator. We now proceed to match this locally exact solution to the WKB solutions in (C.4)-(C.5). For $P < -1$ taking the large- m limit of (C.12) gives

$$G(P) = -2^{\frac{3}{4}(1-d)} m^{\frac{d-3}{2}} (\pi\ell)^{\frac{1-d}{2}} e^{-m\ell\pi} (-1 - P)^{\frac{1-d}{4}} \sin \left(m\ell\sqrt{-2 - 2P} - \frac{\pi(d+1)}{4} \right). \quad (\text{C.14})$$

Using $\arccos P \approx \pi - i\sqrt{2}\sqrt{-1-P}$, (C.4) can be matched to (C.14). This fixes the constants to be

$$\alpha = \frac{d-3}{2}, \quad a_-^{(1)} = i^{d-1} 2^{-\frac{d+1}{2}} (\pi\ell)^{\frac{1-d}{2}}, \quad a_+^{(1)} = 2^{-\frac{d+1}{2}} (\pi\ell)^{\frac{1-d}{2}}, \quad c_-^{(1)} = 2\pi, \quad c_+^{(1)} = 0.$$

Plugging these back into (C.4), we obtain the simple expression

$$G^{(1)}(P) = m^{\frac{d-3}{2}} (2\pi\ell)^{\frac{1-d}{2}} \operatorname{Re} \left[\frac{e^{-m\ell \arccos P}}{(1-P^2)^{\frac{d-1}{4}}} \right], \quad \text{valid for } P < -1. \quad (\text{C.15})$$

This expression recovers (2.14), which has been obtained from a large- m limit of the exact (hypergeometric) solution to (C.1). Similarly, for $P > -1$ taking the large- m limit of (C.12) gives

$$G(P) = 2^{-\frac{3d+1}{4}} m^{\frac{d-3}{2}} (\pi\ell)^{\frac{1-d}{2}} (1+P)^{\frac{1-d}{4}} e^{m\ell\sqrt{2+2P}-m\ell\pi}. \quad (\text{C.16})$$

Using $\arccos P \approx \pi - \sqrt{2}\sqrt{P+1}$, this can be matched to the solution in (C.5) with the plus sign,

$$a_-^{(2)} = 0, \quad a_+^{(2)} = 2^{-\frac{d+1}{2}} (\pi\ell)^{\frac{1-d}{2}}, \quad c_+^{(2)} = 0.$$

Note that the only difference compared to the $P < -1$ solution is that the X_- component is exponentially suppressed and therefore no longer present. The WKB solution to the correlator becomes

$$G^{(2)}(P) = \frac{1}{2} \times m^{\frac{d-3}{2}} (2\pi\ell)^{\frac{1-d}{2}} \frac{e^{-m\ell \arccos P}}{(1-P^2)^{\frac{d-1}{4}}}, \quad \text{valid for } -1 < P < 1. \quad (\text{C.17})$$

The expression recovers (2.15). In order to connect the solution in the middle domain to that in $P > 1$, we need to investigate the $P \approx 1$ region. Here we have the locally exact solution

$$G(P) = (1-P)^{\frac{2-d}{4}} \left[\tilde{a} I_{\frac{d}{2}-1} \left(m\ell\sqrt{2-2P} \right) + \tilde{b} K_{\frac{d}{2}-1} \left(m\ell\sqrt{2-2P} \right) \right]. \quad (\text{C.18})$$

Matching it to (C.17) fixes the constants

$$\tilde{a} = 0, \quad \tilde{b} = 2^{\frac{1}{2}-\frac{3d}{4}} \left(\frac{\ell}{m} \right)^{1-\frac{d}{2}} \pi^{-\frac{d}{2}}. \quad (\text{C.19})$$

These coefficients can also be independently verified by matching (C.18) to the flat space short distance singularity (2.8), and using the asymptotic expansion of the modified Bessel

K function,

$$K_{\frac{d}{2}-1}(z) \sim \begin{cases} -\log\left(\frac{z}{2}\right) + \Gamma'(1) & d = 2, \\ \frac{\Gamma\left(\frac{d}{2} - 1\right)}{2} \left(\frac{2}{z}\right)^{\frac{d}{2}-1} & d > 2, \end{cases} \quad (\text{C.20})$$

which is valid for $0 < |z| \ll \sqrt{\frac{d}{2}}$. The $d = 2$ case reproduces (2.9) up to an overall additive constant. We note that matching (C.18) to (C.6) implies that (C.17) remains valid in the $P > 1$ region,

$$G^{(3)}(P) = G^{(2)}(P), \quad \text{valid for } P > 1. \quad (\text{C.21})$$

Finally, note that in this WKB approximation the equation is solved order-by-order in m , and so this method validates the subtle limit of the hypergeometric function that we took in the main text.

Appendix D

Quantum mechanical path integral

In this appendix, we would like to evaluate the following (Euclidean) path integral,

$$Z(\Phi_0, \Phi_N) = \int_{\delta\Theta(\Phi_0)=0}^{\delta\Theta(\Phi_N)=0} D\delta\Theta \exp \left(-m \int_{\Phi_0}^{\Phi_N} d\Phi L(\Phi, \delta\Theta, \delta\dot{\Theta}) \right), \quad (\text{D.1})$$

for a generic quadratic Lagrangian of the form

$$L(\Phi, \delta\Theta, \delta\dot{\Theta}) = \frac{\ell}{2} \left(\delta\dot{\Theta}^2 + \alpha(\Phi)\delta\Theta^2 \right), \quad (\text{D.2})$$

with $\alpha(\Phi)$ an arbitrary function of Φ . This path integral is the quadratic correction to the saddle-point solution, and so we want the fluctuations to vanish at the endpoints. This is a textbook path integral that can be solved by discretising the Φ interval, see for instance [223]. By definition, we would like to compute

$$Z(\Phi_0, \Phi_N) = \lim_{N \rightarrow \infty} \left(\frac{m\ell}{2\pi\Delta\Phi} \right)^{N/2} \int d\delta\Theta_1 \cdots \int d\delta\Theta_{N-1} \exp \left(-m\ell\Delta\Phi \sum_{j=0}^{N-1} \left(\frac{(\delta\Theta_{j+1} - \delta\Theta_j)^2}{2\Delta\Phi^2} + \frac{\alpha_j}{2} \delta\Theta_j^2 \right) \right), \quad (\text{D.3})$$

where $\Phi_j = \Phi_0 + j\Delta\Phi$ and $\alpha_j = \alpha(\Phi_j)$. The exponent in this equation can be written in a quadratic form,

$$\left(-m\ell\Delta\Phi \sum_{j=0}^{N-1} \left(\frac{(\delta\Theta_{j+1} - \delta\Theta_j)^2}{2\Delta\Phi^2} + \frac{\alpha_j}{2} \delta\Theta_j^2 \right) \right) = - \sum_{j,k=1}^{N-1} \delta\Theta_j a_{jk} \delta\Theta_k, \quad (\text{D.4})$$

where a_{jk} are the matrix elements of the following $(N - 1) \times (N - 1)$ matrix,

$$(a_{jk}) = \frac{m\ell}{2\Delta\Phi} \begin{bmatrix} 2 & -1 & 0 & \dots & 0 & 0 \\ -1 & 2 & -1 & \dots & 0 & 0 \\ 0 & -1 & 2 & \dots & 0 & 0 \\ \vdots & \vdots & \vdots & \ddots & \vdots & \vdots \\ 0 & 0 & 0 & \dots & 2 & -1 \\ 0 & 0 & 0 & \dots & -1 & 2 \end{bmatrix} + \frac{m\ell\Delta\Phi}{2} \begin{bmatrix} \alpha_1 & 0 & 0 & \dots & 0 & 0 \\ 0 & \alpha_2 & 0 & \dots & 0 & 0 \\ 0 & 0 & \alpha_3 & \dots & 0 & 0 \\ \vdots & \vdots & \vdots & \ddots & \vdots & \vdots \\ 0 & 0 & 0 & \dots & \alpha_{N-2} & 0 \\ 0 & 0 & 0 & \dots & 0 & \alpha_{N-1} \end{bmatrix}. \quad (\text{D.5})$$

If $\det(a_{jk}) \neq 0$, then we can do the multiple Gaussian integrals to obtain,

$$\begin{aligned} Z(\Phi_0, \Phi_N) &= \lim_{N \rightarrow \infty} \left(\frac{m\ell}{2\pi\Delta\Phi} \right)^{N/2} \left(\frac{\pi^{N-1}}{\det a_{jk}} \right)^{1/2} \\ &= \lim_{N \rightarrow \infty} \left(\frac{m\ell}{2\pi} \frac{1}{\Delta\Phi \left(\frac{2\Delta\Phi}{m\ell} \right)^{N-1} \det a_{jk}} \right)^{1/2}. \end{aligned} \quad (\text{D.6})$$

It is convenient to define the following function,

$$f(\Phi_0, \Phi_N) \equiv \lim_{N \rightarrow \infty} \left(\Delta\Phi \left(\frac{2\Delta\Phi}{m\ell} \right)^{N-1} \det a_{jk} \right). \quad (\text{D.7})$$

In order to take the $N \rightarrow \infty$ limit, we first define the discrete determinant,

$$\begin{aligned} D_{N-1} &\equiv \left(\frac{2\Delta\Phi}{m\ell} \right)^{N-1} \det a_{jk} \\ &= \begin{vmatrix} 2 + \Delta\Phi^2\alpha_1 & -1 & 0 & \dots & 0 & 0 \\ -1 & 2 + \Delta\Phi^2\alpha_2 & -1 & \dots & 0 & 0 \\ 0 & -1 & 2 + \Delta\Phi^2\alpha_3 & \dots & 0 & 0 \\ \vdots & \vdots & \vdots & \ddots & \vdots & \vdots \\ 0 & 0 & 0 & \dots & 2 + \Delta\Phi^2\alpha_{N-2} & -1 \\ 0 & 0 & 0 & \dots & -1 & 2 + \Delta\Phi^2\alpha_{N-1} \end{vmatrix}. \end{aligned} \quad (\text{D.8})$$

Now we assume that the dimension of the matrix is variable, so $n = N - 1$ can vary. We take the determinant using the last column to obtain the following recursion relation,

$$D_n = (2 + \Delta\Phi^2\alpha_n) D_{n-1} - D_{n-2}. \quad (\text{D.9})$$

The first two determinants are given by $D_1 = 2 + \Delta\Phi^2\alpha_1$ and $D_2 = 3 + 2\Delta\Phi^2(\alpha_1 + \alpha_2) + \Delta\Phi^4\alpha_1\alpha_2$. Using these along with (D.9), we can analytically continue the discrete determinant to $n \in \mathbb{Z}_{\leq 0}$, finding, for example, $D_0 = 1$ and $D_{-1} = 0$. Rewriting the recursion relation in a more suggestive way, we obtain

$$\frac{D_{n+1} - 2D_n + D_{n-1}}{\Delta\Phi^2} = \alpha_{n+1}D_n. \quad (\text{D.10})$$

But now we are interested in the continuum limit of this expression, where $\Delta\Phi \rightarrow 0$ (or $N \rightarrow \infty$), so we may interpret the above recursion relation as a second order differential equation in the variable $\Phi = N\Delta\Phi + \Phi_0$. Note that the extra factor of $\Delta\Phi$ in (D.7) cancels since the above equation is linear in D . We then get,

$$\frac{d^2 f(\Phi_0, \Phi)}{d\Phi^2} = \alpha(\Phi)f(\Phi_0, \Phi). \quad (\text{D.11})$$

The boundary conditions $D_0 = 1$ and $D_{-1} = 0$ give,

$$f(\Phi_0, \Phi_0) = \lim_{N \rightarrow \infty} \Delta\Phi D_{-1} = 0, \quad (\text{D.12})$$

$$\left. \frac{df(\Phi_0, \Phi)}{d\Phi} \right|_{\Phi=\Phi_0} = \lim_{N \rightarrow \infty} \Delta\Phi \frac{(D_0 - D_{-1})}{\Delta\Phi} = 1. \quad (\text{D.13})$$

Now that we have f , we can go back to (D.6) to find the final result for the path integral, which reads

$$Z(\Phi_0, \Phi_N) = \sqrt{\frac{m\ell}{2\pi f(\Phi_0, \Phi_N)}}. \quad (\text{D.14})$$

In Chapter 2 we had $\alpha(\Phi) = -1$, so we get $f(\Phi_0, \Phi_N) = \sin(\Phi_N - \Phi_0)$. This is the result we used in the main text to compute the first correction to the geodesic length, see (2.42).

Appendix E

Geodesic equation in higher dimensions

Here we show that the geodesic equations for the d -dimensional sphere are solved by $\Theta_i = 0$. The metric of dS_d can be written compactly as

$$\frac{ds^2}{\ell^2} = \sum_{a=1}^d \left(\prod_{m=1}^{a-1} \cos^2 \Theta_m \right) d\Theta_a^2, \quad (\text{E.1})$$

where $-\frac{\pi}{2} \leq \Theta_i \leq \frac{\pi}{2}$ for $1 \leq i < d-1$ and $0 \leq \Theta_d < 2\pi$ with $\Theta_d \equiv \Phi$. As in the two-dimensional case, we can use Φ to parameterise the geodesic so that it will follow a path $(\Theta_1(\Phi), \dots, \Theta_{d-1}(\Phi))$, that extremises the length functional,

$$\tilde{L}^d = \ell \int d\Phi \sqrt{\sum_{a=1}^d \left(\prod_{m=1}^{a-1} \cos^2 \Theta_m \right) \dot{\Theta}_a^2}, \quad (\text{E.2})$$

where again the dot represents a derivative with respect to $\Phi \equiv \Theta_d$, so that $\dot{\Theta}_d = 1$. The Euler-Lagrange equations are

$$\frac{\partial \mathcal{L}}{\partial \Theta_i} - \frac{d}{d\Phi} \left(\frac{\partial \mathcal{L}}{\partial \dot{\Theta}_i} \right) = 0, \quad (\text{E.3})$$

where \mathcal{L} is the integrand of (E.2). We find that

$$\begin{aligned} \frac{\partial \mathcal{L}}{\partial \dot{\Theta}_i} &= \frac{\dot{\Theta}_i}{\mathcal{L}} \prod_{m=1}^{i-1} \cos^2 \Theta_m, \\ \frac{\partial \mathcal{L}}{\partial \Theta_i} &= -\frac{\sin \Theta_i \cos \Theta_i}{\mathcal{L}} \left(\prod_{n=1}^{i-1} \cos^2 \Theta_n \right) \left(\sum_{a=i+1}^d \left(\prod_{m=i+1}^{a-1} \cos^2 \Theta_m \right) \dot{\Theta}_a^2 \right). \end{aligned} \quad (\text{E.4})$$

with $i = 1, \dots, d - 1$. It can be shown that

$$\frac{d}{d\Phi} \left(\frac{\partial \mathcal{L}}{\partial \dot{\Theta}_i} \right) = \left(\frac{\ddot{\Theta}_i}{\mathcal{L}} - \frac{\dot{\Theta}_i}{\mathcal{L}^2} \frac{d\mathcal{L}}{d\Phi} - \frac{2\dot{\Theta}_i}{\mathcal{L}} \sum_{j=1}^{i-1} \tan \Theta_j \dot{\Theta}_j \right) \prod_{n=1}^{i-1} \cos^2 \Theta_n. \quad (\text{E.5})$$

The equation of motion will therefore have an overall factor of $\prod_{n=1}^{i-1} \cos^2 \Theta_n$. We will choose the endpoints of the geodesics to lie at $\Theta_i(\Phi_1) = 0$ and $\Theta_i(\Phi_2) = 0$ for all $i = 1, \dots, d - 1$. Therefore, although it appears that $\Theta_i = \pm \frac{\pi}{2}$ would solve the equation of motion for $i = 2, \dots, d - 1$, this solution does not obey the boundary conditions and so we neglect it. For $i = 1$ this product evaluates to 1, and so we can focus on the equation without this overall factor. Therefore, the equation of motion is

$$\left(\sin \Theta_i \cos \Theta_i \left(\sum_{a=i+1}^d \left(\prod_{m=i+1}^{a-1} \cos^2 \Theta_m \right) \dot{\Theta}_a^2 \right) + \ddot{\Theta}_i - \frac{\dot{\Theta}_i}{\mathcal{L}} \frac{d\mathcal{L}}{d\Phi} - 2\dot{\Theta}_i \sum_{j=1}^{i-1} \tan \Theta_j \dot{\Theta}_j \right) = 0, \quad (\text{E.6})$$

where

$$\frac{d\mathcal{L}}{d\Phi} = \frac{\partial \mathcal{L}}{\partial \dot{\Theta}_i} \ddot{\Theta}_i + \frac{\partial \mathcal{L}}{\partial \Theta_i} \dot{\Theta}_i, \quad (\text{E.7})$$

with the various terms above defined in equation (E.4). Therefore, we can see that $\Theta_i = 0$, for $i = 1, \dots, d - 1$ is a solution to equation (E.6).

Appendix F

Details on the stretched horizon

To find the geodesics between complimentary stretched horizons, it is useful to relate the global (5) and static coordinates (8) in embedding space. These are related to the three-dimensional Minkowski coordinates by

$$\begin{aligned} X_0 &= \ell \sinh T &= \ell \sqrt{1-r^2} \sinh t, \\ X_1 &= \ell \cos \varphi \cosh T &= \ell r, \\ X_2 &= \ell \sin \varphi \cosh T &= \ell \sqrt{1-r^2} \cosh t. \end{aligned} \tag{F.1}$$

Rearranging, we can write the global coordinates in terms of the static ones as

$$T(r, t) = \operatorname{arcsinh} \left(\sqrt{1-r^2} \sinh t \right), \tag{F.2}$$

$$\varphi(r, t) = \arccos \left(\frac{r}{\sqrt{\cosh^2 t - r^2 \sinh^2 t}} \right). \tag{F.3}$$

It is clear from this that the points opposite each other with a fixed $r = r_{st}$ will have the same T_0 and their angles will be at φ_0 and $-\varphi_0$. This gives the de Sitter invariant distance written in the main text,

$$P_{X,Y}^{st} = \frac{1}{\ell^2} [-(X_0)^2 + (X_1)^2 - (X_2)^2] = (r_{st}^2 - 1) \cosh 2t + r_{st}^2. \tag{F.4}$$

We can also recover the critical time from geometric arguments. Starting from $t = 0$ and increasing in time, note that there are two final geodesics at a time $|t| = t_c$ that are almost null. After this, there are no more real geodesics. Let us compute $P_{X,Y}$ for the endpoints of the final geodesics. Recall that in $d = 2$ the full Penrose diagram is two copies of the usual square. If we call Y the point on the right of the Penrose diagram, it is easy to see that its

antipodal point \bar{Y} will be outside the Penrose diagram and will be null separated to X , the left endpoint of the geodesic, see Figure F.1. If X is null separated from the antipodal point of Y , then the last geodesics have $P_{X,Y} = -1$. To compute t_c we just need to use the metric in static coordinates (7), and find a null ray that passes through the point $(r = 0, t = 0)$. That ray intersects $r = r_{st}$ at exactly the t_c given by (2.57). So, we have recovered this time scale from a geometric point of view.

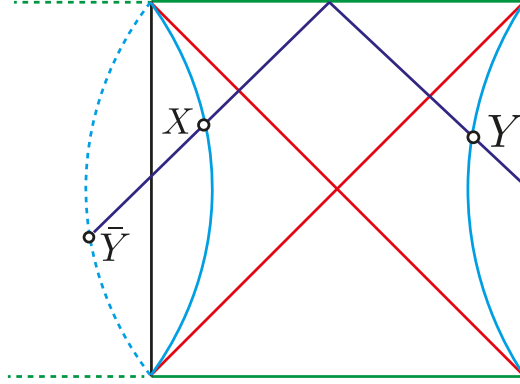


Figure F.1: Illustration of the null rays involved in fixing the critical static time t_c , after which symmetric geodesics between the two stretched horizons do not exist anymore.

Appendix G

Chern-Simons determinant on S^3

In this appendix, we consider the determinant that stems from the quadratic part of Chern-Simons theory on S^3 . We first recall that the canonical mass dimension of $A_\mu(x)$ is zero, as is the mass dimension for the gauge parameter $\alpha(x)$. We define the normalisation of our path integration measures to be

$$1 \equiv \int \mathcal{D}\alpha e^{-\ell_{\text{uv}}^{-3} \int d^3x \sqrt{g} \alpha(x)^2/2}, \quad (\text{G.1})$$

$$1 \equiv \int \mathcal{D}A_\mu^T e^{-\ell_{\text{uv}}^{-1} \int d^3x \sqrt{g} g^{\mu\nu} A_\nu^T(x) A_\mu^T(x)/2}, \quad (\text{G.2})$$

$$1 \equiv \int \mathcal{D}\bar{c} \mathcal{D}c e^{\ell_{\text{uv}}^{-2} \int d^3x \sqrt{g} \bar{c}(x) c(x)}, \quad (\text{G.3})$$

where $\nabla^\mu A_\mu^T(x) = 0$ and $\alpha(x)$ is a real scalar, while $\bar{c}(x)$ and $c(x)$ are Grassmann valued fields. To render the exponents dimensionless, we multiply by the appropriate powers of the UV cutoff length scale $\ell_{\text{uv}} = 1/\Lambda_{\text{uv}}$. In fixing the above normalisation, we fix any ultraviolet ambiguities stemming from field rescalings. The fields can be expanded in a complete basis of eigenfunctions of the Laplacian on the round three-sphere. For instance,

$$\alpha(x) = \sum_l \alpha_l \phi_l(x), \quad -\nabla^2 \phi_l = \xi_l \phi_l, \quad \int d^3x \sqrt{g} \phi_l(x) \phi_{l'}(x) = \delta_{ll'}, \quad (\text{G.4})$$

such that mass dimension of α_l is $-3/2$. Following similar steps for the other fields, we obtain the following path integration measures

$$\mathcal{D}\alpha \equiv \prod_l \Lambda_{\text{uv}}^{3/2} \frac{d\alpha_l}{\sqrt{2\pi}}, \quad \mathcal{D}\bar{c} \mathcal{D}c \equiv \prod_l' \Lambda_{\text{uv}}^{-2} d\bar{c}_l dc_l, \quad \mathcal{D}A_\mu^T \equiv \prod_l \Lambda_{\text{uv}}^{1/2} \frac{dA_l}{\sqrt{2\pi}}. \quad (\text{G.5})$$

With the above definitions of the path integration measures, and the Chern-Simons action normalised as

$$S_{\text{CS}} = \frac{1}{2} \int d^3x \varepsilon^{\mu\nu\rho} A_\mu \partial_\nu A_\rho, \quad (\text{G.6})$$

we can proceed via the Fadeev-Popov gauge fixing procedure. We take the metric on S^3 to be

$$ds^2 = \ell^2 (d\theta^2 + \sin^2 \theta d\Omega_2^2), \quad (\text{G.7})$$

with volume $\text{vol } S^3 = 2\pi^2 \ell^3$. Working in the Lorenz gauge $\nabla_\mu A^\mu = 0$, one finds

$$|Z_{U(1)_k}[S^3]| = \sqrt{\frac{2\pi}{k}} \times \frac{\sqrt{2\pi} (\text{vol } S^3 \Lambda_{\text{uv}}^3)^{-1/2}}{\text{vol } U(1)} \times \sqrt{\frac{\det'[-\nabla^2/\Lambda_{\text{uv}}^2]}{\det[LL^\dagger/\Lambda_{\text{uv}}^2]^{1/2}}}, \quad (\text{G.8})$$

where $\text{vol } U(1) = 2\pi$. The term $\sqrt{2\pi} (\text{vol } S^3 \Lambda_{\text{uv}}^3)^{-1/2} / \text{vol } U(1)$ follows from the zero-mode contribution $d\alpha_0$. It originates from the residual part of the gauge group volume that is not cancelled by the Lorenz gauge.

After the dust settles, we are left to evaluate the following ratio of functional determinants

$$r^2 = \frac{\det'(-\nabla^2/\Lambda_{\text{uv}}^2)}{\sqrt{\det LL^\dagger/\Lambda_{\text{uv}}^2}}, \quad (\text{G.9})$$

where the Laplacian $-\nabla^2$ acts on scalar functions on S^3 and LL^\dagger acts on transverse vector fields on S^3 . The prime indicates we are dropping the zero mode of $-\nabla^2$. The respective spectra are well known [224]. For the scalar Laplacian we have

$$\lambda_n = \frac{1}{\ell^2} \times n(n+2), \quad d_n = (n+1)^2, \quad n = 0, 1, \dots \quad (\text{G.10})$$

For the LL^\dagger operator, the eigenvalues and degeneracies are given by

$$\lambda_n = \frac{1}{\ell^2} \times (n+1)^2, \quad d_n = 2n(n+2), \quad n = 1, 2, \dots \quad (\text{G.11})$$

Using a heat kernel regularisation,¹ we have that

$$-\log \det' \left(-\frac{\nabla^2}{\Lambda_{\text{uv}}^2} \right) = \sum_{n=1}^{\infty} (n+1)^2 \int_0^{\infty} \frac{d\tau}{\tau} e^{-\frac{\varepsilon^2}{4\tau}} e^{-\tau n(n+2)}, \quad (\text{G.12})$$

¹For a ζ -function regularisation scheme, see [225].

where the dimensionless cutoff parameter is taken to be $\varepsilon \equiv 2e^{-\gamma}/\ell\Lambda_{\text{uv}}$ with γ being the Euler constant. It is convenient to rewrite the above in the following form

$$-\log \det' \left(-\frac{\nabla^2}{\Lambda_{\text{uv}}^2} \right) = \int_{\mathcal{C}} \frac{du}{\sqrt{u^2 + \varepsilon^2}} e^{-i\sqrt{u^2 + \varepsilon^2}} \left(\frac{1 + e^{iu}}{1 - e^{iu}} \frac{e^{iu}}{(1 - e^{iu})^2} - e^{iu} \right). \quad (\text{G.13})$$

The contour $\mathcal{C} = \mathbb{R} + i\delta$ is parallel to the real axis but has a small positive imaginary part $0 < \delta < \varepsilon$. We can deform the contour to go down the branch cut from the left and up from the right. We find

$$-\log \det' \left(-\frac{\nabla^2}{\Lambda_{\text{uv}}^2} \right) = \int_{\varepsilon}^{\infty} \frac{dt}{\sqrt{t^2 - \varepsilon^2}} \left(\frac{1 + e^{-t}}{1 - e^{-t}} \frac{e^{-t}}{(1 - e^{-t})^2} - e^{-t} \right) \left(e^{\sqrt{t^2 - \varepsilon^2}} + e^{-\sqrt{t^2 - \varepsilon^2}} \right). \quad (\text{G.14})$$

Similar considerations lead to

$$-\frac{1}{2} \log \det LL^\dagger = 2 \int_{\varepsilon}^{\infty} \frac{dt}{\sqrt{t^2 - \varepsilon^2}} \frac{3e^{-2t} - e^{-3t}}{(1 - e^{-t})^3}. \quad (\text{G.15})$$

The ultraviolet behaviour is encoded in the small- t regime of the integrands. Setting $\varepsilon = 0$ in the integrand and performing a small- t expansion we find that there is no $\sim 1/\varepsilon^3$ divergence, and moreover that the leading divergence goes as $\sim 1/\varepsilon$. There is also a logarithmic $\sim \log \varepsilon$ divergence. Since we are in odd dimensions there should be no logarithmic divergences contributing to $\log Z[S^3]$. Recalling the expression (G.8) we see that this is indeed the case once we take into account the overall factor $\ell_{\text{uv}}^{-3/2}$. Evaluating the t -integral in the heat kernel regularisation in the small- ε limit leads to

$$\log r^2 = -\frac{3\pi}{2\varepsilon} - 3 \log \frac{e^\gamma \varepsilon}{2} + \log 2\pi^2 = -\frac{3\pi}{2\varepsilon} + 3 \log \ell\Lambda_{\text{uv}} + \log 2\pi^2. \quad (\text{G.16})$$

Combining the above with (G.8) and recalling that $\text{vol } S^3 = 2\pi^2 \ell^3$, we find

$$|Z_{U(1)_k}(S^3)| = \sqrt{\frac{1}{k}} e^{-\frac{3\pi}{4\varepsilon}}. \quad (\text{G.17})$$

A similar picture holds for Chern-Simons theories with more general gauge group in the perturbative, large k regime. The coefficient of the $1/\varepsilon$ term in (G.17) can be tuned by adding a local background dependent term

$$S_b = \Lambda_b \int d^3x \sqrt{g} R = 12\pi^2 \ell \Lambda_b, \quad (\text{G.18})$$

where we recall that $R = 6/\ell^2$. For the particular choice $\Lambda_b = -e^\gamma \Lambda_{\text{uv}}/32\pi$ we can set the divergent term to zero.

As a final remark, we note that the choices of normalisation (G.1) serve another physical purpose, namely to set the partition function of the theory on $S^1 \times S^2$ equal to unity (up to $1/\varepsilon$ divergences, which can be absorbed into local counterterms). This agrees well with the fact that Chern Simons theory quantised on a spatial S^2 has a unique state with vanishing energy. To compute the partition function in this case, one must take into account the non-trivial moduli space of flat connections due to the presence of a non-contractible cycle [226]. The volume of this moduli space is crucial to cancel the k dependence of the partition function.

Appendix H

Euclidean path-integral of Abelian edge-mode theory

Here we provide a derivation of the thermal partition function (3.48) from the Euclidean path integral. We must Wick rotate the edge-mode theory (3.38) to Euclidean signature by taking $t = -i\xi$ and imposing the thermal periodicity condition $\xi \sim \xi + \beta_T$. Notice that although the original Chern-Simons theory, being topological, is insensitive to the signature of space-time, the edge-mode theory can sense it. The reason for this is that from the gauge theory perspective we should also continue $A_t = iA_\xi$ when continuing $t = -i\xi$. This would violate the reality conditions of the gauge-fixing condition (3.21) unless we also continue $v = -iv_E$. If we also analytically continue v , the edge-mode theory would remain unchanged, and hence unaware of the underlying signature. For the purposes of computing the thermal partition function, we keep v unchanged upon continuation to Euclidean signature.

It is convenient to expand the non-winding sector in a Fourier basis

$$\zeta(\xi, \varphi) = \frac{1}{\sqrt{2\pi}} \sum_{(m,n) \in \mathbb{Z}^2} e^{2\pi m i \xi / \beta_T + i n \varphi} \zeta_{m,n}, \quad (\text{H.1})$$

with $\bar{\zeta}_{m,n} = \zeta_{-m,-n}$. Performing the Gaussian path integral over the non-winding sector, we are led to evaluate

$$Z_{\text{non-winding}}[\beta_T] = \mathcal{N} \prod_{m,n=1}^{\infty} \frac{1}{1 + (\beta_T v n / 2\pi m)^2}. \quad (\text{H.2})$$

We will be rather cavalier about the overall normalisation \mathcal{N} as we can determine it by imposing that there is a unique vacuum state and hence $\lim_{\beta_T \rightarrow \infty} (1 - \beta_T \partial_{\beta_T}) \log Z_{\text{non-winding}}[\beta_T] =$

0. Using the infinite product representation of $\sinh z$, we can express the above as

$$Z_{\text{non-winding}}[\beta_T] = e^{-\beta_T v \epsilon_0} \times e^{\beta_T v / 24} \prod_{n=1}^{\infty} \frac{1}{1 - e^{-\beta_T v n}} = \frac{e^{-\beta_T v \epsilon_0}}{\eta(q)}, \quad (\text{H.3})$$

where we have absorbed any divergences of the overall energy scale into ϵ_0 and $q = e^{-v\beta_T}$. If we further incorporate the winding mode sector wrapping the φ cycle, we get an additional contribution given by

$$Z_{\text{winding}}[\beta_T] = \sum_{n \in \mathbb{Z}} e^{-kv\beta_T n^2 / 2} = \vartheta_3(0, q^{k/2}). \quad (\text{H.4})$$

Combining the two, we find agreement with (3.48).

Appendix I

Lorentzian edge-mode Hamiltonian

In this appendix, we show how the Lorentzian edge-mode Hamiltonian reduces to that of a conformal quantum mechanics. We start with the Hamiltonian in the form (3.86). Since the modes carrying fixed momentum n on the circle decouple, it is sufficient to study the Hamiltonian of a single mode number n :

$$\hat{Q}_t^{(n)} = \frac{\sqrt{k^2 + \lambda^2}}{8\pi} n^2 \left(v_{re} \left(\hat{A}_n^+ \hat{A}_n^- - \hat{B}_n^+ \hat{B}_n^- \right) + i v_{im} \left(\hat{A}_n^+ \hat{B}_n^+ - \hat{A}_n^- \hat{B}_n^- \right) \right). \quad (\text{I.1})$$

where $\hat{Q}_t = \frac{1}{2} \sum_n \hat{Q}_t^{(n)}$. We represent the raising and lowering operators as

$$\hat{A}_n^\pm = \left(\frac{4\pi}{n\sqrt{k^2 + \lambda^2}} \right)^{1/2} \left(x_n \pm \frac{d}{dx_n} \right), \quad \hat{B}_n^\pm = \left(\frac{4\pi}{n\sqrt{k^2 + \lambda^2}} \right)^{1/2} \left(y_n \pm \frac{d}{dy_n} \right). \quad (\text{I.2})$$

In these new coordinates, the Hamiltonian is

$$\hat{Q}_t^{(n)} = \frac{n}{2} \left[v_{re} \left(- \left(\frac{d}{dx_n} \right)^2 + \left(\frac{d}{dy_n} \right)^2 + x_n^2 - y_n^2 \right) + 2i v_{im} \left(x_n \frac{d}{dy_n} + y_n \frac{d}{dx_n} \right) \right]. \quad (\text{I.3})$$

We then make the following change of coordinates:

$$x_n = w_n \cosh t_n, \quad y_n = w_n \sinh t_n, \quad (t_n, w_n) \in \mathbb{R}^2, \quad (\text{I.4})$$

covering the region $|x| > |y|$, shown in Figure I.1. In terms of (w_n, t_n) , our Hamiltonian is

$$\hat{Q}_t^{(n)} = \frac{n}{2} \left[v_{re} \left(- \frac{d^2}{dw_n^2} - \frac{1}{w_n} \frac{d}{dw_n} + \frac{1}{w_n^2} \frac{d^2}{dt_n^2} + w_n^2 \right) + 2i v_{im} \frac{d}{dt_n} \right]. \quad (\text{I.5})$$

For $|x| < |y|$ the Hamiltonian is given by

$$\hat{Q}_t^{(n)} = -\frac{n}{2} \left[v_{re} \left(-\frac{d^2}{dw_n^2} - \frac{1}{w_n} \frac{d}{dw_n} + \frac{1}{w_n^2} \frac{d^2}{dt_n^2} + w_n^2 \right) + 2iv_{im} \frac{d}{dt_n} \right]. \quad (\text{I.6})$$

We can then find the Schrödinger equation for each mode. By expanding the wavefunction in a Fourier basis as

$$\Psi(w_n, t_n) = \int_{\mathbb{R}} \frac{dp_n}{2\pi} \psi_n(w_n) e^{ip_n t_n}, \quad p_n \in \mathbb{R}, \quad (\text{I.7})$$

and taking $|x| > |y|$, we find

$$\frac{1}{2} \left(-\frac{d^2}{dw_n^2} - \frac{1}{w_n} \frac{d}{dw_n} - \frac{p_n^2}{w_n^2} + w_n^2 \right) \psi_n = \frac{1}{v_{re}} \left(\frac{E_n}{n} + v_{im} p_n \right) \psi_n. \quad (\text{I.8})$$

To get this in the Schrödinger form, we then make the substitution $\psi_n \rightarrow \frac{1}{\sqrt{w_n}} \psi_n$, and this becomes

$$\frac{1}{2} \left(-\frac{d^2}{dw_n^2} + w_n^2 - \frac{1/4 + p_n^2}{w_n^2} \right) \psi_n = \frac{1}{v_{re}} \left(\frac{E_n}{n} + v_{im} p_n \right) \psi_n, \quad (\text{I.9})$$

which is the conformal quantum mechanics problem studied in [193, 194]. We need to patch this solution to the one for $|y| > |x|$ which can be found by exchanging $x_n \leftrightarrow y_n$ in (I.4) and following the same steps. The result is a change of sign in the left-hand side of (I.9).

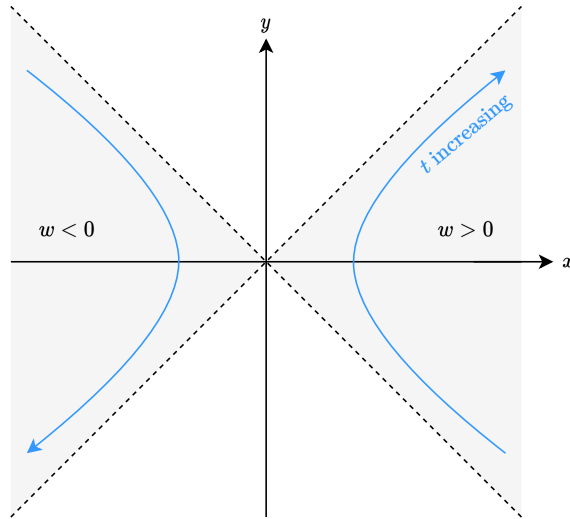


Figure I.1: Plot showing the shaded regions $|x| > |y|$, where the Hamiltonian (I.5) is valid. The blue arrows indicate increasing $t = \text{arctanh}(y/x)$. By gluing this solution along $|x| = |y|$ with the one in the $|y| > |x|$ region, we arrive at the solution (3.91).

Appendix J

$SL(2, \mathbb{C})$ WZW central charge

To calculate the current algebra and central charge of the chiral $SL(2, \mathbb{C})$ WZW model (3.115), we first study the non-chiral WZW model and then take the anti-holomorphic sector to describe the current algebra of the chiral theory. This is because the chiral theory is invariant under

$$g(z, \bar{z}) \rightarrow g(z, \bar{z})\bar{\Omega}^{-1}(\bar{z}), \quad (\text{J.1})$$

where (z, \bar{z}) are coordinates on the complex plane. The $SL(2, \mathbb{C})$ WZW model is given by

$$S = \frac{k + i\lambda}{8\pi} \int d^2x \text{Tr} (\partial^\mu g^{-1} \partial_\mu g) - \frac{i(k + i\lambda)}{12\pi} \int d^3y \varepsilon^{\mu\nu\rho} \text{Tr} (g^{-1} \partial_\mu g g^{-1} \partial_\nu g g^{-1} \partial_\rho g) + \text{c.c.}, \quad (\text{J.2})$$

where $g \in SL(2, \mathbb{C})$. By computing the equations of motion for this action, we find the following conserved currents

$$\begin{aligned} J_z &= -\frac{1}{2}(k + i\lambda)\partial_z g g^{-1}, & J_{\bar{z}} &= \frac{1}{2}(k + i\lambda)g^{-1}\partial_{\bar{z}} g, \\ \tilde{J}_{\bar{z}} &= -\frac{1}{2}(k - i\lambda)\partial_{\bar{z}} \bar{g} \bar{g}^{-1}, & \tilde{J}_z &= \frac{1}{2}(k - i\lambda)\bar{g}^{-1}\partial_z \bar{g}, \end{aligned} \quad (\text{J.3})$$

Here the subscripts label which currents are holomorphic/ anti-holomorphic. We can calculate the current algebra (using the procedure described for instance in [172]) and find

$$\begin{aligned} [J_{z,n}^a, J_{z,m}^b] &= \frac{1}{2}(k + i\lambda)n\delta_{ab}\delta_{n+m,0} + \sum_c i f_{abc} J_{z,n+m}^c, \\ [J_{\bar{z},n}^a, J_{\bar{z},m}^b] &= \frac{1}{2}(k + i\lambda)n\delta_{ab}\delta_{n+m,0} - \sum_c i f_{abc} J_{\bar{z},n+m}^c, \\ [\tilde{J}_{\bar{z},n}^a, \tilde{J}_{\bar{z},m}^b] &= \frac{1}{2}(k - i\lambda)n\delta_{ab}\delta_{n+m,0} - \sum_c i f_{abc} \tilde{J}_{\bar{z},n+m}^c, \\ [\tilde{J}_{z,n}^a, \tilde{J}_{z,m}^b] &= \frac{1}{2}(k - i\lambda)n\delta_{ab}\delta_{n+m,0} + \sum_c i f_{abc} \tilde{J}_{z,n+m}^c. \end{aligned} \quad (\text{J.4})$$

The anti-holomorphic sector is then given by the second and third of these. Following the Sugawara construction, we find the anti-holomorphic energy-momentum tensor

$$\bar{T}(\bar{z}) = \frac{1}{k + i\lambda + 2} \sum_a (J_{\bar{z}}^a J_{\bar{z}}^a)(\bar{z}) + \frac{1}{k - i\lambda + 2} \sum_a (\tilde{J}_{\bar{z}}^a \tilde{J}_{\bar{z}}^a)(\bar{z}), \quad (\text{J.5})$$

where we have used $f_{abc}f_{cbd} = \epsilon_{abc}\epsilon_{cbd} = 2\delta_{ad}$. From the OPE

$$\bar{T}(z)\bar{T}(w) = \left(\frac{3(k + i\lambda)}{2(k + i\lambda + 2)} + \frac{3(k - i\lambda)}{2(k - i\lambda + 2)} \right) \frac{1}{(\bar{z} - \bar{w})^4} + \frac{2\bar{T}(\bar{w})}{(\bar{z} - \bar{w})^2} + \frac{\partial\bar{T}(\bar{w})}{\bar{z} - \bar{w}}, \quad (\text{J.6})$$

we can find the central charge

$$c_{SL(2,\mathbb{C})} = \frac{3(k + i\lambda)}{(k + i\lambda + 2)} + \frac{3(k - i\lambda)}{(k - i\lambda + 2)} = \frac{6(k(k + 2) + \lambda^2)}{(k + 2)^2 + \lambda^2}. \quad (\text{J.7})$$

Bibliography

- [1] Adam G. Riess et al. Observational evidence from supernovae for an accelerating universe and a cosmological constant. *Astron. J.*, 116:1009–1038, 1998. [arXiv:astro-ph/9805201](#), [doi:10.1086/300499](#).
- [2] Saul Perlmutter et al. Measurements of Ω and Λ from 42 high redshift supernovae. *Astrophys. J.*, 517:565–586, 1999. [arXiv:astro-ph/9812133](#), [doi:10.1086/307221](#).
- [3] Pierre Astier and Reynald Pain. Observational Evidence of the Accelerated Expansion of the Universe. *Comptes Rendus Physique*, 13:521–538, 2012. [arXiv:1204.5493](#), [doi:10.1016/j.crhy.2012.04.009](#).
- [4] Scott Dodelson and Lam Hui. A Horizon ratio bound for inflationary fluctuations. *Phys. Rev. Lett.*, 91:131301, 2003. [arXiv:astro-ph/0305113](#), [doi:10.1103/PhysRevLett.91.131301](#).
- [5] Andrew R Liddle and Samuel M Leach. How long before the end of inflation were observable perturbations produced? *Phys. Rev. D*, 68:103503, 2003. [arXiv:astro-ph/0305263](#), [doi:10.1103/PhysRevD.68.103503](#).
- [6] Alan H. Guth. The Inflationary Universe: A Possible Solution to the Horizon and Flatness Problems. *Phys. Rev. D*, 23:347–356, 1981. [doi:10.1103/PhysRevD.23.347](#).
- [7] Andrei D. Linde. A New Inflationary Universe Scenario: A Possible Solution of the Horizon, Flatness, Homogeneity, Isotropy and Primordial Monopole Problems. *Phys. Lett. B*, 108:389–393, 1982. [doi:10.1016/0370-2693\(82\)91219-9](#).
- [8] Andreas Albrecht and Paul J. Steinhardt. Cosmology for Grand Unified Theories with Radiatively Induced Symmetry Breaking. *Phys. Rev. Lett.*, 48:1220–1223, 1982. [doi:10.1103/PhysRevLett.48.1220](#).
- [9] Alan H. Guth. Eternal inflation and its implications. *J. Phys. A*, 40:6811–6826, 2007. [arXiv:hep-th/0702178](#), [doi:10.1088/1751-8113/40/25/S25](#).

- [10] Willem de Sitter. On the relativity of inertia. Remarks concerning Einstein's latest hypothesis. *Koninklijke Nederlandse Akademie van Wetenschappen Proceedings Series B Physical Sciences*, 19:1217–1225, March 1917.
- [11] Jacob D. Bekenstein. Black holes and the second law. *Lett. Nuovo Cim.*, 4:737–740, 1972. [doi:10.1007/BF02757029](https://doi.org/10.1007/BF02757029).
- [12] Stephen W. Hawking. Particle Creation by Black Holes. *Commun. Math. Phys.*, 43:199–220, 1975. [Erratum: *Commun.Math.Phys.* 46, 206 (1976)]. [doi:10.1007/BF02345020](https://doi.org/10.1007/BF02345020).
- [13] Gary W. Gibbons and Stephen W. Hawking. Action Integrals and Partition Functions in Quantum Gravity. *Phys. Rev. D*, 15:2752–2756, 1977. [doi:10.1103/PhysRevD.15.2752](https://doi.org/10.1103/PhysRevD.15.2752).
- [14] Gary W. Gibbons and Stephen W. Hawking. Cosmological Event Horizons, Thermodynamics, and Particle Creation. *Phys. Rev. D*, 15:2738–2751, 1977. [doi:10.1103/PhysRevD.15.2738](https://doi.org/10.1103/PhysRevD.15.2738).
- [15] Juan Martin Maldacena. The Large N limit of superconformal field theories and supergravity. *Adv. Theor. Math. Phys.*, 2:231–252, 1998. [arXiv:hep-th/9711200](https://arxiv.org/abs/hep-th/9711200), [doi:10.4310/ATMP.1998.v2.n2.a1](https://doi.org/10.4310/ATMP.1998.v2.n2.a1).
- [16] Maximo Banados, Claudio Teitelboim, and Jorge Zanelli. The Black hole in three-dimensional space-time. *Phys. Rev. Lett.*, 69:1849–1851, 1992. [arXiv:hep-th/9204099](https://arxiv.org/abs/hep-th/9204099), [doi:10.1103/PhysRevLett.69.1849](https://doi.org/10.1103/PhysRevLett.69.1849).
- [17] Francesco Benini, Kiril Hristov, and Alberto Zaffaroni. Black hole microstates in AdS₄ from supersymmetric localization. *JHEP*, 05:054, 2016. [arXiv:1511.04085](https://arxiv.org/abs/1511.04085), [doi:10.1007/JHEP05\(2016\)054](https://doi.org/10.1007/JHEP05(2016)054).
- [18] Alejandro Cabo-Bizet, Davide Cassani, Dario Martelli, and Sameer Murthy. Microscopic origin of the Bekenstein-Hawking entropy of supersymmetric AdS₅ black holes. *JHEP*, 10:062, 2019. [arXiv:1810.11442](https://arxiv.org/abs/1810.11442), [doi:10.1007/JHEP10\(2019\)062](https://doi.org/10.1007/JHEP10(2019)062).
- [19] Edward Witten. Quantum gravity in de Sitter space. In *Strings 2001: International Conference*, 6 2001. [arXiv:hep-th/0106109](https://arxiv.org/abs/hep-th/0106109).
- [20] Andrew Strominger. The dS / CFT correspondence. *JHEP*, 10:034, 2001. [arXiv:hep-th/0106113](https://arxiv.org/abs/hep-th/0106113), [doi:10.1088/1126-6708/2001/10/034](https://doi.org/10.1088/1126-6708/2001/10/034).

- [21] Dionysios Anninos, Thomas Hartman, and Andrew Strominger. Higher Spin Realization of the dS/CFT Correspondence. *Class. Quant. Grav.*, 34(1):015009, 2017. [arXiv:1108.5735](#), [doi:10.1088/1361-6382/34/1/015009](#).
- [22] Dionysios Anninos, Sean A. Hartnoll, and Diego M. Hofman. Static Patch Solipsism: Conformal Symmetry of the de Sitter Worldline. *Class. Quant. Grav.*, 29:075002, 2012. [arXiv:1109.4942](#), [doi:10.1088/0264-9381/29/7/075002](#).
- [23] Sam Leuven, Erik Verlinde, and Manus Visser. Towards non-AdS Holography via the Long String Phenomenon. *JHEP*, 06:097, 2018. [arXiv:1801.02589](#), [doi:10.1007/JHEP06\(2018\)097](#).
- [24] Leonard Susskind, Larus Thorlacius, and John Uglum. The Stretched horizon and black hole complementarity. *Phys. Rev. D*, 48:3743–3761, 1993. [arXiv:hep-th/9306069](#), [doi:10.1103/PhysRevD.48.3743](#).
- [25] Raphael Bousso. Holography in general space-times. *JHEP*, 06:028, 1999. [arXiv:hep-th/9906022](#), [doi:10.1088/1126-6708/1999/06/028](#).
- [26] Tom Banks, Bartomeu Fiol, and Alexander Morisse. Towards a quantum theory of de Sitter space. *JHEP*, 12:004, 2006. [arXiv:hep-th/0609062](#), [doi:10.1088/1126-6708/2006/12/004](#).
- [27] Xi Dong, Eva Silverstein, and Gonzalo Torroba. De Sitter Holography and Entanglement Entropy. *JHEP*, 07:050, 2018. [arXiv:1804.08623](#), [doi:10.1007/JHEP07\(2018\)050](#).
- [28] Leonard Susskind. Entanglement and Chaos in De Sitter Space Holography: An SYK Example. *JHAP*, 1(1):1–22, 2021. [arXiv:2109.14104](#), [doi:10.22128/jhap.2021.455.1005](#).
- [29] Edgar Shaghoulian. The central dogma and cosmological horizons. *JHEP*, 01:132, 2022. [arXiv:2110.13210](#), [doi:10.1007/JHEP01\(2022\)132](#).
- [30] Edgar Shaghoulian and Leonard Susskind. Entanglement in De Sitter space. *JHEP*, 08:198, 2022. [arXiv:2201.03603](#), [doi:10.1007/JHEP08\(2022\)198](#).
- [31] Lars Onsager. Crystal statistics. 1. A Two-dimensional model with an order disorder transition. *Phys. Rev.*, 65:117–149, 1944. [doi:10.1103/PhysRev.65.117](#).
- [32] Sidney R. Coleman. There are no Goldstone bosons in two-dimensions. *Commun. Math. Phys.*, 31:259–264, 1973. [doi:10.1007/BF01646487](#).

- [33] Gerard 't Hooft. A Two-Dimensional Model for Mesons. *Nucl. Phys. B*, 75:461–470, 1974. [doi:10.1016/0550-3213\(74\)90088-1](https://doi.org/10.1016/0550-3213(74)90088-1).
- [34] Edward Witten. (2+1)-Dimensional Gravity as an Exactly Soluble System. *Nucl. Phys. B*, 311:46, 1988. [doi:10.1016/0550-3213\(88\)90143-5](https://doi.org/10.1016/0550-3213(88)90143-5).
- [35] Ana Achúcarro and Paul K. Townsend. A Chern-Simons Action for Three-Dimensional anti-De Sitter Supergravity Theories. *Phys. Lett. B*, 180:89, 1986. [doi:10.1016/0370-2693\(86\)90140-1](https://doi.org/10.1016/0370-2693(86)90140-1).
- [36] Alexander A. Belavin, Alexander M. Polyakov, and Alexander B. Zamolodchikov. Infinite Conformal Symmetry in Two-Dimensional Quantum Field Theory. *Nucl. Phys. B*, 241:333–380, 1984. [doi:10.1016/0550-3213\(84\)90052-X](https://doi.org/10.1016/0550-3213(84)90052-X).
- [37] Phil Saad, Stephen H. Shenker, and Douglas Stanford. JT gravity as a matrix integral. 3 2019. [arXiv:1903.11115](https://arxiv.org/abs/1903.11115).
- [38] T. Banks. Some thoughts on the quantum theory of de sitter space. In *The Davis Meeting on Cosmic Inflation*, 5 2003. [arXiv:astro-ph/0305037](https://arxiv.org/abs/astro-ph/0305037).
- [39] T. Banks and W. Fischler. The holographic approach to cosmology. In *8th International Conference on Particle Physics and the Early Universe*, 12 2004. [arXiv:hep-th/0412097](https://arxiv.org/abs/hep-th/0412097).
- [40] Maulik K. Parikh and Erik P. Verlinde. De Sitter holography with a finite number of states. *JHEP*, 01:054, 2005. [arXiv:hep-th/0410227](https://arxiv.org/abs/hep-th/0410227), [doi:10.1088/1126-6708/2005/01/054](https://doi.org/10.1088/1126-6708/2005/01/054).
- [41] Tom Banks and W. Fischler. The holographic spacetime model of cosmology. *Int. J. Mod. Phys. D*, 27(14):1846005, 2018. [arXiv:1806.01749](https://arxiv.org/abs/1806.01749), [doi:10.1142/S0218271818460057](https://doi.org/10.1142/S0218271818460057).
- [42] Hao Geng. Some Information Theoretic Aspects of De-Sitter Holography. *JHEP*, 02:005, 2020. [arXiv:1911.02644](https://arxiv.org/abs/1911.02644), [doi:10.1007/JHEP02\(2020\)005](https://doi.org/10.1007/JHEP02(2020)005).
- [43] Lars Aalsma and Gary Shiu. Chaos and complementarity in de Sitter space. *JHEP*, 05:152, 2020. [arXiv:2002.01326](https://arxiv.org/abs/2002.01326), [doi:10.1007/JHEP05\(2020\)152](https://doi.org/10.1007/JHEP05(2020)152).
- [44] Hao Geng. Non-local entanglement and fast scrambling in de-Sitter holography. *Annals Phys.*, 426:168402, 2021. [arXiv:2005.00021](https://arxiv.org/abs/2005.00021), [doi:10.1016/j.aop.2021.168402](https://doi.org/10.1016/j.aop.2021.168402).

- [45] Lars Aalsma and Watse Sybesma. The Price of Curiosity: Information Recovery in de Sitter Space. *JHEP*, 05:291, 2021. [arXiv:2104.00006](#), [doi:10.1007/JHEP05\(2021\)291](#).
- [46] Vasudev Shyam. $T\bar{T} + \Lambda_2$ deformed CFT on the stretched dS_3 horizon. *JHEP*, 04:052, 2022. [arXiv:2106.10227](#), [doi:10.1007/JHEP04\(2022\)052](#).
- [47] Evan Coleman, Edward A. Mazenc, Vasudev Shyam, Eva Silverstein, Ronak M. Soni, Gonzalo Torroba, and Sungyeon Yang. De Sitter microstates from $T\bar{T} + \Lambda_2$ and the Hawking-Page transition. *JHEP*, 07:140, 2022. [arXiv:2110.14670](#), [doi:10.1007/JHEP07\(2022\)140](#).
- [48] Andrew Svesko, Evita Verheijden, Erik P. Verlinde, and Manus R. Visser. Quasi-local energy and microcanonical entropy in two-dimensional nearly de Sitter gravity. *JHEP*, 08:075, 2022. [arXiv:2203.00700](#), [doi:10.1007/JHEP08\(2022\)075](#).
- [49] Batoul Banihashemi and Ted Jacobson. Thermodynamic ensembles with cosmological horizons. *JHEP*, 07:042, 2022. [arXiv:2204.05324](#), [doi:10.1007/JHEP07\(2022\)042](#).
- [50] Eva Silverstein. Black hole to cosmic horizon microstates in string/M theory: timelike boundaries and internal averaging. *JHEP*, 12 2022. [arXiv:2212.00588](#).
- [51] Yasunori Nomura, Pratik Rath, and Nico Salzetta. Spacetime from Unentanglement. *Phys. Rev. D*, 97(10):106010, 2018. [arXiv:1711.05263](#), [doi:10.1103/PhysRevD.97.106010](#).
- [52] Yasunori Nomura. Spacetime and Universal Soft Modes — Black Holes and Beyond. *Phys. Rev. D*, 101(6):066024, 2020. [arXiv:1908.05728](#), [doi:10.1103/PhysRevD.101.066024](#).
- [53] Chitraang Murdia, Yasunori Nomura, and Kyle Ritchie. Black hole and de Sitter microstructures from a semiclassical perspective. *Phys. Rev. D*, 107(2):026016, 2023. [arXiv:2207.01625](#), [doi:10.1103/PhysRevD.107.026016](#).
- [54] Edward Farhi, Alan H. Guth, and Jemal Guven. Is It Possible to Create a Universe in the Laboratory by Quantum Tunneling? *Nucl. Phys. B*, 339:417–490, 1990. [doi:10.1016/0550-3213\(90\)90357-J](#).
- [55] Ben Freivogel, Veronika E. Hubeny, Alexander Maloney, Robert C. Myers, Mukund Rangamani, and Stephen Shenker. Inflation in AdS/CFT. *JHEP*, 03:007, 2006. [arXiv:hep-th/0510046](#), [doi:10.1088/1126-6708/2006/03/007](#).

- [56] Dionysios Anninos and Diego M. Hofman. Infrared Realization of dS_2 in AdS_2 . *Class. Quant. Grav.*, 35(8):085003, 2018. [arXiv:1703.04622](#), [doi:10.1088/1361-6382/aab143](#).
- [57] Dionysios Anninos, Damián A. Galante, and Diego M. Hofman. De Sitter horizons & holographic liquids. *JHEP*, 07:038, 2019. [arXiv:1811.08153](#), [doi:10.1007/JHEP07\(2019\)038](#).
- [58] Alexei Kitaev and John Preskill. Topological entanglement entropy. *Phys. Rev. Lett.*, 96:110404, 2006. [arXiv:hep-th/0510092](#), [doi:10.1103/PhysRevLett.96.110404](#).
- [59] Michael Levin and Xiao-Gang Wen. Detecting Topological Order in a Ground State Wave Function. *Phys. Rev. Lett.*, 96:110405, 2006. [arXiv:cond-mat/0510613](#), [doi:10.1103/PhysRevLett.96.110405](#).
- [60] Dionysios Anninos and Eleanor Harris. Interpolating geometries and the stretched dS_2 horizon. *JHEP*, 11:166, 2022. [arXiv:2209.06144](#), [doi:10.1007/JHEP11\(2022\)166](#).
- [61] Shira Chapman, Damián A. Galante, Eleanor Harris, Sameer U. Sheorey, and David Vegh. Complex geodesics in de Sitter space. *JHEP*, 03:006, 2023. [arXiv:2212.01398](#), [doi:10.1007/JHEP03\(2023\)006](#).
- [62] Dionysios Anninos and Eleanor Harris. Three-dimensional de Sitter horizon thermodynamics. *JHEP*, 10:091, 2021. [arXiv:2106.13832](#), [doi:10.1007/JHEP10\(2021\)091](#).
- [63] Dionysios Anninos, Frederik Denef, Y. T. Albert Law, and Zimo Sun. Quantum de Sitter horizon entropy from quasicanonical bulk, edge, sphere and topological string partition functions. *JHEP*, 01:088, 2022. [arXiv:2009.12464](#), [doi:10.1007/JHEP01\(2022\)088](#).
- [64] Y. T. Albert Law. A compendium of sphere path integrals. *JHEP*, 12:213, 2021. [arXiv:2012.06345](#), [doi:10.1007/JHEP12\(2021\)213](#).
- [65] Justin R. David and Jyotirmoy Mukherjee. Partition functions of p-forms from Harish-Chandra characters. *JHEP*, 09:094, 2021. [arXiv:2105.03662](#), [doi:10.1007/JHEP09\(2021\)094](#).
- [66] Shira Chapman, Damián A. Galante, and Eric David Kramer. Holographic complexity and de Sitter space. *JHEP*, 02:198, 2022. [arXiv:2110.05522](#), [doi:10.1007/JHEP02\(2022\)198](#).

- [67] Dionysios Anninos and Damián A. Galante. Constructing AdS₂ flow geometries. *JHEP*, 02:045, 2021. [arXiv:2011.01944](#), [doi:10.1007/JHEP02\(2021\)045](#).
- [68] Juan Maldacena, Douglas Stanford, and Zhenbin Yang. Conformal symmetry and its breaking in two dimensional Nearly Anti-de-Sitter space. *PTEP*, 2016(12):12C104, 2016. [arXiv:1606.01857](#), [doi:10.1093/ptep/ptw124](#).
- [69] Dionysios Anninos, Damián A. Galante, and Beatrix Mühlmann. Finite features of quantum de Sitter space. *Class. Quant. Grav.*, 40(2):025009, 2023. [arXiv:2206.14146](#), [doi:10.1088/1361-6382/acaba5](#).
- [70] Victor Gorbenko, Eva Silverstein, and Gonzalo Torroba. dS/dS and $T\bar{T}$. *JHEP*, 03:085, 2019. [arXiv:1811.07965](#), [doi:10.1007/JHEP03\(2019\)085](#).
- [71] Florian Ecker, Daniel Grumiller, and Robert McNees. dS₂ as excitation of AdS₂. *SciPost Phys.*, 13:119, 2022. [arXiv:2204.00045](#), [doi:10.21468/SciPostPhys.13.6.119](#).
- [72] James W. York, Jr. Black hole thermodynamics and the Euclidean Einstein action. *Phys. Rev. D*, 33:2092–2099, 1986. [doi:10.1103/PhysRevD.33.2092](#).
- [73] Bernard F. Whiting and James W. York, Jr. Action Principle and Partition Function for the Gravitational Field in Black Hole Topologies. *Phys. Rev. Lett.*, 61:1336, 1988. [doi:10.1103/PhysRevLett.61.1336](#).
- [74] Geoff Hayward. Euclidean action and the thermodynamics of manifolds without boundary. *Phys. Rev. D*, 41:3248–3251, 1990. [doi:10.1103/PhysRevD.41.3248](#).
- [75] Bo-Bo Wang and Chao-Guang Huang. Thermodynamics of de Sitter space-time in York’s formalism. *Mod. Phys. Lett. A*, 16:1487–1492, 2001. [doi:10.1142/S0217732301004637](#).
- [76] Dionysios Anninos, Tarek Anous, Irene Bredberg, and Gim Seng Ng. Incompressible Fluids of the de Sitter Horizon and Beyond. *JHEP*, 05:107, 2012. [arXiv:1110.3792](#), [doi:10.1007/JHEP05\(2012\)107](#).
- [77] Batoul Banihashemi, Ted Jacobson, Andrew Svesko, and Manus Visser. The minus sign in the first law of de Sitter horizons. *JHEP*, 01:054, 2023. [arXiv:2208.11706](#), [doi:10.1007/JHEP01\(2023\)054](#).

- [78] David J. Gross, Jorrit Kruthoff, Andrew Rolph, and Edgar Shaghoulian. $T\bar{T}$ in AdS₂ and Quantum Mechanics. *Phys. Rev. D*, 101(2):026011, 2020. [arXiv:1907.04873](#), [doi:10.1103/PhysRevD.101.026011](#).
- [79] David J. Gross, Jorrit Kruthoff, Andrew Rolph, and Edgar Shaghoulian. Hamiltonian deformations in quantum mechanics, $T\bar{T}$, and the SYK model. *Phys. Rev. D*, 102(4):046019, 2020. [arXiv:1912.06132](#), [doi:10.1103/PhysRevD.102.046019](#).
- [80] Luca V. Iliesiu, Jorrit Kruthoff, Gustavo J. Turiaci, and Herman Verlinde. JT gravity at finite cutoff. *SciPost Phys.*, 9:023, 2020. [arXiv:2004.07242](#), [doi:10.21468/SciPostPhys.9.2.023](#).
- [81] Douglas Stanford and Zhenbin Yang. Finite-cutoff JT gravity and self-avoiding loops. 4 2020. [arXiv:2004.08005](#).
- [82] Luca Griguolo, Rodolfo Panerai, Jacopo Papalini, and Domenico Seminara. Nonperturbative effects and resurgence in Jackiw-Teitelboim gravity at finite cutoff. *Phys. Rev. D*, 105(4):046015, 2022. [arXiv:2106.01375](#), [doi:10.1103/PhysRevD.105.046015](#).
- [83] Richard C. Tolman. On the Weight of Heat and Thermal Equilibrium in General Relativity. *Phys. Rev.*, 35:904–924, 1930. [doi:10.1103/PhysRev.35.904](#).
- [84] Stephen W. Hawking and Don N. Page. Thermodynamics of Black Holes in anti-De Sitter Space. *Commun. Math. Phys.*, 87:577, 1983. [doi:10.1007/BF01208266](#).
- [85] Edward Witten. Matrix Models and Deformations of JT Gravity. *Proc. Roy. Soc. Lond. A*, 476(2244):20200582, 2020. [arXiv:2006.13414](#), [doi:10.1098/rspa.2020.0582](#).
- [86] Henry Maxfield and Gustavo J. Turiaci. The path integral of 3D gravity near extremality; or, JT gravity with defects as a matrix integral. *JHEP*, 01:118, 2021. [arXiv:2006.11317](#), [doi:10.1007/JHEP01\(2021\)118](#).
- [87] Lorenz Eberhardt and Gustavo J. Turiaci. 2D dilaton gravity and the Weil-Petersson volumes with conical defects. 4 2023. [arXiv:2304.14948](#).
- [88] Daniel L. Jafferis, David K. Kolchmeyer, Baur Mukhametzhanov, and Julian Sonner. JT gravity with matter, generalized ETH, and Random Matrices. 9 2022. [arXiv:2209.02131](#).
- [89] Christian Schubert. Perturbative quantum field theory in the string inspired formalism. *Phys. Rept.*, 355:73–234, 2001. [arXiv:hep-th/0101036](#), [doi:10.1016/S0370-1573\(01\)00013-8](#).

- [90] Fiorenzo Bastianelli. Path integrals in curved space and the worldline formalism. In *8th International Conference on Path Integrals from Quantum Information to Cosmology*, 8 2005. [arXiv:hep-th/0508205](#).
- [91] Jacob D. Bekenstein and Leonard Parker. Path Integral Evaluation of Feynman Propagator in Curved Space-time. *Phys. Rev. D*, 23:2850–2869, 1981. [doi:10.1103/PhysRevD.23.2850](#).
- [92] Leonard Parker. Path integrals for a particle in curved space. *Phys. Rev. D*, 19:438–441, 1979. [doi:10.1103/PhysRevD.19.438](#).
- [93] Leonard Parker and David Toms. *Quantum Field Theory in Curved Spacetime: Quantized Field and Gravity*. Cambridge Monographs on Mathematical Physics. Cambridge University Press, 8 2009. [doi:10.1017/CB09780511813924](#).
- [94] Stephen W. Hawking and George F. R. Ellis. *The Large Scale Structure of Space-Time*. Cambridge Monographs on Mathematical Physics. Cambridge University Press, 2 2023. [doi:10.1017/9781009253161](#).
- [95] Bruce Allen and Theodore Jacobson. Vector Two Point Functions in Maximally Symmetric Spaces. *Commun. Math. Phys.*, 103:669, 1986. [doi:10.1007/BF01211169](#).
- [96] Robert M. Wald. *General Relativity*. Chicago Univ. Pr., Chicago, USA, 1984. [doi:10.7208/chicago/9780226870373.001.0001](#).
- [97] Marcus Spradlin, Andrew Strominger, and Anastasia Volovich. Les Houches lectures on de Sitter space. In *Les Houches Summer School: Session 76: Euro Summer School on Unity of Fundamental Physics: Gravity, Gauge Theory and Strings*, pages 423–453, 10 2001. [arXiv:hep-th/0110007](#).
- [98] Dionysios Anninos. De Sitter Musings. *Int. J. Mod. Phys. A*, 27:1230013, 2012. [arXiv:1205.3855](#), [doi:10.1142/S0217751X1230013X](#).
- [99] Vijay Balasubramanian, Jan de Boer, and Djordje Minic. Notes on de Sitter space and holography. *Class. Quant. Grav.*, 19:5655–5700, 2002. [arXiv:hep-th/0207245](#), [doi:10.1016/S0003-4916\(02\)00020-9](#).
- [100] Naureen Goheer, Matthew Kleban, and Leonard Susskind. The Trouble with de Sitter space. *JHEP*, 07:056, 2003. [arXiv:hep-th/0212209](#), [doi:10.1088/1126-6708/2003/07/056](#).

- [101] Sebastian Fischetti, Donald Marolf, and Aron C. Wall. A paucity of bulk entangling surfaces: AdS wormholes with de Sitter interiors. *Class. Quant. Grav.*, 32:065011, 2015. [arXiv:1409.6754](#), [doi:10.1088/0264-9381/32/6/065011](#).
- [102] Alejandra Castro, Philippe Sabella-Garnier, and Claire Zukowski. Gravitational Wilson Lines in 3D de Sitter. *JHEP*, 07:202, 2020. [arXiv:2001.09998](#), [doi:10.1007/JHEP07\(2020\)202](#).
- [103] Yasuaki Hikida, Tatsuma Nishioka, Tadashi Takayanagi, and Yusuke Taki. CFT duals of three-dimensional de Sitter gravity. *JHEP*, 05:129, 2022. [arXiv:2203.02852](#), [doi:10.1007/JHEP05\(2022\)129](#).
- [104] Lars Aalsma, Mir Mehedi Faruk, Jan Pieter van der Schaar, Manus Visser, and Job de Witte. Late-Time Correlators and Complex Geodesics in de Sitter Space. *SciPost Phys.*, 15:031, 2023. [arXiv:2212.01394](#), [doi:10.21468/SciPostPhys.15.1.031](#).
- [105] Vijay Balasubramanian and Simon F. Ross. Holographic particle detection. *Phys. Rev. D*, 61:044007, 2000. [arXiv:hep-th/9906226](#), [doi:10.1103/PhysRevD.61.044007](#).
- [106] Jorma Louko, Donald Marolf, and Simon F. Ross. On geodesic propagators and black hole holography. *Phys. Rev. D*, 62:044041, 2000. [arXiv:hep-th/0002111](#), [doi:10.1103/PhysRevD.62.044041](#).
- [107] Balasubramanian, Vijay and Bernamonti, Alice and de Boer, Jan and Copland, Neil B. and Craps, Ben and Keski-Vakkuri, Esko and Müller, Berndt and Schäfer, Andreas and Shigemori, Masaki and Staessens, Wieland. Holographic Thermalization. *Phys. Rev. D*, 84:026010, 2011. [arXiv:1103.2683](#), [doi:10.1103/PhysRevD.84.026010](#).
- [108] Joao Aparicio and Esperanza Lopez. Evolution of Two-Point Functions from Holography. *JHEP*, 12:082, 2011. [arXiv:1109.3571](#), [doi:10.1007/JHEP12\(2011\)082](#).
- [109] Hong Liu and S. Josephine Suh. Entanglement Tsunami: Universal Scaling in Holographic Thermalization. *Phys. Rev. Lett.*, 112:011601, 2014. [arXiv:1305.7244](#), [doi:10.1103/PhysRevLett.112.011601](#).
- [110] Stephen H. Shenker and Douglas Stanford. Black holes and the butterfly effect. *JHEP*, 03:067, 2014. [arXiv:1306.0622](#), [doi:10.1007/JHEP03\(2014\)067](#).
- [111] Stephen H. Shenker and Douglas Stanford. Multiple Shocks. *JHEP*, 12:046, 2014. [arXiv:1312.3296](#), [doi:10.1007/JHEP12\(2014\)046](#).

- [112] Roman Jackiw. Lower Dimensional Gravity. *Nucl. Phys. B*, 252:343–356, 1985. doi:[10.1016/0550-3213\(85\)90448-1](https://doi.org/10.1016/0550-3213(85)90448-1).
- [113] Claudio Teitelboim. Gravitation and Hamiltonian Structure in Two Space-Time Dimensions. *Phys. Lett. B*, 126:41–45, 1983. doi:[10.1016/0370-2693\(83\)90012-6](https://doi.org/10.1016/0370-2693(83)90012-6).
- [114] Edward Witten. A note on boundary conditions in Euclidean gravity. *Rev. Math. Phys.*, 33(10):2140004, 2021. arXiv:[1805.11559](https://arxiv.org/abs/1805.11559), doi:[10.1142/S0129055X21400043](https://doi.org/10.1142/S0129055X21400043).
- [115] Tomas Andrade, William R. Kelly, Donald Marolf, and Jorge E. Santos. On the stability of gravity with Dirichlet walls. *Class. Quant. Grav.*, 32(23):235006, 2015. arXiv:[1504.07580](https://arxiv.org/abs/1504.07580), doi:[10.1088/0264-9381/32/23/235006](https://doi.org/10.1088/0264-9381/32/23/235006).
- [116] Zhongshan An and Michael T. Anderson. The initial boundary value problem and quasi-local Hamiltonians in General Relativity. *Classical and Quantum Gravity*, 38:154001, 3 2021. arXiv:[2103.15673](https://arxiv.org/abs/2103.15673), doi:[10.1088/1361-6382/ac0a86](https://doi.org/10.1088/1361-6382/ac0a86).
- [117] Michael T. Anderson. Extension of symmetries on Einstein manifolds with boundary. *Selecta Mathematica*, 16:343–375, 4 2007. arXiv:[0704.3373](https://arxiv.org/abs/0704.3373).
- [118] Daniel Grumiller and Robert McNees. Thermodynamics of black holes in two (and higher) dimensions. *JHEP*, 04:074, 2007. arXiv:[hep-th/0703230](https://arxiv.org/abs/hep-th/0703230), doi:[10.1088/1126-6708/2007/04/074](https://doi.org/10.1088/1126-6708/2007/04/074).
- [119] Edward Witten. Deformations of JT Gravity and Phase Transitions. 6 2020. arXiv:[2006.03494](https://arxiv.org/abs/2006.03494).
- [120] Patrick Draper and Szilard Farkas. Euclidean de Sitter black holes and microcanonical equilibrium. *Phys. Rev. D*, 105(12):126021, 2022. arXiv:[2203.01871](https://arxiv.org/abs/2203.01871), doi:[10.1103/PhysRevD.105.126021](https://doi.org/10.1103/PhysRevD.105.126021).
- [121] Dionysios Anninos, Teresa Bautista, and Beatrix Mühlmann. The two-sphere partition function in two-dimensional quantum gravity. *JHEP*, 09:116, 2021. arXiv:[2106.01665](https://arxiv.org/abs/2106.01665), doi:[10.1007/JHEP09\(2021\)116](https://doi.org/10.1007/JHEP09(2021)116).
- [122] Beatrix Mühlmann. The two-sphere partition function from timelike Liouville theory at three-loop order. *JHEP*, 05:057, 2022. arXiv:[2202.04549](https://arxiv.org/abs/2202.04549), doi:[10.1007/JHEP05\(2022\)057](https://doi.org/10.1007/JHEP05(2022)057).
- [123] Beatrix Mühlmann. The two-sphere partition function in two-dimensional quantum gravity at fixed area. *JHEP*, 09(189):189, 2021. arXiv:[2106.04532](https://arxiv.org/abs/2106.04532), doi:[10.1007/JHEP09\(2021\)189](https://doi.org/10.1007/JHEP09(2021)189).

- [124] Jens C. Niemeyer and Raphael Bousso. The Nonlinear evolution of de Sitter space instabilities. *Phys. Rev. D*, 62:023503, 2000. [arXiv:gr-qc/0004004](#), [doi:10.1103/PhysRevD.62.023503](#).
- [125] Dionysios Anninos and Tarek Anous. A de Sitter Hoedown. *JHEP*, 08:131, 2010. [arXiv:1002.1717](#), [doi:10.1007/JHEP08\(2010\)131](#).
- [126] Dionysios Anninos, Diego M. Hofman, and Stathis Vitouladitis. One-dimensional Quantum Gravity and the Schwarzian theory. *JHEP*, 03:121, 2022. [arXiv:2112.03793](#), [doi:10.1007/JHEP03\(2022\)121](#).
- [127] Dionysios Anninos and Beatrix Mühlmann. Matrix integrals & finite holography. *JHEP*, 06:120, 2021. [arXiv:2012.05224](#), [doi:10.1007/JHEP06\(2021\)120](#).
- [128] Subir Sachdev and Jinwu Ye. Gapless spin fluid ground state in a random, quantum Heisenberg magnet. *Phys. Rev. Lett.*, 70:3339, 1993. [arXiv:cond-mat/9212030](#), [doi:10.1103/PhysRevLett.70.3339](#).
- [129] Alexei Kitaev and S. Josephine Suh. The soft mode in the Sachdev-Ye-Kitaev model and its gravity dual. *JHEP*, 05:183, 2018. [arXiv:1711.08467](#), [doi:10.1007/JHEP05\(2018\)183](#).
- [130] Juan Maldacena and Douglas Stanford. Remarks on the Sachdev-Ye-Kitaev model. *Phys. Rev. D*, 94(10):106002, 2016. [arXiv:1604.07818](#), [doi:10.1103/PhysRevD.94.106002](#).
- [131] Dionysios Anninos, Damián A. Galante, and Sameer U. Sheorey. Renormalisation Group Flows of the SYK Model. 12 2022. [arXiv:2212.04944](#).
- [132] Charlotte Sleight. A Mellin Space Approach to Cosmological Correlators. *JHEP*, 01:090, 2020. [arXiv:1906.12302](#), [doi:10.1007/JHEP01\(2020\)090](#).
- [133] Emil Mottola. Particle Creation in de Sitter Space. *Phys. Rev. D*, 31:754, 1985. [doi:10.1103/PhysRevD.31.754](#).
- [134] Bruce Allen. Vacuum States in de Sitter Space. *Phys. Rev. D*, 32:3136, 1985. [doi:10.1103/PhysRevD.32.3136](#).
- [135] George N. Watson. Asymptotic expansions of hypergeometric functions. *Trans. Cambridge Phil. Soc.*, 22:277–308, 1918.

- [136] Mislav Cvitković, Ana-Sunčana Smith, and Jayant Pande. Asymptotic expansions of the hypergeometric function with two large parameters—application to the partition function of a lattice gas in a field of traps. *Journal of Physics A: Mathematical and Theoretical*, 50(26):265206, jun 2017. URL: <https://doi.org/10.1088/1751-8121/50/26/265206>, doi:10.1088/1751-8121/aa7213.
- [137] Eivind Jørstad, Robert C. Myers, and Shan-Ming Ruan. Holographic complexity in dS_{d+1} . *JHEP*, 05:119, 2022. [arXiv:2202.10684](https://arxiv.org/abs/2202.10684), doi:10.1007/JHEP05(2022)119.
- [138] Adam R. Brown, Hrant Gharibyan, Henry W. Lin, Leonard Susskind, LÁrus Thorlacius, and Ying Zhao. Complexity of Jackiw-Teitelboim gravity. *Phys. Rev. D*, 99(4):046016, 2019. [arXiv:1810.08741](https://arxiv.org/abs/1810.08741), doi:10.1103/PhysRevD.99.046016.
- [139] Damian Galante. Geodesics, complexity and holography in (A)dS₂. *PoS, CORFU2021*:359, 2022. doi:10.22323/1.406.0359.
- [140] Lukasz Fidkowski, Veronika Hubeny, Matthew Kleban, and Stephen Shenker. The Black hole singularity in AdS / CFT. *JHEP*, 02:014, 2004. [arXiv:hep-th/0306170](https://arxiv.org/abs/hep-th/0306170), doi:10.1088/1126-6708/2004/02/014.
- [141] Guido Festuccia and Hong Liu. Excursions beyond the horizon: Black hole singularities in Yang-Mills theories. I. *JHEP*, 04:044, 2006. [arXiv:hep-th/0506202](https://arxiv.org/abs/hep-th/0506202), doi:10.1088/1126-6708/2006/04/044.
- [142] Irene Amado and Carlos Hoyos-Badajoz. AdS black holes as reflecting cavities. *JHEP*, 09:118, 2008. [arXiv:0807.2337](https://arxiv.org/abs/0807.2337), doi:10.1088/1126-6708/2008/09/118.
- [143] A. Lopez-Ortega. Quasinormal modes of D-dimensional de Sitter spacetime. *Gen. Rel. Grav.*, 38:1565–1591, 2006. [arXiv:gr-qc/0605027](https://arxiv.org/abs/gr-qc/0605027), doi:10.1007/s10714-006-0335-9.
- [144] Paul Fendley, Matthew P. A. Fisher, and Chetan Nayak. Topological entanglement entropy from the holographic partition function. *J. Statist. Phys.*, 126:1111, 2007. [arXiv:cond-mat/0609072](https://arxiv.org/abs/cond-mat/0609072), doi:10.1007/s10955-006-9275-8.
- [145] Edward Witten. Quantum Field Theory and the Jones Polynomial. *Commun. Math. Phys.*, 121:351–399, 1989. doi:10.1007/BF01217730.
- [146] Edward Witten. Quantization of Chern-Simons Gauge Theory With Complex Gauge Group. *Commun. Math. Phys.*, 137:29–66, 1991. doi:10.1007/BF02099116.

- [147] Edward Witten. Analytic Continuation Of Chern-Simons Theory. *AMS/IP Stud. Adv. Math.*, 50:347–446, 2011. [arXiv:1001.2933](#).
- [148] Sergei Gukov, Marcos Marino, and Pavel Putrov. Resurgence in complex Chern-Simons theory. 5 2016. [arXiv:1605.07615](#).
- [149] Tudor Dimofte, Sergei Gukov, Jonatan Lenells, and Don Zagier. Exact Results for Perturbative Chern-Simons Theory with Complex Gauge Group. *Commun. Num. Theor. Phys.*, 3:363–443, 2009. [arXiv:0903.2472](#), [doi:10.4310/CNTP.2009.v3.n2.a4](#).
- [150] Tudor Dimofte. Perturbative and nonperturbative aspects of complex Chern–Simons theory. *J. Phys. A*, 50(44):443009, 2017. [arXiv:1608.02961](#), [doi:10.1088/1751-8121/aa6a5b](#).
- [151] Cumrun Vafa. Fractional Quantum Hall Effect and M-Theory. 11 2015. [arXiv:1511.03372](#).
- [152] Lee Smolin. Linking topological quantum field theory and nonperturbative quantum gravity. *J. Math. Phys.*, 36:6417–6455, 1995. [arXiv:gr-qc/9505028](#), [doi:10.1063/1.531251](#).
- [153] Cho-pin Soo. Wave function of the universe and Chern-Simons perturbation theory. *Class. Quant. Grav.*, 19:1051–1064, 2002. [arXiv:gr-qc/0109046](#), [doi:10.1088/0264-9381/19/6/303](#).
- [154] Lee Smolin and Chopin Soo. The Chern-Simons invariant as the natural time variable for classical and quantum cosmology. *Nucl. Phys. B*, 449:289–316, 1995. [arXiv:gr-qc/9405015](#), [doi:10.1016/0550-3213\(95\)00222-E](#).
- [155] Alejandra Castro, Ioana Coman, Jackson R. Fliss, and Claire Zukowski. Keeping matter in the loop in dS_3 quantum gravity. *JHEP*, 07:120, 2023. [arXiv:2302.12281](#), [doi:10.1007/JHEP07\(2023\)120](#).
- [156] Steven Carlip. The Sum over topologies in three-dimensional Euclidean quantum gravity. *Class. Quant. Grav.*, 10:207–218, 1993. [arXiv:hep-th/9206103](#), [doi:10.1088/0264-9381/10/2/004](#).
- [157] Enore Guadagnini and Paolo Tomassini. Sum over the geometries of three manifolds. *Phys. Lett. B*, 336:330–336, 1994. [doi:10.1016/0370-2693\(94\)90541-X](#).
- [158] Alejandra Castro, Nima Lashkari, and Alexander Maloney. A de Sitter Farey Tail. *Phys. Rev. D*, 83:124027, 2011. [arXiv:1103.4620](#), [doi:10.1103/PhysRevD.83.124027](#).

- [159] Joseph Polchinski. The Phase of the Sum Over Spheres. *Phys. Lett. B*, 219:251–257, 1989. doi:[10.1016/0370-2693\(89\)90387-0](https://doi.org/10.1016/0370-2693(89)90387-0).
- [160] Mu-In Park. Statistical entropy of three-dimensional Kerr-de Sitter space. *Phys. Lett. B*, 440:275–282, 1998. arXiv:[hep-th/9806119](https://arxiv.org/abs/hep-th/9806119), doi:[10.1016/S0370-2693\(98\)01119-8](https://doi.org/10.1016/S0370-2693(98)01119-8).
- [161] Juan Martin Maldacena and Andrew Strominger. Statistical entropy of de Sitter space. *JHEP*, 02:014, 1998. arXiv:[gr-qc/9801096](https://arxiv.org/abs/gr-qc/9801096), doi:[10.1088/1126-6708/1998/02/014](https://doi.org/10.1088/1126-6708/1998/02/014).
- [162] Maximo Banados, Thorsten Brotz, and Miguel E. Ortiz. Quantum three-dimensional de Sitter space. *Phys. Rev. D*, 59:046002, 1999. arXiv:[hep-th/9807216](https://arxiv.org/abs/hep-th/9807216), doi:[10.1103/PhysRevD.59.046002](https://doi.org/10.1103/PhysRevD.59.046002).
- [163] T. R. Govindarajan, Romesh K. Kaul, and Vardarajan Suneeta. Quantum gravity on dS(3). *Class. Quant. Grav.*, 19:4195–4205, 2002. arXiv:[hep-th/0203219](https://arxiv.org/abs/hep-th/0203219), doi:[10.1088/0264-9381/19/15/320](https://doi.org/10.1088/0264-9381/19/15/320).
- [164] Xi Dong, Bart Horn, Eva Silverstein, and Gonzalo Torroba. Micromanaging de Sitter holography. *Class. Quant. Grav.*, 27:245020, 2010. arXiv:[1005.5403](https://arxiv.org/abs/1005.5403), doi:[10.1088/0264-9381/27/24/245020](https://doi.org/10.1088/0264-9381/27/24/245020).
- [165] D. V. Vassilevich. Heat kernel expansion: User’s manual. *Phys. Rept.*, 388:279–360, 2003. arXiv:[hep-th/0306138](https://arxiv.org/abs/hep-th/0306138), doi:[10.1016/j.physrep.2003.09.002](https://doi.org/10.1016/j.physrep.2003.09.002).
- [166] Pavel V. Buividovich and Mikhail I. Polikarpov. Entanglement entropy in gauge theories and the holographic principle for electric strings. *Phys. Lett. B*, 670:141–145, 2008. arXiv:[0806.3376](https://arxiv.org/abs/0806.3376), doi:[10.1016/j.physletb.2008.10.032](https://doi.org/10.1016/j.physletb.2008.10.032).
- [167] William Donnelly. Decomposition of entanglement entropy in lattice gauge theory. *Phys. Rev. D*, 85:085004, 2012. arXiv:[1109.0036](https://arxiv.org/abs/1109.0036), doi:[10.1103/PhysRevD.85.085004](https://doi.org/10.1103/PhysRevD.85.085004).
- [168] William Donnelly. Entanglement entropy and nonabelian gauge symmetry. *Class. Quant. Grav.*, 31(21):214003, 2014. arXiv:[1406.7304](https://arxiv.org/abs/1406.7304), doi:[10.1088/0264-9381/31/21/214003](https://doi.org/10.1088/0264-9381/31/21/214003).
- [169] Horacio Casini, Marina Huerta, and Jose Alejandro Rosabal. Remarks on entanglement entropy for gauge fields. *Phys. Rev. D*, 89(8):085012, 2014. arXiv:[1312.1183](https://arxiv.org/abs/1312.1183), doi:[10.1103/PhysRevD.89.085012](https://doi.org/10.1103/PhysRevD.89.085012).

- [170] Sudip Ghosh, Ronak M Soni, and Sandip P. Trivedi. On The Entanglement Entropy For Gauge Theories. *JHEP*, 09:069, 2015. [arXiv:1501.02593](#), [doi:10.1007/JHEP09\(2015\)069](#).
- [171] Jennifer Lin and Dorde Radičević. Comments on defining entanglement entropy. *Nucl. Phys. B*, 958:115118, 2020. [arXiv:1808.05939](#), [doi:10.1016/j.nuclphysb.2020.115118](#).
- [172] Philippe Di Francesco, Pierre Mathieu, and David Senechal. *Conformal Field Theory*. Graduate Texts in Contemporary Physics. Springer-Verlag, New York, 1997. [doi:10.1007/978-1-4612-2256-9](#).
- [173] Hiroshi Ooguri and Cumrun Vafa. World sheet derivation of a large N duality. *Nucl. Phys. B*, 641:3–34, 2002. [arXiv:hep-th/0205297](#), [doi:10.1016/S0550-3213\(02\)00620-X](#).
- [174] Dionysios Anninos and Beatrix Mühlmann. Notes on matrix models (matrix musings). *J. Stat. Mech.*, 2008:083109, 2020. [arXiv:2004.01171](#), [doi:10.1088/1742-5468/aba499](#).
- [175] Gerald V. Dunne, Roman W. Jackiw, and Carlo A. Trugenberger. Chern-Simons Theory in the Schrodinger Representation. *Annals Phys.*, 194:197, 1989. [doi:10.1016/0003-4916\(89\)90036-5](#).
- [176] Shmuel Elitzur, Gregory W. Moore, Adam Schwimmer, and Nathan Seiberg. Remarks on the Canonical Quantization of the Chern-Simons-Witten Theory. *Nucl. Phys. B*, 326:108–134, 1989. [doi:10.1016/0550-3213\(89\)90436-7](#).
- [177] David Tong. Lectures on the Quantum Hall Effect. 6 2016. [arXiv:1606.06687](#).
- [178] Simone Giombi, Igor R. Klebanov, and Grigory Tarnopolsky. Conformal QED_d, F-Theorem and the ϵ Expansion. *J. Phys. A*, 49(13):135403, 2016. [arXiv:1508.06354](#), [doi:10.1088/1751-8113/49/13/135403](#).
- [179] Roberto Floreanini and Roman W. Jackiw. Selfdual Fields as Charge Density Solitons. *Phys. Rev. Lett.*, 59:1873, 1987. [doi:10.1103/PhysRevLett.59.1873](#).
- [180] Xiao-Gang Wen. Chiral Luttinger Liquid and the Edge Excitations in the Fractional Quantum Hall States. *Phys. Rev. B*, 41:12838–12844, 1990. [doi:10.1103/PhysRevB.41.12838](#).

- [181] Gerard 't Hooft. On the Quantum Structure of a Black Hole. *Nucl. Phys. B*, 256:727–745, 1985. [doi:10.1016/0550-3213\(85\)90418-3](https://doi.org/10.1016/0550-3213(85)90418-3).
- [182] Diptarka Das and Shouvik Datta. Universal features of left-right entanglement entropy. *Phys. Rev. Lett.*, 115(13):131602, 2015. [arXiv:1504.02475](https://arxiv.org/abs/1504.02475), [doi:10.1103/PhysRevLett.115.131602](https://doi.org/10.1103/PhysRevLett.115.131602).
- [183] Marc Geiller. Edge modes and corner ambiguities in 3d Chern–Simons theory and gravity. *Nucl. Phys. B*, 924:312–365, 2017. [arXiv:1703.04748](https://arxiv.org/abs/1703.04748), [doi:10.1016/j.nuclphysb.2017.09.010](https://doi.org/10.1016/j.nuclphysb.2017.09.010).
- [184] Gabriel Wong. A note on entanglement edge modes in Chern Simons theory. *JHEP*, 08:020, 2018. [arXiv:1706.04666](https://arxiv.org/abs/1706.04666), [doi:10.1007/JHEP08\(2018\)020](https://doi.org/10.1007/JHEP08(2018)020).
- [185] A. N. Schellekens. Introduction to conformal field theory. *Fortsch. Phys.*, 44:605–705, 1996.
- [186] Shiyong Dong, Eduardo Fradkin, Robert G. Leigh, and Sean Nowling. Topological Entanglement Entropy in Chern-Simons Theories and Quantum Hall Fluids. *JHEP*, 05:016, 2008. [arXiv:0802.3231](https://arxiv.org/abs/0802.3231), [doi:10.1088/1126-6708/2008/05/016](https://doi.org/10.1088/1126-6708/2008/05/016).
- [187] Eran Sagi and Raul A. Santos. Supersymmetry in the Fractional Quantum Hall Regime. *Phys. Rev. B*, 95(20):205144, 2017. [arXiv:1610.07627](https://arxiv.org/abs/1610.07627), [doi:10.1103/PhysRevB.95.205144](https://doi.org/10.1103/PhysRevB.95.205144).
- [188] Krzysztof Pilch, Peter van Nieuwenhuizen, and M. F. Sohnius. De Sitter Superalgebras and Supergravity. *Commun. Math. Phys.*, 98:105, 1985. [doi:10.1007/BF01211046](https://doi.org/10.1007/BF01211046).
- [189] Tarek Anous, Daniel Z. Freedman, and Alexander Maloney. de Sitter Supersymmetry Revisited. *JHEP*, 07:119, 2014. [arXiv:1403.5038](https://arxiv.org/abs/1403.5038), [doi:10.1007/JHEP07\(2014\)119](https://doi.org/10.1007/JHEP07(2014)119).
- [190] Danny Birmingham, Matthias Blau, Mark Rakowski, and George Thompson. Topological field theory. *Phys. Rept.*, 209:129–340, 1991. [doi:10.1016/0370-1573\(91\)90117-5](https://doi.org/10.1016/0370-1573(91)90117-5).
- [191] Alberto S. Cattaneo, Paolo Cotta-Ramusino, Jurg Frohlich, and Maurizio Martellini. Topological BF theories in three-dimensions and four-dimensions. *J. Math. Phys.*, 36:6137–6160, 1995. [arXiv:hep-th/9505027](https://arxiv.org/abs/hep-th/9505027), [doi:10.1063/1.531238](https://doi.org/10.1063/1.531238).
- [192] Gerald V. Dunne and Roman W. Jackiw. 'Peierls substitution' and Chern-Simons quantum mechanics. *Nucl. Phys. B Proc. Suppl.*, 33:114–118, 1993. [arXiv:hep-th/9204057](https://arxiv.org/abs/hep-th/9204057), [doi:10.1016/0920-5632\(93\)90376-H](https://doi.org/10.1016/0920-5632(93)90376-H).

- [193] Vittorio de Alfaro, Sergio Fubini, and G. Furlan. Conformal Invariance in Quantum Mechanics. *Nuovo Cim. A*, 34:569, 1976. doi:[10.1007/BF02785666](https://doi.org/10.1007/BF02785666).
- [194] Tarek Anous and Jim Skulte. An invitation to the principal series. *SciPost Phys.*, 9(3):028, 2020. arXiv:[2007.04975](https://arxiv.org/abs/2007.04975), doi:[10.21468/SciPostPhys.9.3.028](https://doi.org/10.21468/SciPostPhys.9.3.028).
- [195] Krzysztof Andrzejewski and Joanna Gonera. On the geometry of conformal mechanics. 8 2011. arXiv:[1108.1299](https://arxiv.org/abs/1108.1299).
- [196] Krzysztof Andrzejewski. Quantum conformal mechanics emerging from unitary representations of $SL(2, \mathbb{R})$. *Annals Phys.*, 367:227–250, 2016. arXiv:[1506.05596](https://arxiv.org/abs/1506.05596), doi:[10.1016/j.aop.2016.01.020](https://doi.org/10.1016/j.aop.2016.01.020).
- [197] Steven Carlip. The Statistical mechanics of the (2+1)-dimensional black hole. *Phys. Rev. D*, 51:632–637, 1995. arXiv:[gr-qc/9409052](https://arxiv.org/abs/gr-qc/9409052), doi:[10.1103/PhysRevD.51.632](https://doi.org/10.1103/PhysRevD.51.632).
- [198] Maximo Banados and Andres Gomberoff. Black hole entropy in the Chern-Simons formulation of (2+1) gravity. *Phys. Rev. D*, 55:6162–6167, 1997. arXiv:[gr-qc/9611044](https://arxiv.org/abs/gr-qc/9611044), doi:[10.1103/PhysRevD.55.6162](https://doi.org/10.1103/PhysRevD.55.6162).
- [199] Giovanni Arcioni, Matthias Blau, and Martin O’Loughlin. On the boundary dynamics of Chern-Simons gravity. *JHEP*, 01:067, 2003. arXiv:[hep-th/0210089](https://arxiv.org/abs/hep-th/0210089), doi:[10.1088/1126-6708/2003/01/067](https://doi.org/10.1088/1126-6708/2003/01/067).
- [200] Vijay Balasubramanian and Per Kraus. A Stress tensor for Anti-de Sitter gravity. *Commun. Math. Phys.*, 208:413–428, 1999. arXiv:[hep-th/9902121](https://arxiv.org/abs/hep-th/9902121), doi:[10.1007/s002200050764](https://doi.org/10.1007/s002200050764).
- [201] Juan Maldacena and Guilherme L. Pimentel. Entanglement entropy in de Sitter space. *JHEP*, 02:038, 2013. arXiv:[1210.7244](https://arxiv.org/abs/1210.7244), doi:[10.1007/JHEP02\(2013\)038](https://doi.org/10.1007/JHEP02(2013)038).
- [202] Anton Kapustin, Brian Willett, and Itamar Yaakov. Exact Results for Wilson Loops in Superconformal Chern-Simons Theories with Matter. *JHEP*, 03:089, 2010. arXiv:[0909.4559](https://arxiv.org/abs/0909.4559), doi:[10.1007/JHEP03\(2010\)089](https://doi.org/10.1007/JHEP03(2010)089).
- [203] Nadav Drukker, Marcos Marino, and Pavel Putrov. From weak to strong coupling in ABJM theory. *Commun. Math. Phys.*, 306:511–563, 2011. arXiv:[1007.3837](https://arxiv.org/abs/1007.3837), doi:[10.1007/s00220-011-1253-6](https://doi.org/10.1007/s00220-011-1253-6).
- [204] Edward Witten. Anti-de Sitter space, thermal phase transition, and confinement in gauge theories. *Adv. Theor. Math. Phys.*, 2:505–532, 1998. arXiv:[hep-th/9803131](https://arxiv.org/abs/hep-th/9803131), doi:[10.4310/ATMP.1998.v2.n3.a3](https://doi.org/10.4310/ATMP.1998.v2.n3.a3).

- [205] Lauren McGough and Herman Verlinde. Bekenstein-Hawking Entropy as Topological Entanglement Entropy. *JHEP*, 11:208, 2013. [arXiv:1308.2342](#), [doi:10.1007/JHEP11\(2013\)208](#).
- [206] John Chalker. Quantum theory of condensed matter. <https://www-thphys.physics.ox.ac.uk/people/JohnChalker/qtcm/lecture-notes.pdf>, 2013. Accessed: 06-04-2023.
- [207] Mukund Rangamani and Tadashi Takayanagi. *Holographic Entanglement Entropy*, volume 931. Springer, 2017. [arXiv:1609.01287](#), [doi:10.1007/978-3-319-52573-0](#).
- [208] Leonard Susskind. Three Lectures on Complexity and Black Holes. SpringerBriefs in Physics. Springer, 10 2018. [arXiv:1810.11563](#), [doi:10.1007/978-3-030-45109-7](#).
- [209] Shira Chapman and Giuseppe Policastro. Quantum computational complexity from quantum information to black holes and back. *Eur. Phys. J. C*, 82(2):128, 2022. [arXiv:2110.14672](#), [doi:10.1140/epjc/s10052-022-10037-1](#).
- [210] Jacques Bros. Complexified de Sitter space: Analytic causal kernels and Kallen-Lehmann type representation. *Nucl. Phys. B Proc. Suppl.*, 18:22–28, 1991. [doi:10.1016/0920-5632\(91\)90119-Y](#).
- [211] Leonard Susskind. Black Holes Hint Towards De Sitter-Matrix Theory. 9 2021. [arXiv:2109.01322](#).
- [212] Henry Lin and Leonard Susskind. Infinite Temperature’s Not So Hot. 6 2022. [arXiv:2206.01083](#).
- [213] Leonard Susskind. De Sitter Space, Double-Scaled SYK, and the Separation of Scales in the Semiclassical Limit. 9 2022. [arXiv:2209.09999](#).
- [214] Adel A. Rahman. dS JT Gravity and Double-Scaled SYK. 9 2022. [arXiv:2209.09997](#).
- [215] Antonio M. García-García, Lucas Sá, Jacobus J. M. Verbaarschot, and Jie Ping Zheng. Keldysh wormholes and anomalous relaxation in the dissipative Sachdev-Ye-Kitaev model. *Phys. Rev. D*, 107(10):106006, 2023. [arXiv:2210.01695](#), [doi:10.1103/PhysRevD.107.106006](#).
- [216] Rajesh Gopakumar and Cumrun Vafa. On the gauge theory / geometry correspondence. *Adv. Theor. Math. Phys.*, 3:1415–1443, 1999. [arXiv:hep-th/9811131](#), [doi:10.4310/ATMP.1999.v3.n5.a5](#).

- [217] Elias Kiritsis and Vasilis Niarchos. Large- N limits of 2d CFTs, Quivers and AdS_3 duals. *JHEP*, 04:113, 2011. [arXiv:1011.5900](#), [doi:10.1007/JHEP04\(2011\)113](#).
- [218] Euihun Joung, Prithvi Narayan, and Junggi Yoon. Gravitational Edge Mode in Asymptotically AdS_2 : JT Gravity Revisited. 4 2023. [arXiv:2304.06088](#).
- [219] Thomas G. Mertens, Joan Simón, and Gabriel Wong. A proposal for 3d quantum gravity and its bulk factorization. *JHEP*, 06:134, 2023. [arXiv:2210.14196](#), [doi:10.1007/JHEP06\(2023\)134](#).
- [220] Jose P. S. Lemos. Thermodynamics of the two-dimensional black hole in the Teitelboim-Jackiw theory. *Phys. Rev. D*, 54:6206–6212, 1996. [arXiv:gr-qc/9608016](#), [doi:10.1103/PhysRevD.54.6206](#).
- [221] Marco Cavaglia. Geometrodynamical formulation of two-dimensional dilaton gravity. *Phys. Rev. D*, 59:084011, 1999. [arXiv:hep-th/9811059](#), [doi:10.1103/PhysRevD.59.084011](#).
- [222] Vijay Balasubramanian, Ben Craps, Marine De Clerck, and Kévin Nguyen. Superluminal chaos after a quantum quench. *JHEP*, 12:132, 2019. [arXiv:1908.08955](#), [doi:10.1007/JHEP12\(2019\)132](#).
- [223] Klaus Schulten. Notes on quantum mechanics. <https://www.ks.uiuc.edu/Services/Class/PHYS480/>, April 2000.
- [224] Mark A. Rubin and Carlos R. Ordonez. Symmetric Tensor Eigen Spectrum of the Laplacian on n Spheres. *J. Math. Phys.*, 26:65, 1985. [doi:10.1063/1.526749](#).
- [225] Jackson R. Fliss, Xueda Wen, Onkar Parrikar, Chang-Tse Hsieh, Bo Han, Taylor L. Hughes, and Robert G. Leigh. Interface Contributions to Topological Entanglement in Abelian Chern-Simons Theory. *JHEP*, 09:056, 2017. [arXiv:1705.09611](#), [doi:10.1007/JHEP09\(2017\)056](#).
- [226] Lev Rozansky. Witten’s invariant of three-dimensional manifolds: Loop expansion and surgery calculus. pages 271–299, 6 1993. [arXiv:hep-th/9401060](#).